Ultrastructural studies of cornea and sclera

Thesis

Ultrastructural studies of cornea and sclera.

Nigel James Fullwood, BSc., MPhil.

Thesis submitted for the degree of
Doctor of Philosophy
in the discipline of
Biophysics.

The Biophysics Group,
Oxford Research Unit,
The Open University.

March 1992.

To my parents

Acknowledgements

I must thank first and foremost my supervisor Dr Keith Meek for his constant advice and encouragement during my time at the Unit. Especially for always having time for my problems and for introducing me to the intricacies of X-ray diffraction. I thank Professor Gerald Elliott for looking after me as a student and for generously allowing me to use his beam time at Daresbury for my own experiments.

I acknowledge the help that Dr Andrew Quantock has given me with some of the figures in this thesis, and without whom, my time at Oxford would have been a lot duller.

I also thank my two fellow students Nageena Malik and Ian Rawe for managing to share an office with me; Nageena for setting an example of a model student and for answering biochemical questions, and Ian for always having a definite (though sometimes wrong) answer to any problem. I also thank Dr Rita Wall for help and advice and also, together with Daniel Leonard, for help at the Daresbury synchrotron.

Without the human material supplied by the clinicians, the work on keratoconus could not have been carried out. So I am indebted to Mr Steven Tuft (Moorfields Hospital, London), Mr Alan Ridgway and Mr Andrew Tullo (Royal Eye Hospital, Manchester), Miss Rosalind Harrison (Burton on Trent Eye Hospital), Professor Antony Bron (Nuffield Department of Ophthalmology, Oxford), and Dr Paul Brittan (Wolverhampton Eye Infirmary). I also thank Dr David Troilo for supplying the material used in the myopic section of this thesis.

Finally, I thank the National Keratoconus/Discovery Fund for Eye Research and the Iris Fund for financial support during this project.

EX12

HIGHER DEGREES OFFICE

LIBRARY AUTHORISATION FORM

STUDENT: NIGEL JAMES FULLWOOD SERIAL NO: M7063223

DEGREE: PhD

TITLE OF THESIS: ULTRASTRUCTURAL STUDIES ON CORNEA AND SCLERA.

I confirm that I am willing that my thesis be made available to readers and maybe photocopied, subject to the discretion of the Librarian.

SIGNED: _____ DATE: 17/2/92

Abstract

The work of Goodfellow et al., (*J. Mol. Biol.* **119**: 237. 1978) and Sayers et al., (*J. Mol. Biol.* **160**: 593. 1982), was repeated using fresh, equilibrated cornea, confirming their finding that the plot of interfibrillar spacing^2 against hydration is a linear relationship. Intermolecular spacing in cornea, sclera and rat-tail tendon was shown to increase rapidly over the hydration range H=0 to H≈1, then tail off (physiological hydration is at H=3.2). Intermolecular and interfibrillar spacings rise in unison over the hydration range H=0 to H≈1, after which virtually all of the water goes between the fibrils.

It was found that freezing corneas to -40°C and then thawing had no effect on normally hydrated or dehydrated corneas, but caused damage to swollen corneas. Freezing to -180°C and thawing resulted in permanent damage to normally hydrated corneas.

The changes in intermolecular spacing, D-period spacing, fibril diameter and fibril packing as a result of processing for TEM and SEM have been described. Low temperature embedding in Lowicryl K4M resin produced least disruption in the cornea.

The fibril diameter in cornea at normal hydration was established to be 37.4nm±1.4. X-ray data modelling indicates that fibril packing in the cornea is liquid-like, as proposed by Worthington and Inoyue (*Int. J. Macromol.* **7**: 2. 1985).

It was shown that the water in the corneal stroma is evenly distributed around the fibrils over the hydration range H=0 to H=4. Above H=4 more water is entering the stroma than can be accounted for if its distribution is uniform.

The transmittance of light through the bovine cornea (excluding interference effects), was calculated as $T \approx 12\%$. Thus, most of the transparency of the cornea must be due to constructive interference as first proposed by Maurice (*J. Physiol.* **136**: 263. 1957).

Examination of keratoconus corneas by the the SEM and TEM and showed abnormal epithelial cells, disrupted lamellae, and abnormally

arranged proteoglycans. Analysis of X-ray data proved that stromal thinning in keratoconus was not due to closer fibril packing. Also that keratoconus corneas had increased intermolecular spacing, and an abnormal arrangement of proteoglycans along the fibrils.
No differences were found between the corneal stroma of normal and myopic chicks. Myopic chick sclera was shown to have more aggrecan proteoglycan which was associated with larger empty spaces, than normal sclera. The fibril attachment sites of the proteoglycans was the same in normal and myopic sclera.

Symbols used in mathematical formulaes in this thesis.

a	The cross-sectional volume of a fibril.
c	The volume fraction of collagen in a fibril.
d	Bragg spacing.
f	The volume fraction of fibrils in the corneal stroma.
f_c	The volume fraction of collagen in the cornea at normal hydration.
f_w	The volume fraction of water in the cornea at normal hydration.
g	The volume fraction of extra-fibrillar material in the extra-fibrillar volume of the cornea at physiological hydration.
n	Order of X-ray reflection.
n_c	Refractive index of collagen.
n_f	Refractive index of the fibrils in the cornea.
n_g	Refractive index of the ground substance in the cornea.
n_p	Refractive index of extra-fibrillar material in the cornea.
n_w	Refractive index of water.
p	Volume fraction of extra-fibrillar material in the corneal stroma.
t	Thickness of the cornea.
u	The axial coordinate specifying vector lengths in fractions of a D-period.
w	Percentage weight of water in the corneal stroma at physiological hydration.
w_c	Percentage weight of collagen in the corneal stroma at physiological hydration.
w_p	Percentage weight of extra-fibrillar material in the corneal stroma at physiological hydration.
B	Disorder constant.
E	Function relating to the refractive indices of the ground substance and fibrils in the cornea.
$F(n)$	The structure factor amplitudes.
H	Hydration.
I	Transmitted intensity of light through the cornea.
I_n	Intermolecular spacing at normal hydration.
I_o	Incident intensity of light.

I_r Observed X-ray intensities.

I_v Intermolecular spacing under vacuum.

K Scaling factor.

N Number of fibrils in an aggregate.

$P(u)$ Patterson function.

R R-factor.

R_f Fibril radius at normal hydration.

D_f Fibril diameter at normal hydration.

D_v Fibril diameter under vacuum.

T The transmittance of light through the cornea.

$T(u)$ The scattered intensity function from aggregates of cylinders with short-range order.

V_f Cross-sectional volume of collagen in a fibril.

V_p Volume occupied by extra-fibrillar material in a 'unit cell' of the corneal stroma.

V_C Volume occupied by the non-aqueous component in the corneal stroma.

V_W Volume occupied by water in the corneal stroma.

γ The swelling parameter.

θ Half the scattering angle.

λ Wavelength of radiation.

μ Integrated scattering of light over all possible angles.

ρ_c Density of collagen.

ρ_d Density of the dry cornea.

ρ_p Density of extra-fibrillar material.

ρ_w Density of water.

ϱ The average axially-projected electron density along one D-period of a collagen fibril.

σ The number density of fibrils in the corneal stroma.

ϕ The phase of an X-ray reflection.

Δv The difference between the refractive indices of the fibrils and the ground substance.

Contents

List of Figures

List of Tables

Chapter 1

Introduction

This thesis is concerned with the structure of the cornea, in both normal and in diseased individuals. The investigation will centre on the size and arrangement of the collagen fibrils and the proteoglycans within the corneal stroma. The two techniques used in this study are synchrotron X-ray diffraction, and electron microscopy. X-ray diffraction allows the study of normally hydrated tissue, while electron microscopy can be used to examine a wider range of structures in the cornea, but is more prone to artifacts.

The thesis starts with a study of the changes which occur in normal corneal stroma with variations in hydration of the tissue. This is followed by an investigation of the changes occurring within the corneal stroma during processing for electron microscopy, the results from which will allow a more accurate interpretation of electron micrographs of the cornea. These first two parts of this thesis will give a comprehensive insight into the arrangement of the normal corneal stroma, and will be discussed in reference to particular theories relating to the transparency of the cornea.

This thesis is also concerned with the investigation of the corneal disease keratoconus. In addition to human keratoconus, a form of keratoconus which occurs in the chicken will also be investigated. Finally, a chapter is devoted to the investigation of the structural changes in the cornea and sclera caused by experimentally induced myopia in chickens.

1.1 Anatomy of the Eye

The cornea and sclera form the outermost layer of the eye (Figure 1.1), the two structures are continuous and together they form a tough protective coat. Internally the eye is divided by the lens and suspensory ligaments,

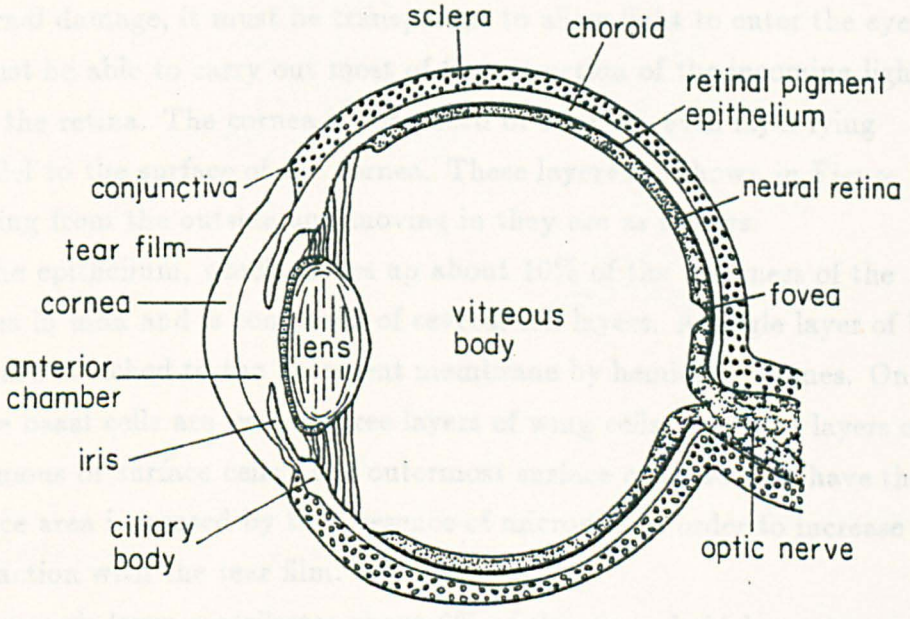

Figure 1.1 Anatomy of the eye

into two chambers. The anterior chamber is filled with aqueous humor, and the chamber posterior to the lens is filled with vitreous humor which occupies 90% of the volume of the eye. The light sensitive retina coats the inner surface of the posterior chamber, and to allow light to reach the retina, all of the components in front of the retina: the corneas, the aqueous humour, the lens, and the vitreous humour are transparent. The cornea and lens are responsible for focusing the incoming light onto the

retina. In man the air/cornea interface accounts for two thirds of the total refraction of light in the eye, while the lens is responsible for the fine adjustment of the focusing.

1.2 The Cornea

The cornea has at least three functions. It must be strong enough to withstand intraocular pressure, and tough enough to protect the eye from external damage, it must be transparent to allow light to enter the eye, and it must be able to carry out most of the refraction of the incoming light onto the retina. The cornea is composed of 5 layers, each layer lying parallel to the surface of the cornea. These layers are shown in Figure 1.2; starting from the outside and moving in they are as follows.

1. The epithelium, which makes up about 10% of the thickness of the cornea in man and is composed of several cell layers. A single layer of basal cells are attached to the basement membrane by hemidesmosomes. On top of the basal cells are two or three layers of wing cells, then two layers of squamous or surface cells. The outermost surface of these cells have their surface area increased by the presence of microvilli in order to increase their interaction with the tear film.

2.Bowman's layer contributes about 2% of the corneal thickness in man, it is an acellular layer composed of collagen. It is very resistant to mechanical deformation, and restrains the cornea anteriorly, ensuring that swelling proceeds in a posterior direction (Buckley, 1987; Kanski,1984).

3. The stroma makes up about 85% of the corneal thickness in man, it is composed of lamellae parallel to the surface of the cornea (Schwarhz 1953), and running the full width of the cornea (Maurice, 1988). It has recently been demonstrated in man (Meek et al, 1987a,b) that the lamellae are biased towards the medial-lateral and inferior-superior directions. In human cornea the stroma is composed of 200 or so of these lamellae, each of which is composed of collagen fibrils of uniform diameter and regular spacing all running in the same direction along the lamella. The fibrils of adjacent

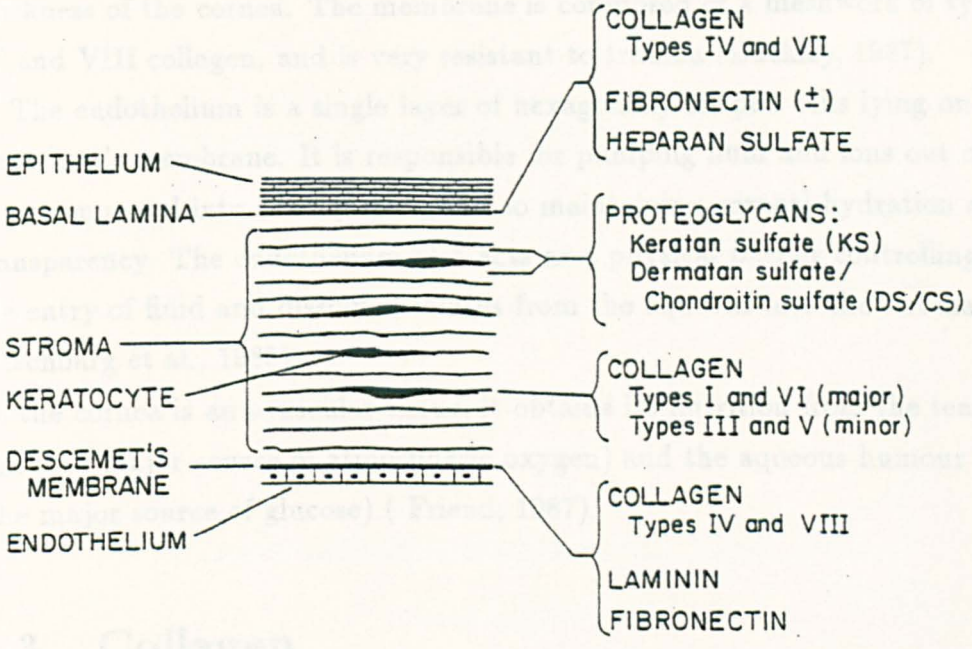

Figure 1.2 The structure of the cornea, showing both the cellular and extracellular layers

lamellae run at approximately right angles to each other. The specialized fibrocytes present in the stroma, called keratocytes, are flattened and lie parallel to the surface of the cornea, the cell processes of these cells interlace with each other.

In man 75% to 80% of the weight of the corneal stroma is due to water. When dry 90-95% of the weight of the cornea is due to collagen, the majority of which is the fibril forming type I collagen. 5% of the dry weight is attributed to glycosaminoglycans, and 1% of the dry weight is attributed to other proteins (Winterhalter, 1988).

4. Descemet's membrane is located between the stroma and the endothelial cells which are responsible at least partially for producing the membrane

(Labermeier and Kenney, 1983). It is approximately 3μm in young humans increasing to 10μm (Murphy et al., 1984), which represents about 3% of the thickness of the cornea. The membrane is composed of a meshwork of type IV and VIII collagen, and is very resistant to trauma (Buckley, 1987).
5. The endothelium is a single layer of hexagonally shaped cells lying on Descemet's membrane. It is responsible for pumping fluid and ions out of the stroma and into the aqueous, and so maintaining corneal hydration and transparency. The endothelium also acts as a physical barrier controlling the entry of fluid and dissolved solutes from the aqueous into the stroma (Fischbarg et al., 1985).
As the cornea is an avascular tissue, it obtains its nutrition from the tear film (the major source of atmospheric oxygen) and the aqueous humour (the major source of glucose) (Friend, 1987).

1.3 Collagen

Type I collagen is the most commonly occurring collagen within the corneal stroma. The cornea also contains quantities of other collagens. Type IV collagen has been found in the epithelial basement membrane in man (Nakayasu et al., 1986), and type VII collagen has been shown to have a role in epithelial adhesion (Gipson et al., 1987). Small quantities of type III and V collagen are found in the corneal stroma; these, like type I, are fibril forming collagens. The corneal stroma also contains a considerable amount of type VI collagen, possibly 30% (Winterhalter, 1988), its function in the corneal stroma is not yet clear.

The abundance of type I collagen makes it the most important collagen within the corneal stroma. It consists of three polypeptide chains each twisted into a left handed triple helix (Figure 1.3). Type I collagen is made up of two different polypeptide chains termed α1(I) and α(2), and the collagen molecule consists of one α(2) chain and two α(1) chains. All of the polypeptide chains have a molecular weight of around 100,000, and contain

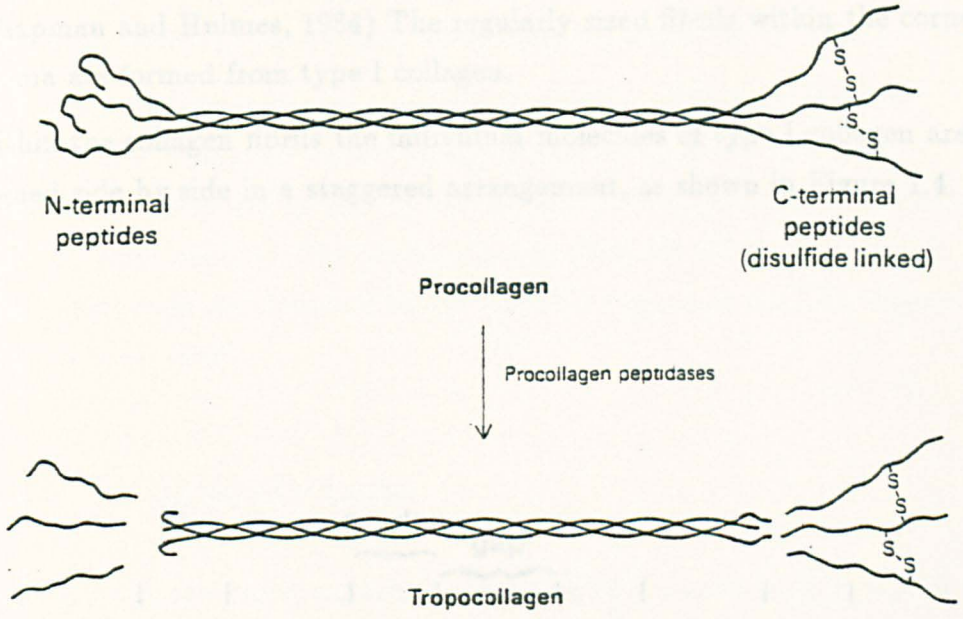

Figure 1.3 The structure of type I collagen and its precursor procollagen.

over 1000 residues. Every third residue in the polypeptide chains is glycine with the other two commonly proline and hydroxyproline, forming a 'triplet' unit. The presence of glycine allows the polypeptides to twist around each other facilitating the the formation of stabilizing hydrogen bonds which involve lysine and hydroxyproline residues (Nimni and Harkness, 1988). In both the $\alpha(1)$ and $\alpha(2)$ chains the triplet region extends for 1014 residues (i.e. 338 triplets) and is terminated by short non-triplet-containing, non-helical sequences called telopeptides, there is one at either end of the collagen molecule an N-terminal telopeptide and a C-terminal telopeptide. Both types of telopeptides contain lysine residues which are involved in the formation of intermolecular crosslinks (Parry, 1988). Evidence from the amino acid sequences of the telopeptides, and

from the staining of the collagen fibril (Chapman and Hulmes, 1984), indicate that the telopeptides are probably in a condensed form. The length of the collagen molecules including the telopeptides is ~300nm (Chapman and Hulmes, 1984) The regularly sized fibrils within the corneal stroma are formed from type I collagen.

Within the collagen fibrils the individual molecules of type I collagen are aligned side by side in a staggered arrangement, as shown in Figure 1.4.

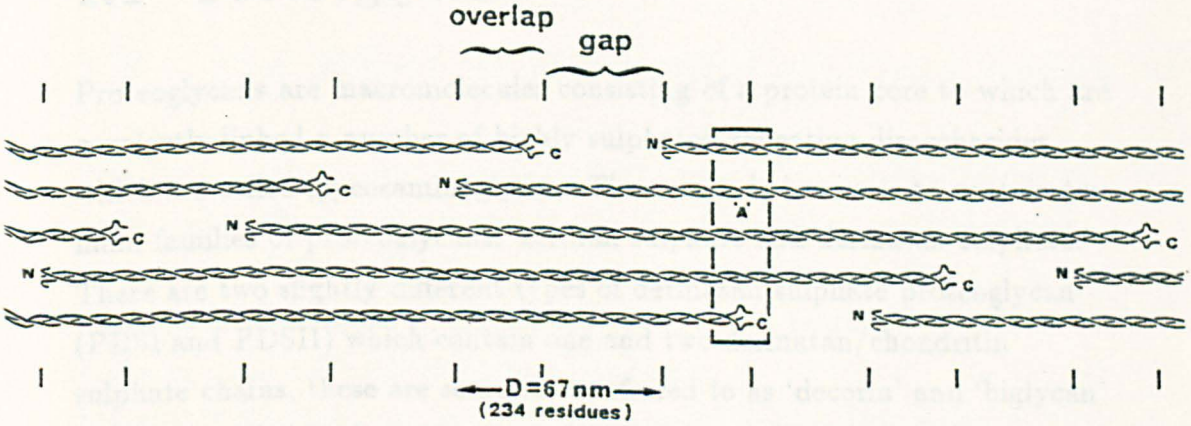

Figure 1.4 The arrangement of type I collagen molecules within a fibril showing the staggered overlap of the molecules which gives rise to the D-periodicity of the fibril. The 'A' corresponds to the 'a' band region of the collagen fibril. Taken from Chapman et al., 1990.

The stagger is approximately equal to a quarter of the length of the collagen molecule. This produces a gap/overlap pattern along the collagen fibril

causing a periodic change in electron density (Tomlin and Worthington, 1956). This is termed the D-period and has a repeat distance of 65nm in cornea as shown by low-angle X-ray diffraction on fresh cornea, and up to 64nm as determined by electron microscopy (Marchini et al., 1986).

Crosslinking between adjacent collagen molecules within the fibril is responsible for collagens tensile strength and resistance to chemical breakdown. These are formed by the joining of two hydroxylysine residues and one lysine residue. The product is a hydroxypryridinium cross-link. These cross-links are confined to the terminal regions in the D-staggered array (Stryer, 1988).

1.4 Proteoglycans

Proteoglycans are macromolecules consisting of a protein core to which are covalently linked a number of highly sulphated repeating disaccharides which are called glycosaminoglycans The cornea is known is to contain two main families of proteoglycans: keratan sulphate and dermatan sulphate. There are two slightly different types of dermatan sulphate proteoglycan (PDSI and PDSII) which contain one and two dermatan/chondritin sulphate chains, these are sometimes referred to as 'decorin' and 'biglycan' (Kjellen and Lindahl, 1991). Keratan sulphate proteoglycan sometimes, referred to as fibromodulin (Kjellen and Lindahl, 1991), is found in the cornea in two slightly different forms: PKSI and PKSII; both contain one keratan sulphate side chain with a molecular weight which can vary between 4,000 and 20,000 (Axelsson and Heinegård, 1978). It is this variation in length which is the distinguishing feature between the two types of proteoglycan.

Two types of dermatan sulphate proteoglycan have been isolated from bovine sclera (Cöster and Fransson, 1981). The large one has a molecular weight of ~160-410 kDa, and the small one a molecular weight of ~70-100 kDa. The small dermatan sulphate proteoglycan in sclera shows an

immunological identity and peptide pattern similar to those in bone, tendon and cornea (Hardingham et al., 1986). In chick sclera two types of proteoglycan are reported to occur (Rada et al., 1991). The small molecular weight proteoglycan ($M_r \approx 43,000$ kDa) is dermatan sulphate PDSI otherwise known as decorin. The second proteoglycan has a much higher molecular weight ($M_r > 1 \times 10^6$) and is the proteoglycan aggrecan which is the major proteoglycan in cartilage and consists of a ~220 kDa core (Kimura et al., 1981) to which 100-150 glycosaminoglycan chains of keratan sulphate and chondroitin sulphate are attached. Due to electrostatic repulsion of the negatively charge glycosaminoglycans, aggrecan is a highly extended molecule and serves a space filling role in cartilage by binding large amounts of water (Muir, 1982).

1.5 The Effect of Hydration on the Cornea

The start of this project involved an investigation into the changes which occur within the corneal stroma as a result of hydration, particularly its influence on the interfibrillar and intermolecular spacings within the cornea. Changes in fibril diameter and fibril spacing are of great importance in understanding the basis of stromal transparency.

Maurice (1957,1984) considered two theoretical models of stromal transparency. In the first model he proposed that the fibrils within the corneal stroma are very hydrated so that their refractive index is the same as the ground substance within the corneal stroma, giving the tissue a uniform refractive index. This theory implies that the diameter of the fibrils, 24-26nm seen under the electron microscope (Jakus,1954), is much lower than the actual diameter in the physiologically hydrated stroma.

In the second model the fibrils are arranged in a regular lattice, and the transparency results from destructive interference of the scattered light. Currently, the second model receives more support for a number of reasons:

1. It explains how large molecules readily diffuse through the stroma.
2. It explains the high structural birefringence of the stroma.

3. It explains the clouding of the stroma under stress.

It has also been demonstrated (Benedek, 1971) that transparency due to destructive interference will occur if the fibrils are arranged in a more or less orderly way rather than in a strict lattice.

Although currently, the destructive interference model receives most support, the uniform refractive index model has not been disproved. Other workers (Smith, 1969) have suggested that electron micrographs may not represent a true picture of the corneal stroma and that the fibrils might be highly swollen. More recent work using freeze-fracture techniques (Itoh et al., 1981) on rabbit corneas has indicated that the fibril diameter could be as high as ~70-80nm. This would bring the fibril surfaces into contact in the cornea, increasing the intrafibrillar volume (decreasing its refractive index), and decreasing the interfibrillar volume (increasing its refractive index). Thus, if the fibrils were as large in diameter as reported by Itoh et al., (1981) the transparency of the cornea could be explained on the basis of the uniform refractive index. Further investigation into the diameter of the fibrils under physiological conditions is obviously desirable as it will allow calculation (along with packing and interfibrillar data) of how much of the transmittance of light through the cornea is due solely to the similarity in refractive indices of the fibrils and the ground substance.

The present investigation was carried out on corneal stroma over a wide range of hydrations including physiological hydration using synchrotron X-ray diffraction in conjunction with electron microscopic techniques.

Investigation into changes in the corneal stroma with hydration was also considered desirable in order to help interpret changes occurring in pathological conditions of the cornea. This was particularly true for the disease keratoconus. Keratoconus corneas are at a different hydration from normal corneas (Sawaguchi et al., 1991), making it necessary to allow for structural changes caused by different hydrations before looking for changes which may be due to other factors, such as abnormal collagens or proteoglycans. This investigation forms the latter part of the thesis.

1.6 Changes in the Cornea caused by Electron Microscope Preparation

During preparation of corneal samples there are numerous possibilities for disruption of the stromal architecture. The processes of chemical fixation, alcohol dehydration, and resin embedding have been shown to have adverse effects on the size and structure of biological tissues, as reviewed in Hayat (1989). Knowledge of the changes occurring during the processing of the cornea for electron microscopy are critical for meaningful interpretation of electron micrographs. This is particularly important since electron micrographs have been used as the basis for theories about the transparency of the cornea, when even minor changes in fibril diameter or in the packing arrangement of the fibrils are critical. The aim of this part of the project was to monitor, stage by stage, the changes in fibril size and arrangement in the corneal stroma which occur during processing for electron microscopy. This was carried out by using the very intense synchrotron X-ray beam at Daresbury which allowed monitoring of interfibrillar spacing, intermolecular spacing, and fibril packing through all stages of electron microscope processing, from a fresh cornea to one which is embedded in polymerized resin. The investigation was carried out for preparation of specimens both for transmission electron microscopy (TEM) and for scanning electron microscopy (SEM).

The use of different preparation regimes, and their effect on the final appearance of the sample under the electron microscope was also assessed.

1.6.1 Determination of Fibril Diameter

Accurate determination of the fibril diameter in the corneal stroma at physiological hydration is a surprisingly difficult thing to achieve. Estimates of the value vary depending on the technique used to determine it. Use of conventional TEM techniques has produced a wide variety of

fibril diameters even for the same species. The diameter of fibrils in rabbit cornea has been reported as 20nm (Cox et al., 1970), 25.5nm (Craig and Parry, 1981), and 30nm (Girauld et al., 1975). Using low temperature embedding techniques Craig et al., (1987) reported fibril diameters larger than previously observed, giving a mean diameter of about 37nm for bovine corneas. Freeze fracture techniques have also been used on cornea in an attempt to determine the fibril diameter, and have also produced conflicting results. Itoh et al., (1981), using a freeze-fracture and etching technique on rabbit corneas has reported fibrils with a diameter of 78nm. Hirsch et al., (1989) using a fast-freeze, deep-etch, rotary shadowing technique, and again working on rabbit cornea, reported fibril diameters of approximately 35nm. Low-angle X-ray diffraction data on bovine cornea analysed by Sayers et al., (1982) gave a fibril diameter of either 40nm or 52nm at physiological hydration depending on the kind of modelling used to interpret the data. Worthington and Inouye (1984) using similar techniques gave a fibril diameter of 39nm for bovine corneas. Potentially, X-ray diffraction should give the most reliable results on fibril diameter since the data are obtained from a fresh untreated specimen, however although the results obtained are consistent, they are open to several possible interpretations. The intention during this thesis was to use several techniques in order to determine the fibril diameter in bovine corneas including specialized preparation procedures for TEM, and the fitting of various models to the X-ray data.

The accurate determination of fibril diameter is of great importance in determining what percentage of the transparency of the cornea is the result of the uniform refractive index theory. If the diameter of the fibrils is in the region reported by Itoh et al., (1981) the uniform refractive index theory could wholly account for the transparency of the cornea. If the fibril diameter is about 50nm or less, most of the transparency is due to destructive interference.

1.7 Keratoconus

A major part of this project is an investigation of the disease keratoconus in humans. Keratoconus is a disorder characterised by the slow development of a non-inflammatory ectasia (bulge) of the cornea. The ectasia occurs on the axial or periaxial region of the cornea and is usually conical in form, and the disease is almost always bilateral. Figure 1.5 shows an advanced case of keratoconus.

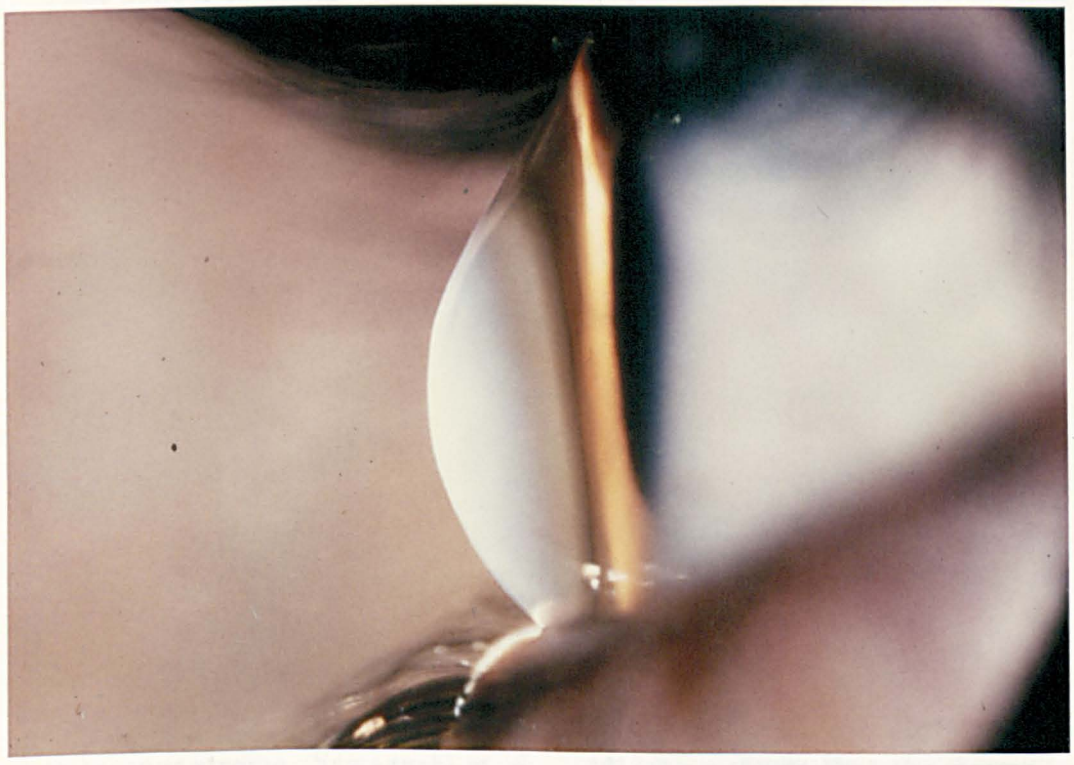

Figure 1.5 An advanced case of keratoconus showing the buldging of the cornea.

Keratoconus is usually detected in the early teens (Nakayasu et al., 1981), progresses at variable rates over the next 10-20 years and can result in visual impairment ranging from mild irregular astigmatism to severe thinning and scarring of the cornea requiring keratoplasty (Krachmer et al.,

1984). Most estimates of the frequency of keratoconus are in the range 4-230 per 100,000 individuals (Krachmer et al., 1984).

The abnormalities in the ultrastructure of keratoconus corneas are well established. Bowman's layer often has breaks in it and is of irregular appearance, the epithelium varies in thickness and has an abnormal basement membrane (Polack, 1976); the destruction of the basement membrane frequently occurs (Newsome et al., 1981). In the stroma there appears to be a reduction in the number of lamellae (Pouliquen et al., 1970) and the lamellae which remain are often formed into Z-shaped folds. There do not appear to be any major differences in collagen types between normal and keratoconus corneas (Nakayasu et al., 1986), although there is evidence for lower levels of collagen in keratoconus corneas (Ihalainen et al., 1986). Cannon and Foster (1978) reported higher levels of lysinonorleucine cross-links in collagen from keratoconus corneas.

Investigations into differences in proteoglycans and glycosaminoglycans between normal and keratoconus corneas have produced a variety of conflicting results. One study has shown a higher hexosamine concentration in keratoconus corneas (Buddecke et al., 1966), while later work (Anseth, 1969) revealed no differences in hexosamine concentration between normal and keratoconus corneas. A recent study has shown high levels of polyanions including glycosaminoglycans in keratoconus corneas (Yue et al., 1988). Funderburgh et al., (1989) have suggested that keratoconus corneas contain an abnormal form of keratan sulphate proteoglycan. This abnormal arrangement appears to be separate from the scarred regions of the keratoconus stroma. Sawaguchi et al., (1991) have shown that the stroma of keratoconus corneas contains increased levels of dermatan sulphate proteoglycan and decreased levels of keratan sulphate proteoglycan compared to normal.

1.7.1 Chicken Keratoconus

Keratoconus has also been reported to occur in the chicken (Whitley et al., 1986). The clinical details of the disease found in the chicken bears a strong resemblance to that reported in humans. The present investigation into human keratoconus is accompanied by a study into the form that the disease takes in chickens. It was hoped that, if the two diseases were similar, the chicken keratoconus could be used to study the early stages of the disease. In humans keratoconus corneal samples are only available when the disease is at a late stage and corneal scarring has started to occur.

Chicken keratoconus is characterised by mild to severe conical protrusion of the corneas with an associated increase in anterior chamber depth. It becomes recognizable at 5 weeks of age, it is bilateral, but by the age of 5 months the bulging of the cornea may be more severe in one eye compared to the other. Ultrastructurally, Bowman's layer is of an irregular thickness, and 'Z' shaped folds are present in the stroma. Descemet's membrane is intact but much thinner than in normal corneas.

1.8 Myopia

This thesis also includes an investigation into myopia, specifically the changes occurring in the cornea and sclera during the development of the condition. In humans myopia is usually associated with increased length of the vitreous chamber (Gernet, 1981; Hosaka, 1988). In chicks, an increase in vitreous chamber length leading to myopia can be induced by partial-field deprivation (Wallman et al., 1978). In chicks there is also an associated increase in corneal curvature. This part of the thesis describes the results of a structural investigation into the collagen and proteoglycans in the cornea and sclera of control and visual-field deprived myopic chicks.

A number of theories have been proposed to account for the increase in vitreous chamber length. One suggestion is that increased intra-ocular

pressure could cause the sclera to stretch passively thus increasing the vitreous chamber size. However, Perkins (1981) failed to find any consistent increase in intra-ocular pressure in humans with myopia. Abnormalities in the appearance of the sclera of humans with high myopia (Curtin et al., 1979) has lead to suggestions that the sclera of myopic individuals is somehow weakened leading to stretching of the sclera under normal intra-ocular pressure. Findings by Raviola and Wiesel (1985) which showed that scleral thinning was associated with myopia in monkeys, and by Curtin and Teng (1957) who reported scleral thinning in humans with high myopia, suggests that some form of stretching may take place. In chicks the development of partial field myopia is not associated with overall thinning of the sclera. However, in chicks the sclera is divided up into an inner cartilaginous layer and an outer fibrous layer. Gottlieb et al., (1990) report that in myopic eyes the cartilaginous layer becomes thicker while the fibrous layer becomes thinner, which again suggests the possibility of stretching of the fibrous sclera.

Recently Christensen and Wallman (1991) have shown that in myopic chicks there is an increase in scleral dry weight as well as increases in DNA synthesis and soluble protein content. There is also a higher level of hydration in myopic chick scleras which suggests that the increase in anterior chamber length is not a passive process.

Recent, work (Rada et al., 1991) has shown that the myopic chick sclera contains slightly increased levels of the small proteoglycan decorin, and greatly increased levels of the proteoglycan aggrecan, compared to controls. The workers propose that the increased levels of aggrecan result in increased hydration of the myopic sclera leading to ocular enlargement.

In this investigation synchrotron X-ray diffraction has been used to study the interfibrillar and intermolecular spacing of collagen in cornea and sclera from control and myopic chicks. Also, the 'critical electrolyte' technique of staining proteoglycans developed by Scott and Orford (1981) was employed to look at the number and distribution of proteoglycans in normal and

myopic chick cornea and sclera. Using these methods, the differences in the structure or distribution of collagen and proteoglycans in cornea and sclera between normal and myopic chicks was demonstrated.

1.9 X-ray Diffraction

The use of synchrotron X-ray diffraction has been central to this thesis. Much of the work carried out has been possible only because of the very high intensity of the synchrotron X-ray beam, and would be impossible using a conventional laboratory based X-ray set.

1.9.1 The Production of Synchrotron X-rays

All of the experimental work involving synchrotron X-rays has been carried out at Daresbury Synchrotron Radiation Source, one of the largest, and for low and high-angle non-crystalline diffraction, probably the best in the world.

To produce synchrotron radiation at Daresbury, electrons are accelerated to 2GeV (99.999997% of the speed of light) by a linear accelerator and injected into the synchrotron ring, a quasi-circular 100m orbit in which the electron beam is constrained by magnets. Whenever the electron beam is bent by the magnetic fields holding the electron beam in its orbit, then synchrotron radiation is emitted tangentially to the ring. The emitted synchrotron radiation is collected along beamlines, and because the spectrum of the synchrotron radiation is continuous from X-rays to the infra-red regions, the wavelength of interest can be isolated by the use of various optical components (eg. mirrors, gratings, monochromators etc.), to give a high intensity focussed beam of a specific wavelength.

1.10 X-ray Diffraction of Cornea and Sclera

X-ray diffraction can be used to study tissues in their normal hydrated state, it is a non-invasive technique that can provide valuable structural information as long as there is a sufficient order within the tissue. It has several advantages over conventional techniques such as electron microscopy, the most obvious of which is the fact that it is possible to carry out X-ray diffraction at normal physiological hydration without the need for fixation, dehydration, embedding, etc, all of which are known to produce artifacts within the tissue. A less obvious advantage, is that an X-ray pattern from a tissue represents an average of the whole thickness of the sample. In the case of electron microscopy typically the area examined is a few hundred μm^2 of the sample.

X-ray diffraction patterns from collagen have several different components (Figure 1.6). There are the sharp meridional reflections which result from the axial changes in electron density caused by the D-periodicity along the collagen fibril. There are also the more diffuse reflections termed equatorial reflections which are caused by diffraction between the fibrils themselves (interfibrillar spacing) or between the laterally packed collagen molecules within the fibril (intermolecular spacing).

1.10.1 Equatorial X-ray Diffraction of Cornea

The low-angle equatorial X-ray pattern from the cornea (which has short-range order) is a scattering intensity profile ($I(kR_f)$), and has two components. These are the scattering intensity resulting from the packing of the fibrils in stroma (packing scattering curve or interference function), and scattering intensity curve resulting from the fibrils themselves (fibril transform).

The scattering intensity profile from the whole cornea ($I(kR_f)$) is therefore given as the product as two functions. $F(kR_f)$ which is the normalized intensity for a single collagen fibril (fibril transform), and $T(2\gamma kR_f)$ which

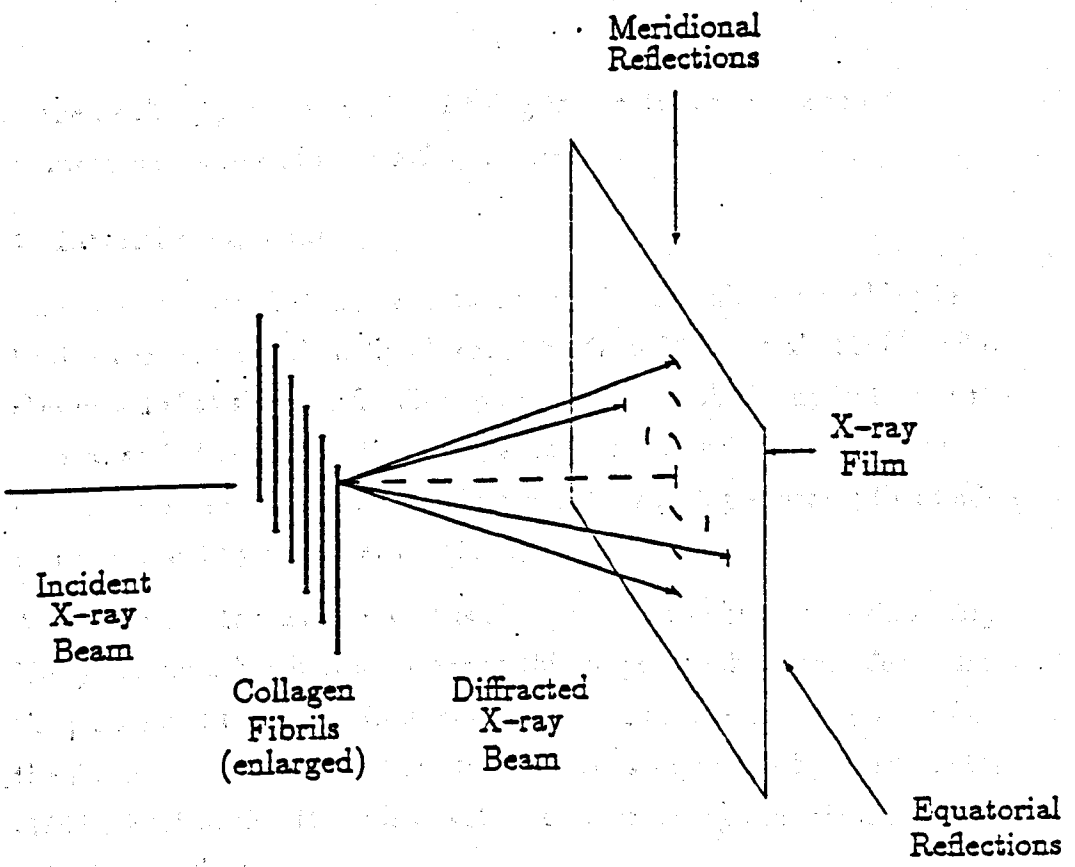

Figure 1.6 X-ray diffraction patterns from a single lamella showing the equatorial and meridional reflections. In a whole cornea the reflections shown would be circular as the 200 or so lamellae in the cornea are all orientated at different angles within the plane of the cornea.

is the normalized interference function that describes the packing of the fibrils. Thus,

$$I(kR_f) = F^2(kR_f)\, T(2\gamma kR_f),$$

where

$$k = \frac{4\pi}{\lambda} \sin\theta,$$

2θ is the scattering angle, λ is the wavelength of the incident X-ray beam, R_f is the collagen fibril radius, and

$$\gamma = \frac{d}{2R_f}$$

is the swelling parameter with d being the centre to centre separation between nearest-neighbour collagen fibrils.

1. Interfibrillar spacing

The first equatorial Bragg reflection from the interfibrillar packing in bovine cornea was originally observed by Goodfellow et al., (1978), who also noted that the interfibrillar spacing varied with the hydration of the cornea, and showed that there was a linear relationship between the hydration of the cornea and the interfibrillar spacing squared; this finding was confirmed by Sayers et al. (1982).

As well as the 1st maximum, it is also possible to obtain two subsidiary X-ray maxima, but it is not clear at this stage whether these derive from the packing of the fibrils (Sayers et al, 1982), or whether they arise from the fibrils themselves (the fibril transform) as suggested by Worthington (1985). Part of this thesis is devoted to determining the origin of these subsidiary reflections.

It is impossible to obtain an X-ray pattern deriving from the interfibrillar spacing in the sclera. This is is because of the large variation in size of the collagen fibrils in the sclera.

2. Intermolecular spacing

Equatorial reflections can also be obtained from the lateral packing of the collagen molecules within the fibrils. Hertel (1933) carried out a limited investigation at various tissue hydrations and was able to identify rings which corresponded to the X-ray pattern of the collagen molecule (Ramachandran, 1967). However, Hertel (1933) froze his specimens to liquid air temperatures which probably produced artifacts. Adler et al., (1949) outlined results which are apparently similar to those of Hertel (1933) but in less detail. Agarwal et al., (1972) investigated dry cornea but were unable to study hydrated tissue because to their experimental setup. Most recently Cooke et al, (1987) carried out the first high-angle investigation of bovine cornea over a range of hydrations, using a

conventional laboratory based X-ray source. Part of this thesis invloves repeating the work of Cooke et al, (1987) on bovine cornea. By using a synchrotron X-ray source, and the equilibration technique described in Chapter 2 to change the hydration of the corneas, it was possible to obtain data of a higher quality than can be obtained using a conventional X-ray set.

1.10.2 Meridional reflections

Meridional reflections arise from the axial electron density profile of the collagen. Measurement of these reflection allows the length of the D-period to be calculated, which is 65nm in cornea. Maurice (1957) was the first worker to observe a meridional X-ray diffraction pattern from cornea, this proved to contain the 3rd and 5th order reflections. More recently Meek et al., (1983) have related the meridional reflections from human cornea to the axial distribution of electron density along the fibrils.

The average axially-projected electron density (above water background) along one D-period of the collagen fibril may be expressed as

$$\varrho(u) = \sum_n F(n) \exp(i\phi(n) - 2\pi n u),$$

where u is the axial coordinate specifying vector lengths in fractions of the D-period. $F(n)$ are the structure factor amplitudes taken as the positive square roots of the observed intensities, n is the order of diffraction and ϕ are the phases. To obtain the phases for just one sample would involve a considerable investment in time (several months) spent collecting experimental data and analysing it, and is beyond the scope of this thesis. Fortunately, it is possible to derive considerable information about the axial electron density on the collagen fibril without knowing the relevant phases. The relative frequency of occurrence of intraperiod electron density vectors (axial spacings between areas of electron density), can be calculated from the measured meridional intensities by means of a Patterson function which is defined by:

$$P(u) = \sum_{n} I_r(n) cos 2\pi n u$$

where $I_r(n)$ are the observed intensities.

1.11 Electron Microscopy

Electron microscopy has been the second main technique used in this investigation. Although the processing procedures necessary for electron microscopy mean that interpretation of micrographs must always be carried out with care, very detailed information can be obtained, and unlike X-ray diffraction the structures studied need not be ordered.

1.11.1 Transmission Electron Microscopy

Conventional TEM was used to investigate the arrangement of the collagen fibrils in normal and diseased corneas under a variety of conditions. When collagen fibrils are stained with heavy salts they exhibit a typical banding pattern caused by the attachment of the heavy metal ions to specific charged amino acid residues (Hodge and Schmitt, 1960). This characteristic staining pattern repeats every D-period. Figure 1.7 shows the staining pattern from a collagen fibril after staining with phosphotungstic acid and uranyl acetate.

The TEM was also used extensively during this project to investigate the arrangement of proteoglycans in the corneal stroma in normal and in diseased tissue. It is normally impossible to visualize proteoglycans under the TEM as their electron density is very low. However they can be stained with the electron opaque dyes cuprolinic blue and cupromeronic blue, both of which are cationic copper based dyes (Scott, 1980; Scott et al., 1981). These two dyes are virtually identical, the only difference being that cupromeronic blue is thought to have a slightly higher specificity, and

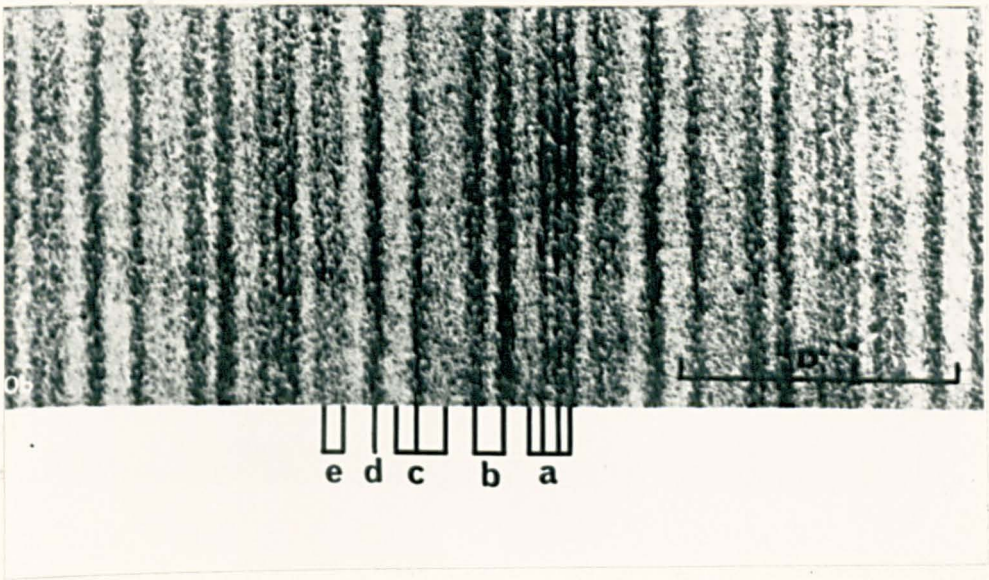

Figure 1.7 The staining pattern of a collagen fibril. The fibril was stained with phosphotungstic acid and uranyl acetate. The notation of the bands is from Hodge and Schmitt 1960. Reproduced from Chapman and Hulmes (1984)

appears to produce finer filaments under the electron microscope. Using these dyes and controlling the concentration of electrolyte ($MgCl_2$) in the solution it is possible to stain the proteoglycans within the corneal stroma. The concentration of the electrolyte influences the extent to which the stain is taken up by the polyanionic glycosaminoglycans on the proteoglycans. If there is an excess of electrolyte the Cl^- ions compete with the anions on the glycosaminoglycans for the attention of the dye. Thus, for optimum staining the electrolyte concentration is critical. Cuprolinic and cupromeronic blue stain the sulphate glycosaminoglycans in the cornea, and the contrast of the dye is further enhanced by attaching tungstate ions to

the dye after it has complexed with the proteoglycans (Scott, 1980).

1.11.2 Scanning Electron Microscopy

SEM was used in this investigation to examine normal corneas under a variety of conditions and also diseased corneas. The SEM proved to be especially useful in the examination of the epithelial surface, and also cross-sections through the corneal stroma. Although the resolution of SEM is low compared to TEM, SEM is far superior for the examination of surface features where its tremendous depth of field, and wide field of view allows large areas of samples to be quickly and comprehensively examined.

Chapter 2

Materials and Methods

2.1 Samples

2.1.1 Bovine corneas

Fresh bovine corneas were obtained immediately after death from the local abattoir. Because these bovine corneas were readily available every day it was possible to use fresh samples in all of the experiments involving bovine corneas.

2.1.2 Human corneas

Keratoconus corneas were obtained from patients who had undergone penetrating keratoplasty. The buttons were obtained a few minutes after surgery, immediately wrapped in clingfilm and stored at -40°C until required. Previous studies had indicated that the freezing process (K.M.Meek, personal communication) has no effect on the inter or intrafibrillar spacings of the corneal stroma, and this was confirmed during this thesis investigation. The majority of normal human corneas were obtained from the Bristol Eye Bank; these were corneas normal in every respect except that they had endothelial cell counts which were too low to allow the corneas to be used for grafting. These corneas had been stored in

	Keratoconus		Normal	
Experiments	No. of patients	Age at surgery	No. of donors	Age of donors
Interfibrillar (H=1-11)	15 f	28.5±6.4	15 c	39.6±27.6
Fig 5.10, Tab 5.1		21-39		1-84
Intermolecular (H=1-11)	15 f	28.5±6.4	30 c	45.1±30.6
Fig 5.12, Tab 5.1		21-39		1-87
Interfibrillar (H=2.4)	13 f	26.2±7.0	20 c	52.1±24.6
Tab 5.2		21-37		4-92
Intermolecular (H=2.4)	16 f	28.8±7.2	23 c	51.3±23.4
Tab 5.2		21-45		4-92
Interfibrillar (H=3.2)	As Row 1	As Row 1	4 f	59±30
Tab 5.3				25-93
Intermolecular (H=3.2)	8 f	35.6±8.2	8 f	77±11.36
Tab 5.3		26-45		55-85
Patterson (H=3.2)	2 f	30, 37	2 f	41,~50
Fig 5.13, Fig 5.14				
Tab 5.4, Tab 5.5				

Table 2.1 Showing the clinical details of donors of keratoconus and normal human corneas used in this investigation. f Control corneas stored frozen. c Control corneas stored in culture medium. H=hydration. Tab. and Fig. refer to the Tables and Figures which summarize the results which have been obtained from the listed specimens.

culture medium (MEM + 2% FCS) for several weeks at 4°C and so had a range of hydrations. Other control human corneas were obtained a few hours after death directly from individuals with no history of ocular disease, and were stored wrapped in clingfilm at -40°C. These controls were at normal physiological hydration.

A summary of the clinical details of the keratoconus and control corneas used in the various experiments can be seen in Table 2.1.

2.1.3 Chicken Keratoconus

The chicken keratoconus and normal chicken eyes were supplied by Dr.R.D.Whitley, (University of Florida, Florida, USA). The chickens (*Gallus gallus domesticus*) were all between 8 and 11 months, by which age the disease had reached its most advanced stage. All of the corneas were immediately frozen after death, and the samples stored at -40°C until required.

2.1.4 Chicken Myopia

Myopic, 6 week old chick (*Gallus gallus domesticus*) eyes were supplied by Dr.D.Troilo (Dept of Physiology, Oxford University.). The myopia in the chicks was induced in one eye only by the use of a hemispherical form occuluder as described in Wallman et al (1978), the other eye was untreated and used as a control. The induction of myopia was carried out by Dr D. Troilo. All of the eyes were immediately frozen at death, and stored at -40°C until required.

2.2 Hydration

The state of hydration of a cornea was calculated according to the equation:

$$H = \frac{wet\ weight - dry\ weight}{dry\ weight}$$

With human specimens the hydration of many corneas varied considerably depending on such factors as how soon after the operation the surgeon wrapped and stored the cornea, and whether the removed cornea was bathed in saline during the operation. When direct comparison between normal and keratoconus corneas at a specific hydration was desirable, an equilibration technique was used. Equilibration was carried out by placing the corneas in 14 kDa cut-off dialysis tubing and leaving them for 5 days at 4°C in a solution of 2% polyethylene glycol (20 kDa) containing 0.15M

NaCl. This resulted in the corneas being equilibrated to a level slightly below physiological hydration.

In the instances where a range of hydrations was required, as during the investigation of the effect of hydration on intermolecular and interfibrillar spacings in the corneal stroma, the percentage of the polyethylene glycol in the equilibrating solution was adjusted between 0% to 25% to produce a range of hydrations from H=10 to H=0.5.

2.3 X-ray Diffraction

X-ray diffraction patterns were recorded at the SERC synchrotron source at Daresbury U.K. When possible, corneas were weighed before and after X-ray exposure in order to determine their hydration. During exposure the corneas were held in air-tight cells and the X-ray beam was directed along the optical axis. Sometimes special cells were used. During the investigation to determine fibril diameter at physiological hydration, it was necessary to design and build a cell which allowed an X-ray pattern to be obtained from a cornea under vacuum.

The X-ray patterns were recorded on Caeverken AB film (Caeverken, Strängnäss, Sweden). Normally, two sheets of film were placed in each cassette allowing more latitude with the length of exposure. The exposed X-ray films were scanned using an Ultrascan XL laser microdensitometer (LKB instruments Inc., Gaithersburg, MD) and background scatter was subtracted from the trace before measurements were made.

2.3.1 Analysis of X-ray Patterns

The basis behind the analysis of X-ray patterns is encapsulated in Bragg's equation:

$$n\lambda = 2dsin\theta$$

where n is the order of the reflection, λ is the wavelength of the radiation and the angle θ shown in Figure 2.1 is half the scattering angle, d is the Bragg spacing, and n refers to the order of the reflection.

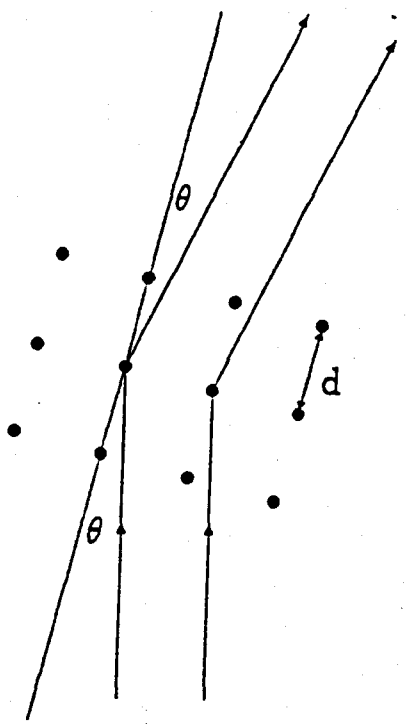

Figure 2.1 Schematic diagram of X-ray diffraction from a perfect lattice showing the derivation of θ and d in Bragg's equation.

Figure 2.2 shows the arrangement of the camera for X-ray diffraction experiments. The specimen-to-film distance can be obtained very accurately by using a calibration specimen of known spacing. Calcite

(d=0.305nm) was used for high-angle work and rat-tail tendon (d=67nm) for low-angle work. Since λ is known and d is known for the calibration specimen, then by using Bragg's equation (for n=1), θ can be obtained; then by measuring the radius of the X-ray pattern, the specimen-to-film distance can be calculated. Once the specimen-to-film distance is accurately known, θ can be obtained by measuring the diameter of X-ray. patterns from unknown specimens, which in turn allows d the Bragg spacing to be obtained for the specimen.

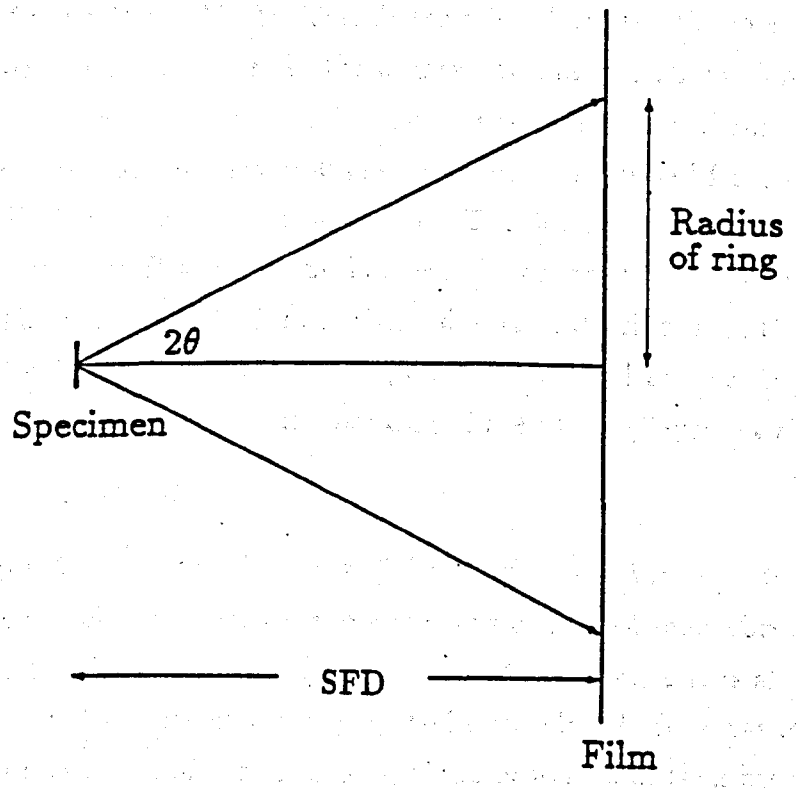

Figure 2.2 Schematic diagram of the X-ray camera arrangements

2.3.2 Low-Angle Pattern

Equatorial Pattern

X-ray patterns arising from the packing of the fibrils were obtained on a low-angle camera on station 8.2 at the Daresbury synchrotron. The beam dimensions were 4 x 0.5mm the wavelength was 0.1540nm, and the specimen to film distance was between 2.5 and 4 m; 90% of this distance was vacuum in order to minimize air scatter. Measurement of the first order diffraction ring from the packing of the collagen fibrils within the corneal stroma allows the first-order Bragg spacing to be obtained. The Bragg spacing is increased by a factor of 1.12 to give the mean centre-to-centre spacing of the collagen fibrils. This factor arises from the the most probable packing arrangement present in the corneal stroma (see Discussion). A typical low angle pattern from a bovine cornea is shown in Figure 2.3, the two diffuse rings at spacings of 40nm and 25nm are derived from the collagen fibrils within the corneal stroma. The 40nm ring is the first order reflection from the Bragg spacing between the collagen fibrils within the stroma. The reflection at 25nm is either due to scattering from the individual cylindrical collagen fibrils (Worthington and Inouye, 1985), or from further reflections from the packing of the fibrils (Sayers et al., 1982).

Meridional Pattern

The sharp reflections seen in Figure 2.3 are reflections resulting from the distribution of electron density along the axis of the collagen fibril (the D-periodicity). Measurement of the spacing of these reflections allows the D-periodicity of a particular specimen to be calculated. By measuring the integrated intensities of several orders of the pattern and then by using Patterson functions it is possible to calculate the electron density vectors within the D-period (these are the axial spacings between areas of high electron density). If the proteoglycans attached to the collagen fibrils within the corneal stroma are stained with an electron-dense dye (cupromeronic blue), then some of the electron density within the D-period

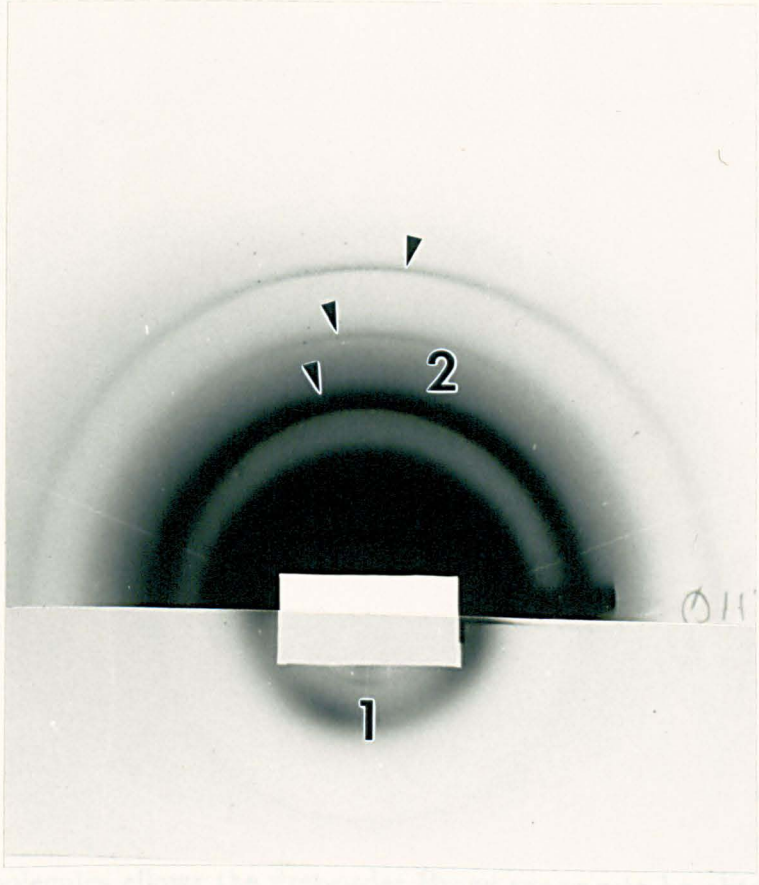

Figure 2.3 Low-angle pattern of fresh bovine cornea showing the meridional and equatorial reflections. The lower half of the figure is the result of a 2 minute exposure, while the upper half is a 30 minute exposure of the same cornea. The meridional reflections are indicated by arrows, and are (inner to outer) the 3rd, 4th, and 5th orders derived from the 65 nm D-periodicity. The 1st (Bragg spacing ~40 nm) and 2nd (Bragg spacing ~25 nm) equatorial reflections are indicated by numbers.

is due to the stained proteoglycans. The electron density vectors demonstrated in a Patterson function calculated from a cupromeronic stained cornea contain a contribution from the frequency and distribution of proteoglycans attached along the D-period of the fibrils.

The cupromeronic blue staining of the proteoglycans in the corneal stroma was carried out by Prof. J.E. Scott (Manchester University) as follows. The specimens were stained overnight in 2.5% glutaraldehyde, 0.1M MgCl in 25mM sodium acetate buffer (pH 5.7) containing 0.5% cupromeronic blue. The electron density of the cupromeronic blue-stained proteoglycans is then further enhanced by three 15 minute washes in 0.5% aqueous sodium tungstate.

2.3.3 High-Angle Pattern

X-ray patterns from the lateral packing of the molecules within the collagen fibrils were obtained on a high-angle camera at station 7.2 at the Daresbury synchrotron. The beam was 0.5mm in diameter with a wavelength of 0.1488nm. The specimen-to-film distance was between 11cm and 12cm; most of this space was filled with helium to minimize air scattering. Measurement of the first-order diffraction ring from the packing of the collagen molecules allows the first-order Bragg spacing to be obtained.

Since it has proved possible to obtain only a first order reflection from the equatorial packing of the molecules in cornea, it is clear that the arrangement of the collagen molecules in cornea is non-crystaline, so there is no lattice from which to directly determine intermolecular distances. The shape of the first order reflection from corneal collagen is very similar to the first order reflection from cartilage collagen (Maroudas et al., 1991), which also only produces a first order reflection. This suggests that the collagen arrangement within the fibrils is similar in cartilage and cornea. Maroudas et al., (1991) report that the type of intermolecular arrangement in cartilage collagen fibrils is the so called 'pseudo-hexagonal' arrangement,

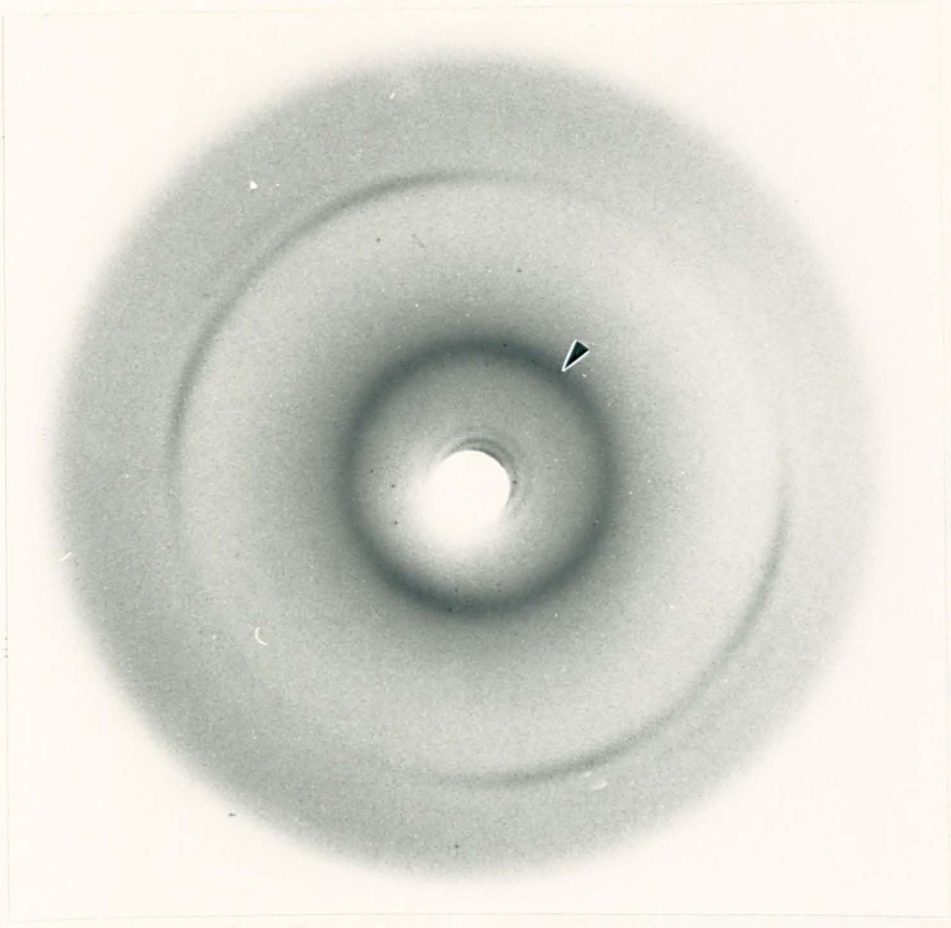

Figure 2.4 Showing the high-angle pattern from bovine cornea. The 1st order reflection is indicated by an arrow and corresponds to a Bragg spacing of ~1.40 nm, the outer ring derives from the mylar window of the X-ray cell.

which is related to the Bragg spacing (d) by the equation

$$I_n = d \times 1.11,$$

where I_n is the intermolecular spacing. It seems that the most probable arrangement of the collagen molecules in cornea is also 'pseudo-hexagonal', consequently the Bragg spacings were increased by the factor 1.11 to obtain the mean centre-to-centre intermolecular spacing in the cornea. The resultant high-angle pattern from a bovine cornea can be seen in Figure 2.4.

2.4 Electron Microscopy

2.4.1 Transmission Electron Microscopy

TEM was used to give detailed information about the arrangement of the fibrils within the corneal stroma, in addition, by using specialized staining techniques it was possible to visualize the proteoglycans within the corneal stroma.

Proteoglycans were stained using the 'critical electrolyte' method of Scott and Orford (1981). Small ($0.5mm^2$) pieces of cornea were stained overnight in 0.05% cuprolinic blue containing 2.5% glutaraldehyde and 0.1M $MgCl_2$ in 25mM sodium acetate buffer pH 5.7. The samples were then rinsed three times (15 minutes each time) in the buffer solution containing glutaraldehyde and $MgCl_2$. After which the samples were stained 'en bloc' in three changes of 0.5% aqueous sodium tungstate. This was followed by a conventional ethanol dehydration, and two 30 minute changes in propylene oxide. The specimens were then transferred to a 3:1 propylene oxide/Polarbed resin mixture overnight, the top was left off the sample tube allowing the propylene oxide to slowly evaporate out of the mixture. The samples were then transferred to 100% Polarbed resin for 12 hrs before being polymerized at 60°C for 24 hrs. Gold or silver sections were cut from the specimen blocks using a Reichert Ultracut E, and stained with aqueous uranyl acetate before being examined with a Philips 301 TEM.

2.4.2 Scanning Electron Microscopy

SEM was used chiefly to examine the surface of corneal epithelium and endothelium, as well as looking at the gross morphology of the stroma. Samples for SEM were fixed in 4% glutaraldehyde in 0.1M sodium cacodylate buffer overnight, then washed for 3 × 15 minutes in 0.1M sodium cacodylate before being postfixed in 2% osmium tetroxide for 2 hours. The samples were then dehydrated in an alcohol series before being

transferred to 100% acetone and critical point dried in a Polaron 'Jumbo' critical point dryer. The processed samples were then mounted on stubs and gold-coated for examination with a JEOL 820 SEM.

2.5 X-Ray Diffraction Studies of Electron Microscope Processing

This section details the processing runs which were monitored using synchrotron X-ray diffraction techniques. Low-angle equatorial and meridional, and high-angle equatorial patterns were taken throughout processing in between the main processing stages.

Fresh bovine corneas were used for this series of experiments.

2.5.1 X-ray Diffraction Studies of Processing for Transmission Electron Microscopy

TEM Processing Run 1:

The corneas were fixed at room temperature in 2.5% glutaraldehyde in 0.1M phosphate buffer at pH 7.2 overnight, followed by 3 × 10 minute washes in 0.1M phosphate buffer at pH 7.2. The samples were then postfixed for 1.5 hours in 1.5% osmium tetroxide, followed by 3 × 10 minute washes in 0.1M phosphate buffer at pH 7.2. This was followed by a dehydration run of 30 minute steps in 50%, 70%, 85%, 95%, 100%, and 100% ethanol. The samples were then placed in propylene oxide for 2 × 30 minutes before being transferred to a mixture of 25% Polarbed resin and 75% propylene oxide in which they were left for 12 hours at which time all of the propylene oxide had evaporated from the mixture. The samples were then transferred to fresh resin and left a further 12 hours before being placed in moulds and polymerized at 60°C for 36 hours.
X-ray diffraction patterns were obtained at the end of the following steps:

1. Glutaraldehyde fixation.
2. Osmium tetroxide post-fixation.
3. Ethanol dehydration.
4. Resin infiltration.
5. Resin polymerization.

The polymerized samples were also sectioned, stained and examined under the TEM to determine fibril diameter and fibril arrangement.

TEM Processing Run 2.

This run is exactly the same as TEM run 1 except that the postfixation step in 1.5% osmium tetroxide was omitted.

X-ray diffraction patterns were obtained at the end of the following steps:

1. Glutaraldehyde fixation.
2. Ethanol dehydration.
3. Resin infiltration.
4. Resin polymerization.

The polymerized samples were also sectioned, stained and examined under the TEM to determine fibril diameter and fibril arrangement.

TEM Processing Run 3.

Processing run TEM 3 was designed to investigate the effects of different embedding resins. Four different resins were used: Polarbed, Lowicryl, L.R. White, and Nanoplast. Table 2.2 gives details of the properties and suppliers of these resins.

Resin	Water tolerance	Supplier
Polarbed (epoxy)	Zero tolerance	Biorad Ltd, U.K.
Lowicryl (methyacrylate)	~1% tolerance	Agar Scientific, U.K.
L.R. White (acrylic)	~12% tolerance	Agar Scientific, U.K.
Nanoplast (melamine)	100% tolerance	Agar Scientific, U.K.

Table 2.2 Details of resins used in processing run TEM 3.

In this run the schedule was as described for run TEM 1 up to the washes

in buffer following glutaraldehyde fixation. The processing run then proceeded separately for the different resins as follows.

Polarbed: The processing was as described for run TEM 2.

Lowicryl: The samples were dehydrated in 30 minute steps through 50%, 70%, 85%, 95%, 99%, ethanol, before being transferred to 2 × 12 hour changes of Lowicryl K4M resin and polymerized for 24 hours in UV light.

L.R. White: The samples were dehydrated in 30 minute steps through 50%, 70%, 85%, and 95% ethanol before being transferred to L.R. White resin for 12 hours after which the samples were polymerized at 60° C for 24 hours.

Nanoplast: The samples were transferred directly from the buffer to the resin and were placed in a dessicator at 40° C for 48 hours before being polymerized at 60° C for 24 hours.

X-ray diffraction patterns were obtained at the end of the following steps:

1. Resin polymerization.

The polymerized samples were also sectioned, stained and examined under the TEM to determine fibril diameter and fibril arrangement.

2.5.2 X-ray diffraction studies on processing for Scanning Electron Microscopy

SEM Processing Run 1:

The corneas were fixed at room temperature in 2.5% glutaraldehyde in 0.1M phosphate buffer at pH 7.2 overnight, followed by 3 × 10 minute washes in 0.1M phosphate buffer at pH 7.2. The samples were then postfixed for 1.5 hours in 1.5% osmium tetroxide, followed by 3 × 10 minute washes in 0.1M phosphate buffer at pH 7.2. This was followed by a dehydration run of 30 minute steps in 50%, 70%, 85%, 95%, 100%, and 100% ethanol. The samples were then transferred to 100% acetone for two changes of 30 minutes each change before being critically point dried in a Polaron 'Jumbo' critical point drier.

X-ray diffraction patterns were obtained at the end of the following steps:

1. Glutaraldehyde fixation.
2. Osmium tetroxide post-fixation.
3. Ethanol dehydration.
4. Critical point drying.

SEM Processing Run 2.

This run is exactly the same as run 1 except that the postfixation step in 1.5% osmium tetroxide was omitted.

X-ray diffraction patterns were obtained at the end of the following steps:

1. Glutaraldehyde fixation.
2. Ethanol dehydration.
3. Critical point drying.

2.5.3 Determination of Fibril Diameter

The fibril diameter in bovine corneal stroma at physiological hydration was obtained through a combination of high-angle X-ray diffraction and electron microscopy. The intermolecular spacing was first obtained for several (n=6) fresh bovine corneas at physiological hydration by the use of high-angle X-ray diffraction. The corneas were then dried under vacuum, and loaded into special X-ray cells which maintained the corneas under vacuum while the intermolecular X-ray pattern was obtained. Next, small pieces of the vacuum-dried corneas were teased out and sandwiched between two grids and loaded into a TEM. When examined, individual collagen fibrils could sometimes be found projecting around the edges of the samples, these individual fibrils were photographed, 10-20 photographs were taken of each sample. During this procedure the intensity of the electron beam was kept as low as possible, so as to minimize any heating of the specimen which might occur. The diameter of the fibrils was calculated using a calibration specimen of a metal replica with 2160 lines per mm; over 25 calibration photographs were taken in order to minimize errors in the calibration.

With both the fibril diameter and intermolecular spacing known for bovine stroma under vacuum, and the intermolecular spacing for bovine stroma at physiological hydration known, it is then a simple matter to calculate the fibril diameter at physiological hydration. If the diameter of the fibril under vacuum is D_v, the intermolecular spacing of the fibril under vacuum is I_v, and the intermolecular spacing of the cornea at physiological hydration is I_n. Then, assuming the water is evenly distributed between the collagen molecules, the fibril diameter at physiological hydration (D_f) is given by

$$D_f = D_v \times \frac{I_n}{I_v}.$$

2.6 X-ray diffraction studies on Freezing

In order to investigate the effect of freezing on the intermolecular spacings in the corneal stroma a special cell was constructed. This cell allowed X-ray patterns to be obtained from corneas while they were being held at temperatures below zero. A range of temperatures could be obtained by using different coolants. A combination of precooling and dry ice was used to give a temperature of around -40°C while liquid nitrogen gave a temperature of around -180°C. Low and high-angle patterns were obtained from bovine corneas before, during, and after freezing.

2.7 Electron microscope studies on freezing

The effect of storage of frozen corneas was also assessed using the SEM. Bovine corneas which had been stored frozen at -40°C were compared to fresh unfrozen bovine corneas. As well as comparing fresh and frozen corneas at physiological hydration, comparison was also carried out over a range of hydrations from H=0 to H=10.

Chapter 3

Hydration of the Cornea

3.1 Introduction

This chapter will detail the results of a series of experiments on corneal hydration carried out on bovine corneas which were equilibrated to specific hydrations using the technique described in Chapter 2. The changes occurring within the corneal stroma were investigated using a number of techniques. These were TEM, SEM, and most importantly low and high-angle X-ray diffraction which allowed changes in interfibrillar and intermolecular spacings to be monitored.

3.2 Electron Microscopy

Electron Microscopy was used to check the effect of the equilibration technique on the corneal stroma, especially with regard to disruption of the collagen fibrils and the loss of proteoglycans which is known to occur if the cornea is placed unprotected into the equilibration solution.

3.2.1 Transmission Electron Microscopy

Equilibrated bovine corneas at a range of hydrations were processed for TEM using the 'cuprolinic blue method' described in Chapter 2, which allows the proteoglycans to be visualized in the TEM.

A bovine cornea at fixed at normal hydration is shown in Figure 3.1. Numerous proteoglycans can be seen associated with the fibrils, the majority are orientated crosswise to the fibrils. Although a proportion of the proteoglycans appear to be associated with the fibril at regular periodic intervals, most of the proteoglycans appear to be randomly distributed.

Figure 3.2 shows that at low hydrations (H=0.5) the collagen fibres are packed into close association with each other, and the number and distribution of the proteoglycans appears normal. Apart from the reduced interfibrillar spacing, the corneal stroma seems to be normal.

Figure 3.3 shows that bovine corneas equilibrated to high hydrations H=8 have widely and fairly evenly spaced collagen fibrils. Proteoglycans are still visible attached to the collagen fibrils. Apart from the increased interfibrillar spacing, the corneal stroma at this hydration appears normal.

Figures 3.2 and 3.3 show that the equilibration technique is effective in allowing very accurate adjustment of the corneas to specific hydrations without disrupting the stroma or causing loss of the proteoglycans, which occurs if the cornea is placed directly into a swelling solution (Gyi, 1988). Corneas which have been left in distilled water or ringer solution for an equivalent period of time lose all their proteoglycans into the solution (personal observation). It is evident however, that the proteoglycans appear longer in the cornea at normal hydration (Figure 3.1), suggesting the possibility that the glycosaminoglycan side chains are duplexing at normal hydration.

Figure 3.1 TEM micrograph showing a longitudinal section through a lamella of bovine cornea stroma which was fixed at physiological hydration. In this micrograph the collagen fibrils are not in contact and the densely stained proteoglycans can be seen orientated both parallel, and crosswise to the fibrils. ×110,000 magnification.

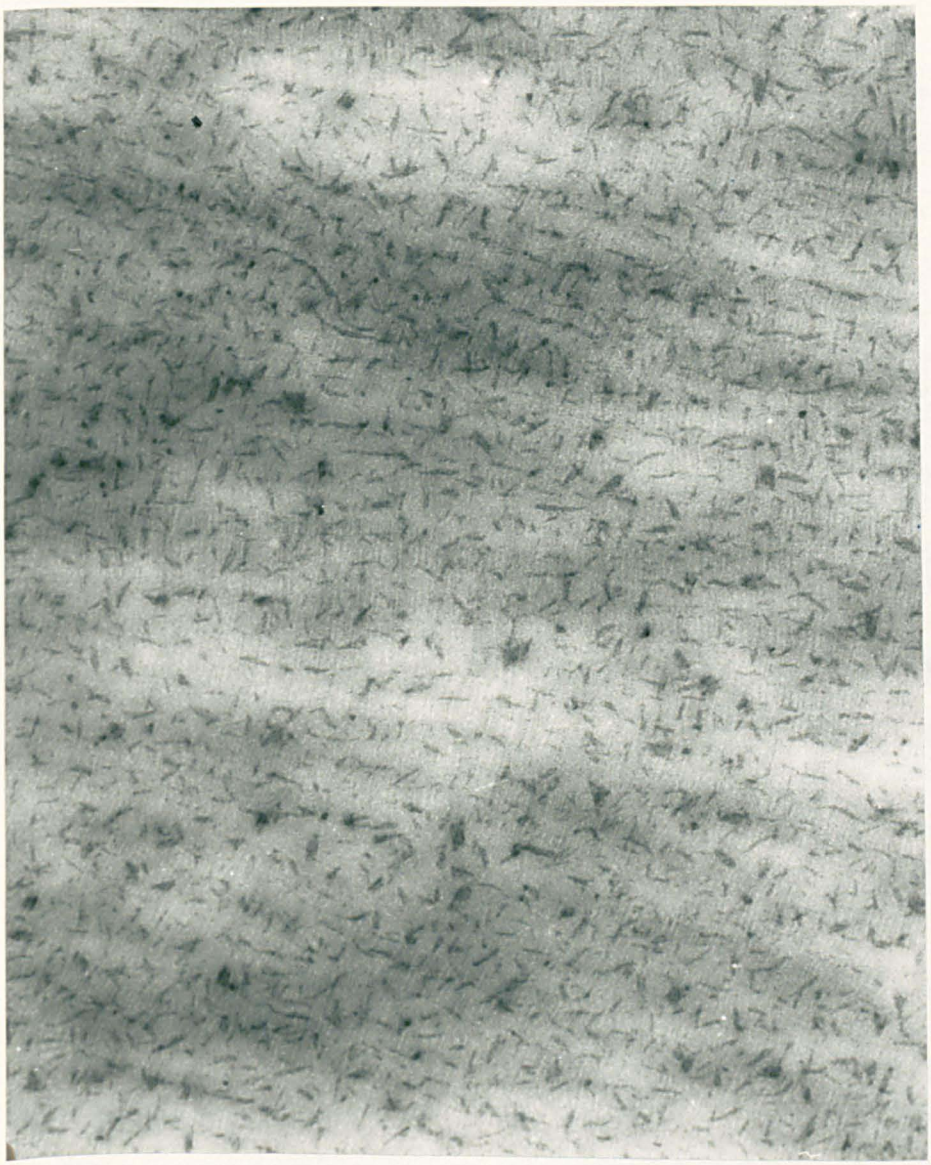

Figure 3.2 TEM micrograph showing a longitudinal section through a lamella of bovine corneal stroma which was equilibrated to H=0.5 before being fixed. In this micrograph the collagen fibrils are touching and the densely stained proteoglycans can be seen orientated both parallel, and crosswise to the fibrils. ×110,000 magnification.

Figure 3.3 TEM micrograph showing a longitudinal section through a lamella from a bovine cornea equilibrated to H=8 before being fixed. The collagen fibrils are spaced very widely at this hydration, however, proteoglycans can still be seen attached to the fibrils. ×110,000 magnification.

3.2.2 Scanning Electron Microscopy

Equilibrated bovine corneas at a range of hydrations were processed for SEM using the technique described in Chapter 2.

Figure 3.4 shows a longitudinal section through the corneal stroma of a bovine cornea. The lamellae can be distinguished, and within the individual lamella aggregates of fibers (they are too large to be individual fibres) are evident running at approximately right-angles to those in adjacent lamella. The appearance of the stroma shown in this micrograph was seen uniformly through the whole thickness of the cornea.

Figure 3.5 shows that at H=0 not much detail is evident, the fibrillar nature of the lamellae is not detectable, presumably as the fibres are so tightly packed. At this hydration even the boundaries between the individual lamellae cannot be seen. It is clear however, that the drying process has resulted in cracks in the stroma running parallel to the lamellae.

Figure 3.6 shows that at H=7 the individual lamellae are distinguishable, the fibrillar nature of the lamellae is evident; the fibres visible must be aggregate rather than individual collagen fibres. The change in direction of the fibres between adjacent lamellae can also be seen at this hydration. Apart from the increased thickness of the cornea there appears to be no difference in the stromal structure when compared to physiologically hydrated stroma.

3.3 X-Ray Diffraction

Fresh bovine corneas were equilibrated to specific hydrations as described in Chapter 2. High-angle synchrotron X-ray diffraction patterns were obtained, and the intermolecular spacing was calculated from the first-order reflection of the Bragg spacing of the collagen molecules, as described in Chapter 2. Low-angle patterns were obtained from the same specimens, and the interfibrillar spacings were calculated from the first-order reflection

Figure 3.4 SEM micrograph showing a longitudinal section of the corneal stroma at physiological hydration. Lamellae are easily distinguished, within them aggregates of collagen fibres can be seen running at approximately right-angles to adjacent lamellae. $\times$12,500 magnification.

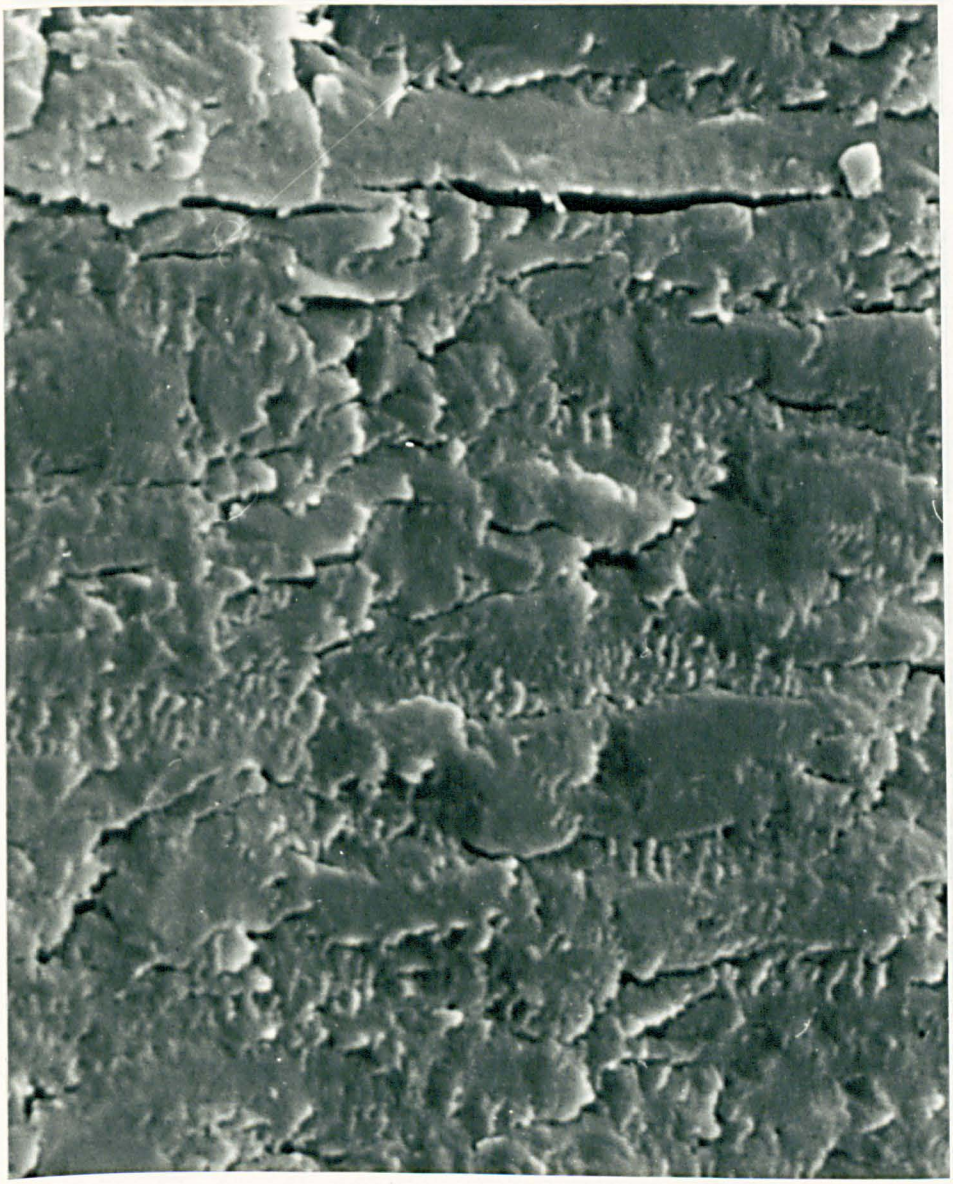

Figure 3.5 SEM micrograph showing a longitudinal section of the corneal stroma at H=0. Little detail is evident apart from cracks running parallel to the lamellae. ×12,500 magnification.

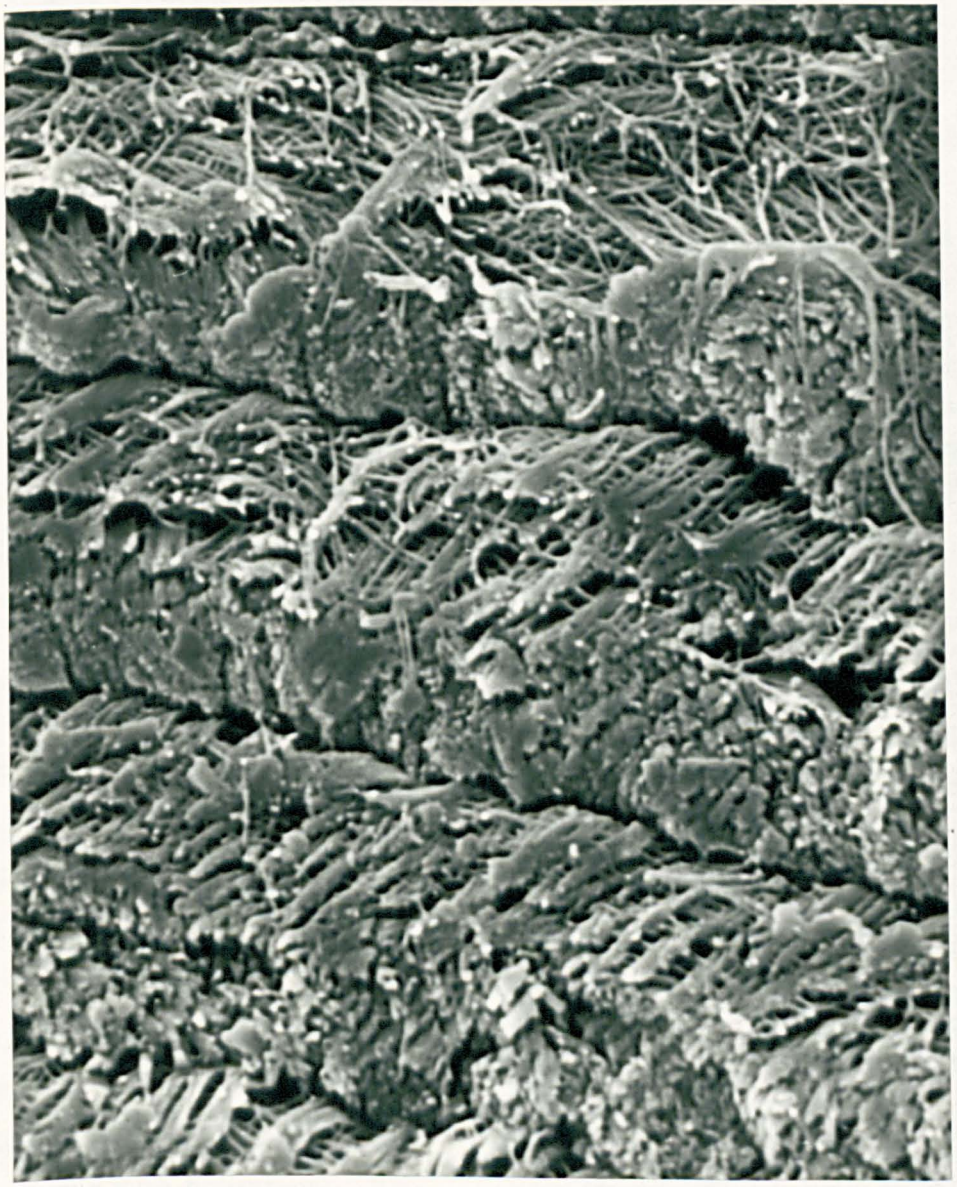

Figure 3.6 SEM micrograph showing a longitudinal section of the corneal stroma at H=7. The boundaries between the lamellae are distinct and the fibers of adjacent lamellae can be seen to be running in different directions. $\times$12,500 magnification.

of the Bragg spacing of the collagen fibrils, again as described in Chapter 2.

3.3.1 Intermolecular Spacing

Figure 3.7 shows the changes in the intermolecular spacings of fresh bovine corneas which have been equilibrated to different hydrations.
The intermolecular spacing can be seen to increase rapidly with hydration from H=0 to H=1 after which it remains almost unchanged, reaching a maximum value of approximately 1.78nm. Figure 3.8 shows the 1st order reflections from the Bragg spacings at different hydrations, and it is clear that the reflections become more diffuse with increasing hydration which implies a larger range of spacings are present at higher hydrations.

The above experiment was repeated with equilibrated rat-tail tendon and the results can be seen plotted on Figure 3.9, which shows that the changes in intermolecular spacing follow the same pattern observed in cornea, a rapid increase in spacing up to H=1, after which there is virtually no change. However, with rat-tail tendon the dry intermolecular spacing is lower than with cornea, and the maximum intermolecular spacing when fully hydrated is also lower than that observed in cornea at the same hydration.

The effect of hydration on bovine sclera was also investigated. Figure 3.10 shows that a similar pattern to cornea and rat-tail tendon is seen. There is a rapid increase in spacing up to ~H=1 after which the spacing increases only slowly with hydration.

3.3.2 Interfibrillar Spacing

Figure 3.11 shows the interfibrillar spacing^2 plotted against tissue hydration. The specimens used to collect these data were the same as used to collect the intermolecular data in the previous section.
From Figure 3.11 it can be seen that the plot of interfibrillar spacing squared against hydration is a straight line, at least over the hydration

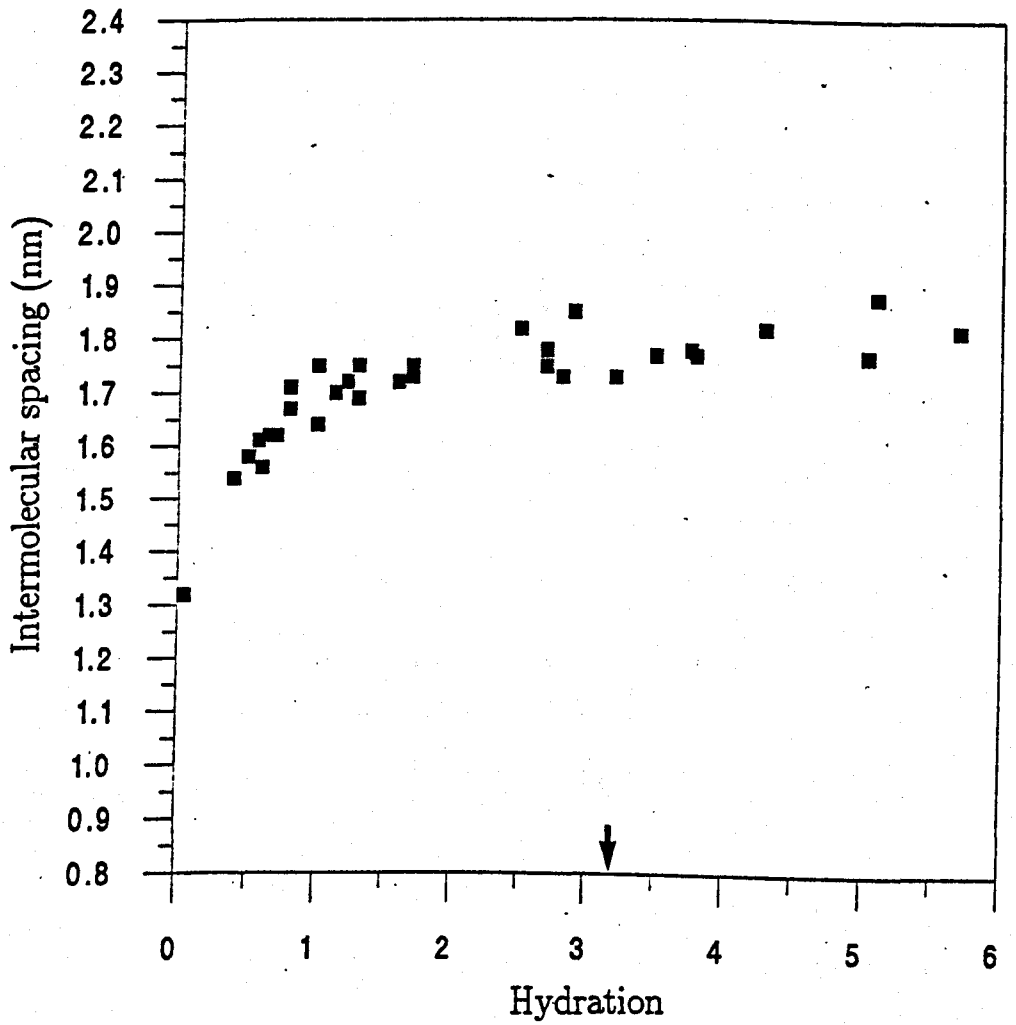

Figure 3.7 Changes in intermolecular spacing in corneas with hydration. Physiological hydration is indicated by the arrow.

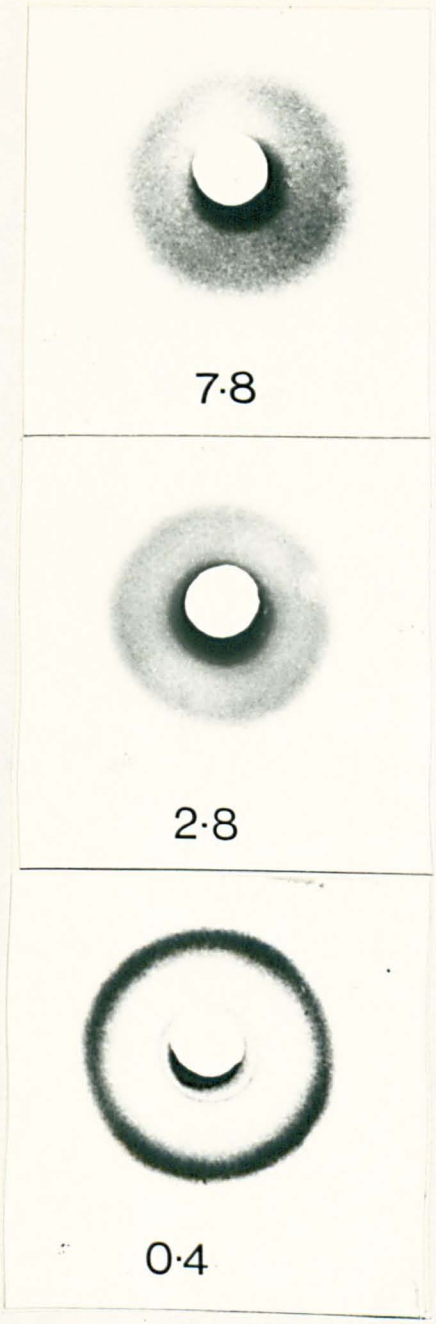

Figure 3.8 Changes in the intermolecular pattern in cornea with hydration. The numbers refer to the hydration.

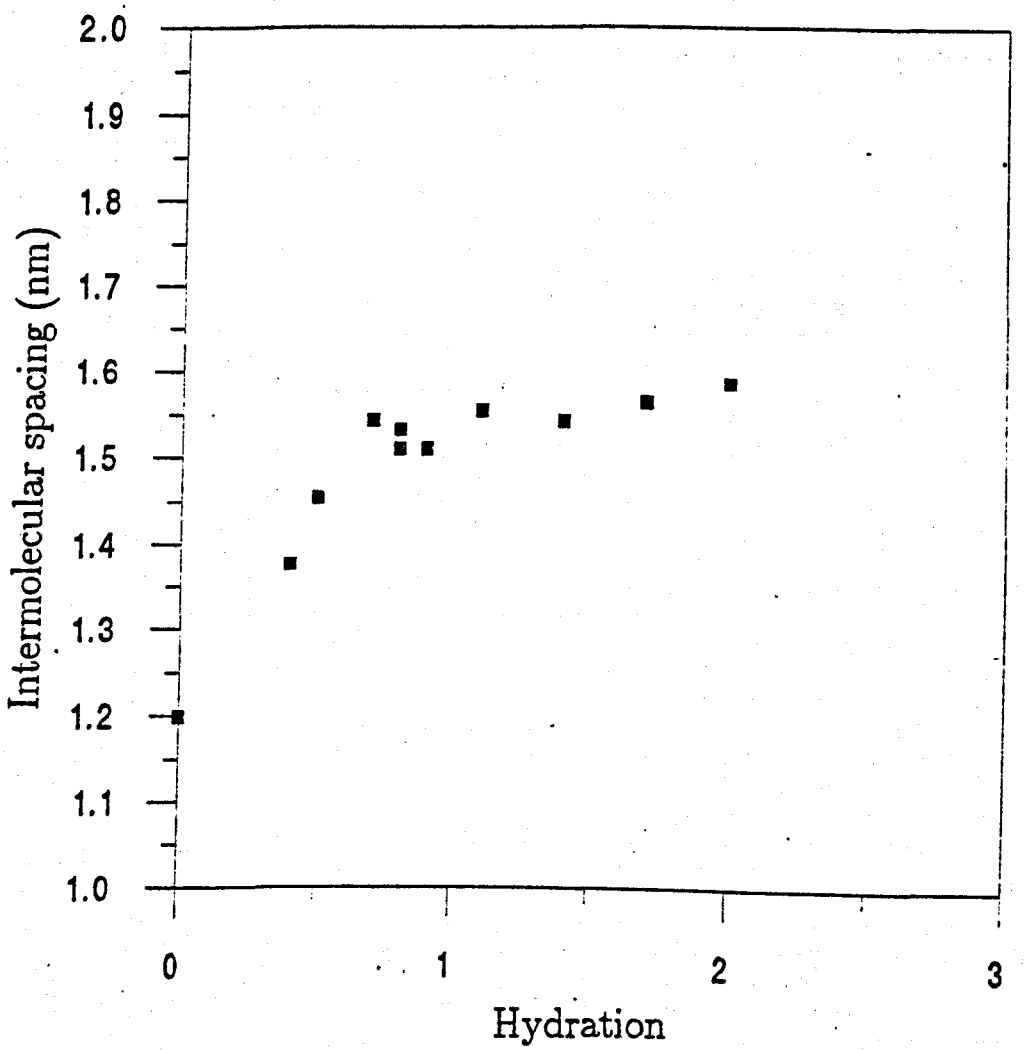

Figure 3.9 Changes in intermolecular spacing in rat-tail tendon with hydration

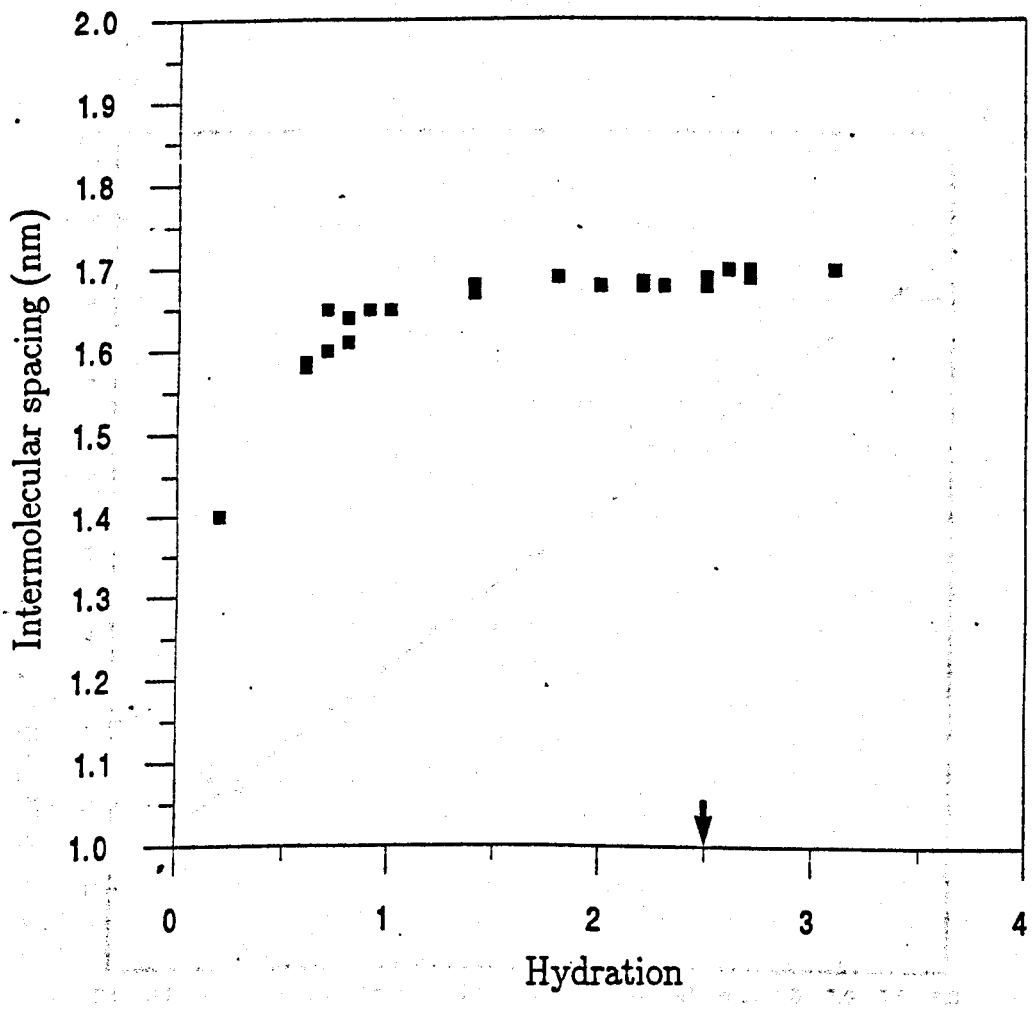

Figure 3.10 Changes in the intermolecular spacing in sclera with hydration, the arrow indicates physiological hydration.

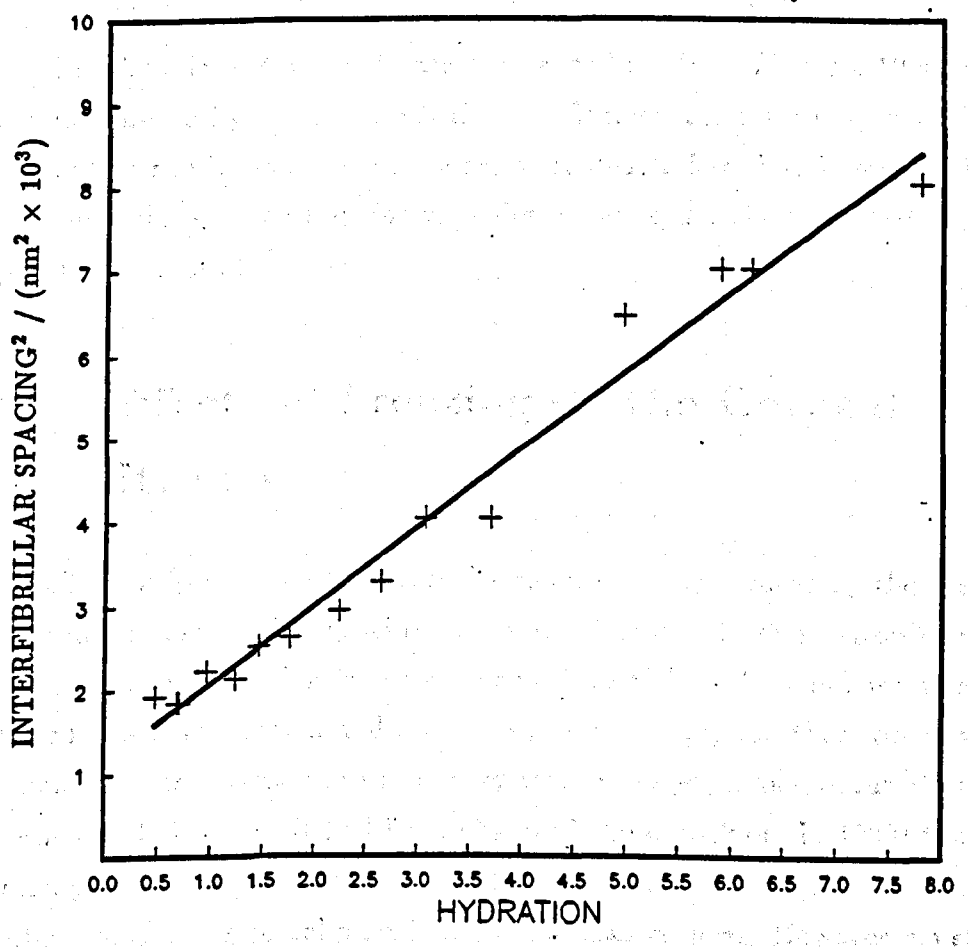

Figure 3.11 Changes in interfibrillar spacing of bovine corneas with hydration, the line is a least-squares best-fit to the experimental data.

range H=0.5 to H=4. It proved impossible to obtain an equatorial low-angle pattern from a cornea at zero hydration.

3.3.3 Correlation between Low and High-angle data

Figure 3.12 shows the interfibrillar and intermolecular data presented together. The two sets of data are normalized at H=0. Figure 3.12 suggests that increase in hydration causes the interfibrillar and intermolecular spacings to rise in unison over the range H=0-1. After H=1 however, the intermolecular spacing remains virtually unchanged while the interfibrillar spacing continues to increase.

3.4 Effects of Freezing on the Corneal Stroma

The effect of freezing on the corneal stroma was investigated by the use of electron microscopy and synchrotron X-ray diffraction. This aspect of the project was of particular importance since most of the human specimens used in this investigation had been frozen for storage, and therefore it was of considerable importance to discover what changes, if any, occur after freezing and thawing. It had been observed (Quantock et al., 1990) that freezing had no observable effect on the interfibrillar spacing, distribution of proteoglycans, or stromal morphology of human corneas. However, no study of the effect of freezing on the intermolecular spacing had been carried out. This study was carried out using low and high-angle X-ray diffraction of specimens in special cells which allowed patterns to be obtained before, during and after freezing. In addition an SEM investigation of the effect of long term storage of corneas at -40°C at both physiological and at a range of hydrations between H=1 to H=8, was carried out.

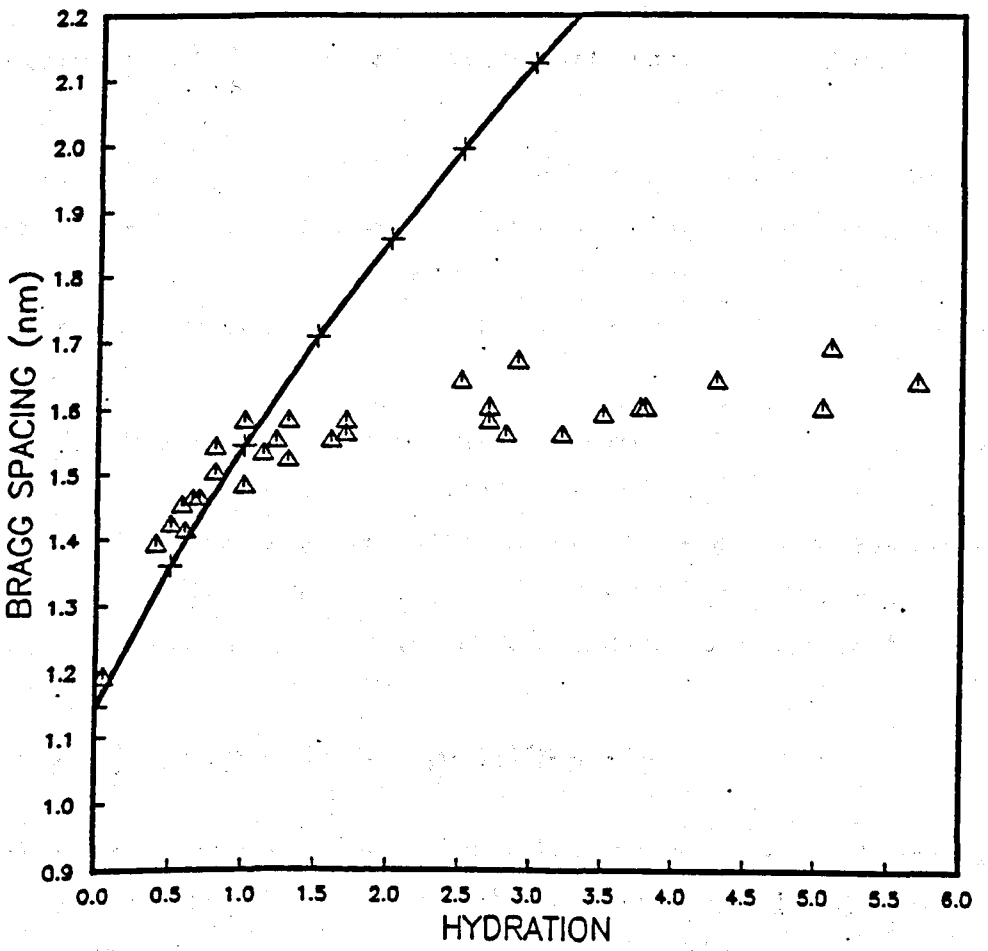

Figure 3.12 High and low-angle data on corneal hydration, the vertical axis (Bragg spacing) refers to the intermolecular data (triangles). The + signs are points calculated from the best-fit interfibrillar data and are not directly related to the vertical axis values. The interfibrillar data is normalized at H=0, and shows the rate of water uptake between the fibrils.

3.4.1 Scanning Electron Microscopy

SEM was used to monitor the changes occurring within the corneal stroma at a variety of hydrations. Bovine corneas which had been stored at -40°C for several weeks were equilibrated to various hydrations, before being processed for SEM according to the preparation procedure outlined in Chapter 2.

At low hydrations (H<4) the stroma of bovine corneas which have been stored at -40°C appears indistinguishable under the SEM to that of fresh bovine corneas. However, above H=4 the corneas which have been frozen show some separation between individual lamellae, as is shown in Figure 3.13.

At high hydrations the disruption within the stroma becomes more evident, with large spaces forming between the lamellae as seen in Figure 3.14 and Figure 3.15. Presumably these are regions where ice formation has pushed apart the lamellae in the frozen tissue.These separations between the lamellae are not visible at physiological hydrations under the SEM.

3.4.2 High-Angle X-ray Diffraction

High-angle patterns were obtained from bovine corneas before, during, and after freezing using the apparatus and procedure described in Chapter 2. The intermolecular spacing of the collagen fibrils within the corneal stroma decreases from 1.78±0.02nm at room temperature to 1.70nm±0.02nm at $\sim -40°C$ the cornea appears opaque while frozen, and the first-order reflection becomes slightly sharper. After thawing back to room temperature, the corneas regain their transparency, and the intermolecular spacings were measured at 1.79±0.02nm, with the reflections appearing identical to the pattern before freezing. When the experiment was repeated at liquid nitrogen temperatures there was a much greater reduction in intermolecular spacing, as much as 18.8%, and the spacing after thawing was slightly lower (~5%) than before freezing.

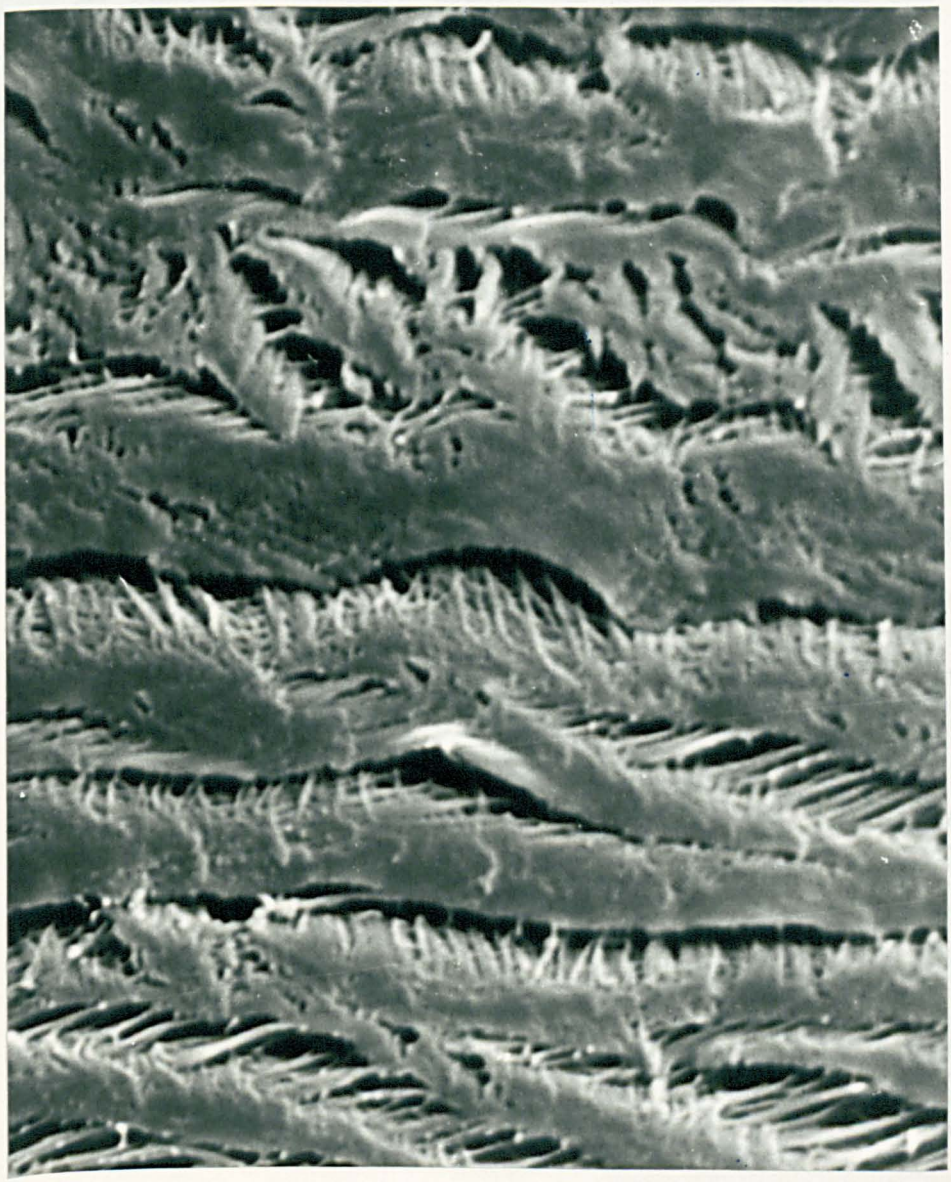

Figure 3.13 SEM micrograph of a thawed bovine cornea at H=4. ×12,500 magnification.

Figure 3.14 SEM micrograph of a thawed bovine cornea at H=7, showing the disruption of the lamella. ×1,200 magnification.

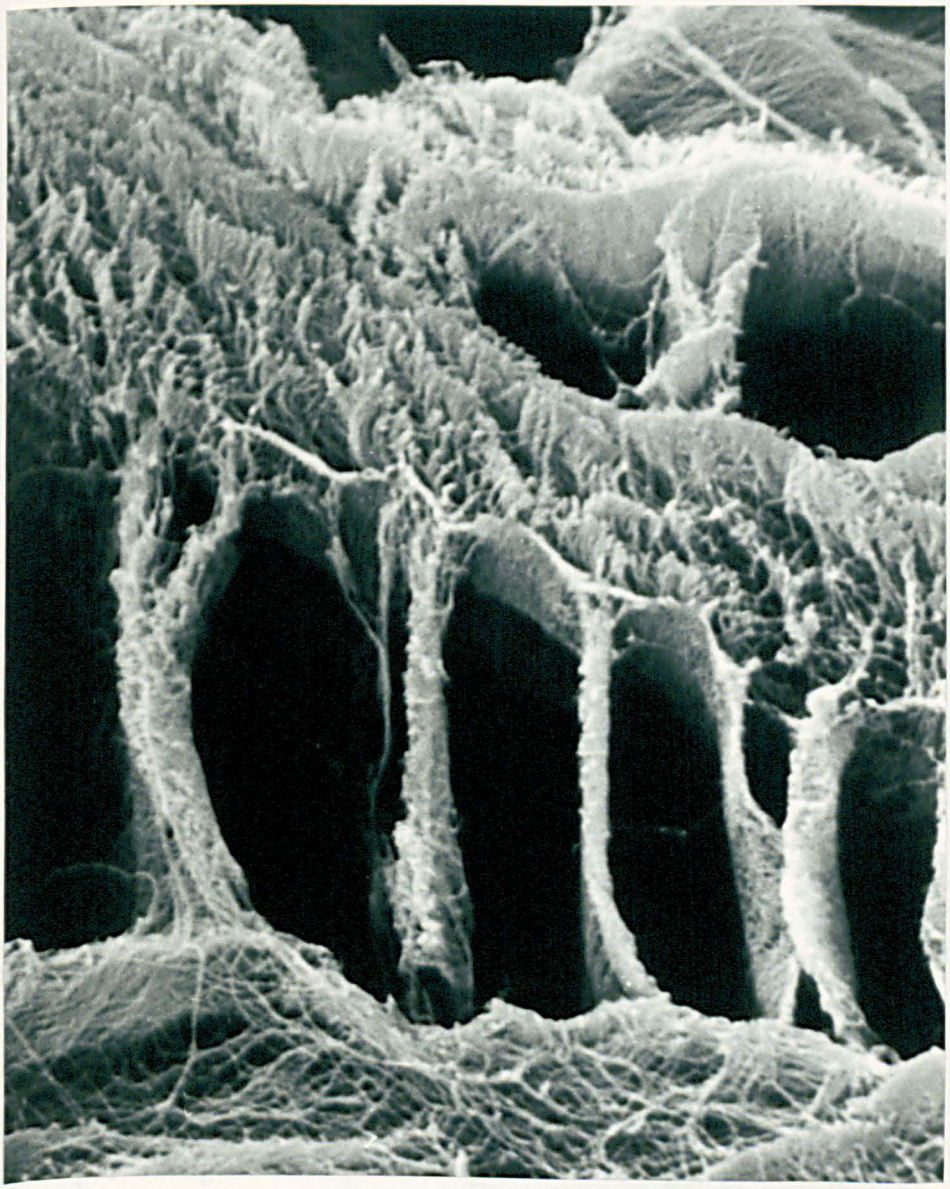

Figure 3.15 SEM micrograph of a thawed bovine cornea at H=7, showing the disruption within a lamella. ×8,000 magnification.

Chapter 4

Electron Microscope Processing of the Cornea.

4.1 Introduction

This section of the work involved an investigation into the changes which occur in the cornea stroma as it is processed for electron microscope examination. Intermolecular and interfibrillar spacings were monitored as well as fibril diameter and fibril packing. Part of this chapter involves a determination of the fibril diameter of bovine cornea at physiological hydration.
The changes were monitored during processing by the use of X-ray diffraction. By using the very intense synchrotron X-ray beam at Daresbury, U.K., it was possible to obtain patterns from corneas at every stage of processing, including those which had been embedded in polymerized resin.

4.2 Transmission Electron Microscopy

Fresh bovine corneas were processed for TEM, using the processing schedules described in Chapter 2, page 48. These were referred to as processing runs TEM 1, TEM 2, and TEM 3. The results are presented one

step at a time.

4.2.1 Fixation

Glutaraldehyde fixation

Table 4.1 shows the effect of glutaraldehyde fixation on bovine corneal stroma during processing run TEM 1. The conclusions are summarized as follows.

1. There is no significant change ($p>0.2$) in interfibrillar spacing.
2. There is a significant ($p<0.05$) increase (5.2%) in intermolecular spacing.
3. There is a significant ($p<0.0001$) decrease (0.6%) in D-period spacing.

Osmium tetroxide post-fixation

Table 4.1 shows the effect of osmium tetroxide post-fixation on bovine corneal stroma during processing run TEM 1. The conclusions are summarized as follows.

1. There is no significant ($p>0.2$) change in interfibrillar spacing.
2. The X-ray pattern derived from the intermolecular spacing is very diffuse making accurate measurement impracticable.
3. There is a significant ($p<0.001$) reduction (0.8%) in D-period spacing.

Processing stage	Interfibrillar spacing(nm)	Intermolecular spacing(nm)	D-period spacing(nm)
Fresh (n=16)	63.8 ± 2.0	1.72 ± 0.06	64.99 ± 0.17
2.5% Glut (n=16)	63.4 ± 2.7	1.81 ± 0.11	64.59 ± 0.23
1.5% $Os0_4$ (n=8)	64.8 ± 2.8	-	64.09 ± 0.17

Table 4.1 Changes occurring in bovine corneal stroma during fixation, n is the number of specimens used.

4.2.2 Dehydration

Table 4.2 shows the effect of ethanol dehydration on bovine corneal stroma during processing run TEM 1. The changes are summarized as follows.

1. There is a significant ($p<0.05$) decrease (3.9%) in interfibrillar spacing.
2. There is no significant ($p>0.1$) change in intermolecular spacing between the stages of glutaraldehyde fixation and ethanol dehydration (the X-ray pattern immediately after osmium tetroxide post-fixation was unmeasurable).
3. There is no significant ($p>0.2$) change in D-period spacing.

Processing stage	Interfibrillar spacing(nm)	Intermolecular spacing(nm)	D-period spacing(nm)
1.5%OsO_4 (n=8)	64.8 ± 2.8	-	64.09 ± 0.17
100% Ethanol (n=8)	62.3 ± 1.6	1.87 ± 0.13	64.17 ± 0.19

Table 4.2 Changes occurring in bovine corneal stroma during ethanol dehydration in processing run TEM 1, n is the number of specimens used.

Table 4.3 shows the effect of ethanol dehydration on corneas during processing run TEM 2. The conclusions are summarized as follows.
1. There is no significant ($p>0.2$) change in interfibrillar spacing.
2. There is no significant ($p>0.05$) change in intermolecular spacing.
3. There is no significant ($p>0.05$) change in the D-period spacing.

Processing stage	Interfibrillar spacing(nm)	Intermolecular spacing(nm)	D-period spacing(nm)
2.5% Glut (n=16)	63.4 ± 2.7	1.81 ± 0.11	64.59 ±0.23
100% Ethanol (n=8)	63.6 ± 4.1	1.94 ± 0.20	64.35 ± 0.09

Table 4.3 Changes occurring in bovine corneal stroma during ethanol dehydration in processing run TEM 2, n is the number of specimens used.

4.2.3 Resin Infiltration

Table 4.4 shows the effect of resin infiltration on bovine corneal stroma during processing run TEM 1. The changes are summarized as follows.
1. There is no significant ($p>0.05$) change in interfibrillar spacing.

2. It proved impossible to obtain an X-ray pattern derived from the intermolecular spacing after resin infiltration.

3. There is a significant ($p>0.005$) decrease (0.8%) in D-period spacing.

Processing stage	Interfibrillar spacing(nm)	Intermolecular spacing(nm)	D-period spacing(nm)
100% Ethanol (n=8)	62.3 ± 1.6	1.87 ± 0.13	64.17 ± 0.19
100% Resin (n=4)	60.9 ± 1.7	-	63.68 ± 0.37

Table 4.4 Changes occurring in bovine corneal stroma during resin infiltration in processing run TEM 1, n is the number of specimens used.

Table 4.5 shows the effect of resin infiltration on bovine corneal stroma during processing run TEM 2. The changes are summarized as follows.

1. There is no significant ($p>0.2$) change in interfibrillar spacing.

2. It proved impossible to obtain a X-ray pattern derived from the intermolecular spacing after resin infiltration.

Processing stage	Interfibrillar spacing(nm)	Intermolecular spacing(nm)	D-period spacing(nm)
100% Ethanol (n=8)	63.6 ± 4.1	1.94 ± 0.20	64.07 ± 0.09
100% Resin (n=4)	62.2 ± 1.2	-	-

Table 4.5 Changes occurring in bovine corneal stroma during resin infiltration in processing run TEM 2, n is the number of specimens used.

4.2.4 Resin Polymerization

Table 4.6 shows the effect of resin polymerization on bovine corneal stroma during processing run TEM 1. The changes are summarized as follows.

1. There is a significant ($p<0.05$) decrease (1.7%) in interfibrillar spacing.

2. It proved impossible to obtain an X-ray pattern derived from the intermolecular spacing after resin infiltration.

3. There is a significant ($p>0.002$) decrease (4.5%) in D-period spacing.

Processing stage	Interfibrillar spacing(nm)	Intermolecular spacing(nm)	D-period spacing(nm)
100% Resin (n=4)	60.9 ± 1.7	-	63.68 ± 0.37
Poly. Resin (n=4)	58.2 ± 2.0	-	60.82 ± 0.35

Table 4.6 Changes occurring in bovine corneal stroma during resin polymerization in processing run TEM 1, n is the number of specimens used.

Table 4.7 shows the effect of resin polymerization on bovine corneal stroma during processing run TEM 2. The changes are summarized as follows.

1. There is a significant ($p<0.5$) decrease (3.2%) in interfibrillar spacing.
2. It proved impossible to obtain an X-ray pattern derived from the intermolecular spacing after resin infiltration.
3. There is a significant ($p>0.0001$) decrease (1.9%) in D-period spacing between the stages of ethanol dehydration and resin polymerization.

Processing stage	Interfibrillar spacing(nm)	Intermolecular spacing(nm)	D-period spacing(nm)
100% Resin (n=4)	62.2 ± 1.2	-	-
Poly. Resin (n=4)	60.2 ± 1.8	-	63.00 ± 0.10

Table 4.7 Changes occurring in bovine corneal stroma during resin polymerization during processing run TEM 2, n is the number of specimens used.

4.2.5 Overall Changes

The changes in the various spacings during processing runs TEM 1 and TEM 2 are represented graphically. Figure 4.1 compares the changes in interfibrillar spacing that occur during processing runs TEM 1 and TEM 2. Figure 4.2 compares the changes that occur in intermolecular spacing during processing runs TEM 1 and TEM 2. Figure 4.3 compares the changes that occur in D-period spacing during processing runs TEM 1 and TEM 2.

The overall changes in bovine corneal stroma between the stages of fresh to embedded, are also compared statistically is this section.

Processing Run TEM 1

1. There is a significant ($p<0.0001$) decrease (8.7%) in interfibrillar spacing.
2. The intermolecular pattern was lost after resin infiltration.
3. There is a significant ($p<0.0001$) decrease (6.4%) in D-period spacing.

Processing Run TEM 2

1. There is a significant ($p<0.05$) decrease (5.6%) in the interfibrillar spacing.
2. The intermolecular pattern was lost after resin infiltration.
3. There is a significant ($p<0.0002$) decrease (3.2%) in D-period spacing.

4.2.6 Comparison of Processing Runs

This section compares the spacings of embedded bovine corneas of processing runs TEM 1 and TEM 2, the differences are summarized as follows.

1. There is a significantly ($p<0.05$) lower (10.2%) interfibrillar spacing for corneas embedded by processing run TEM 1 compared to those prepared by processing run TEM 2.
2. There is a significantly ($p<0.0001$) reduced (3.3%) D-period spacing for corneas embedded by processing run TEM 1 compared to processing run TEM 2.

4.2.7 The Effect of Different Resins

Table 4.8 shows the changes in the bovine corneal stroma as a result of processing run TEM 3. This run compares the effect of different resins (and their associated preparation procedures) on the bovine corneal stroma. The preparation procedures for the different resins are described in Chapter 2. The main conclusions are as follows.

1. No significant differences were found in interfibrillar spacings between the different resins, with the sample sizes used.

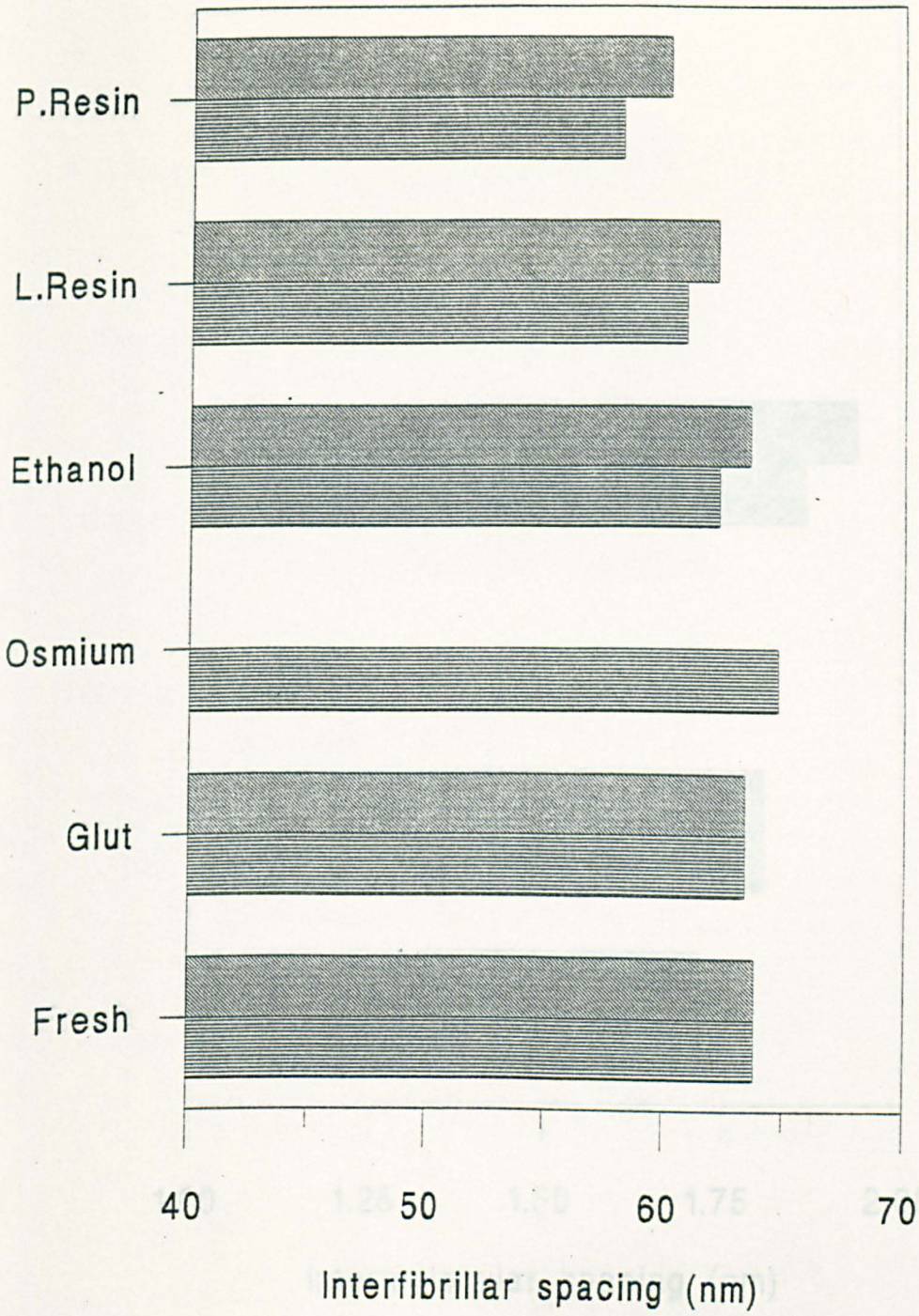

Figure 4.1 Histogram showing the changes that occur in interfibrillar spacing in the bovine cornea during processing runs TEM 1 (lower bars) and TEM 2 (upper bars).

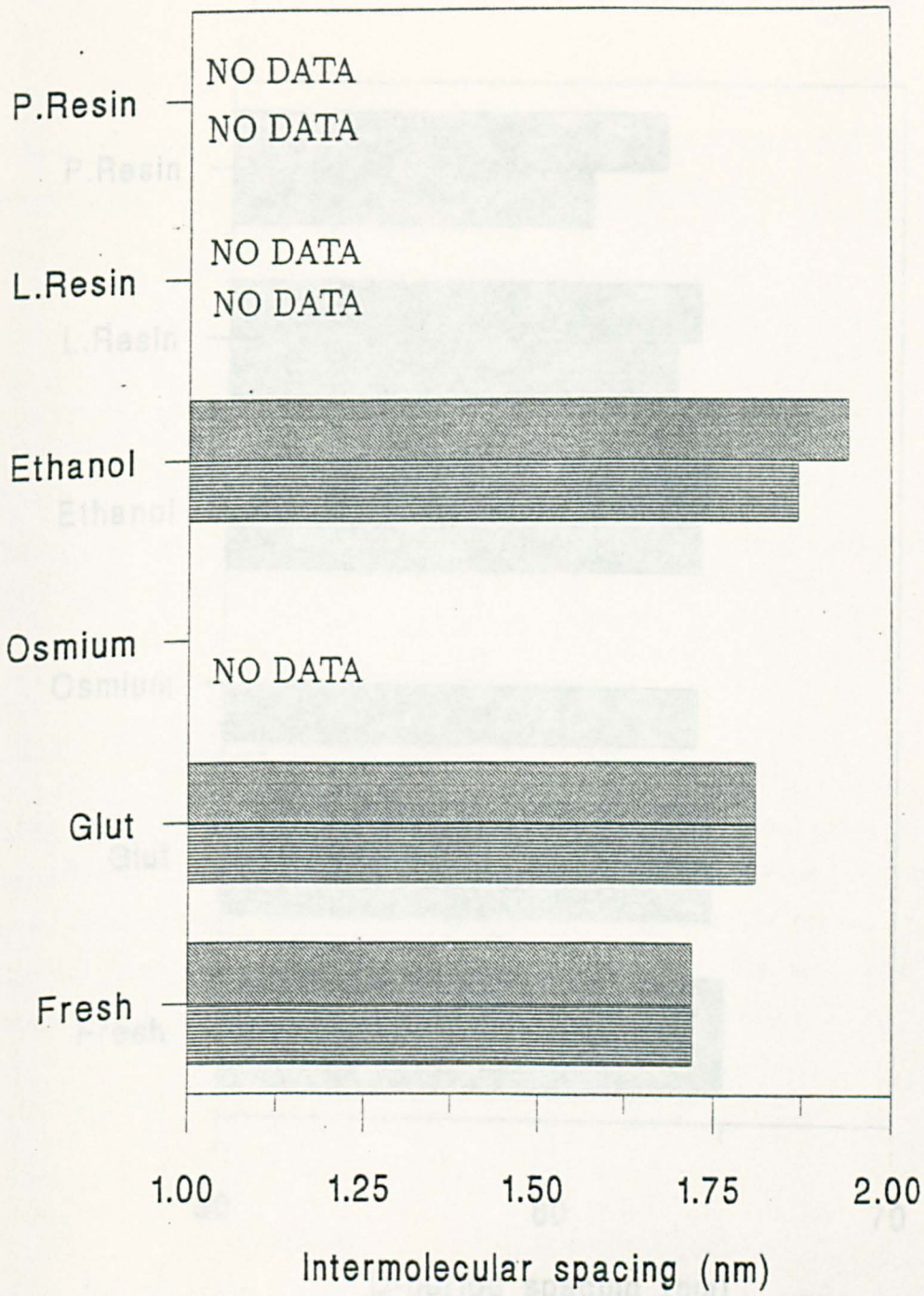

Figure 4.2 Histogram showing the changes that occur in intermolecular spacing in the bovine cornea during processing runs TEM 1 (lower bars) and TEM 2 (upper bars).

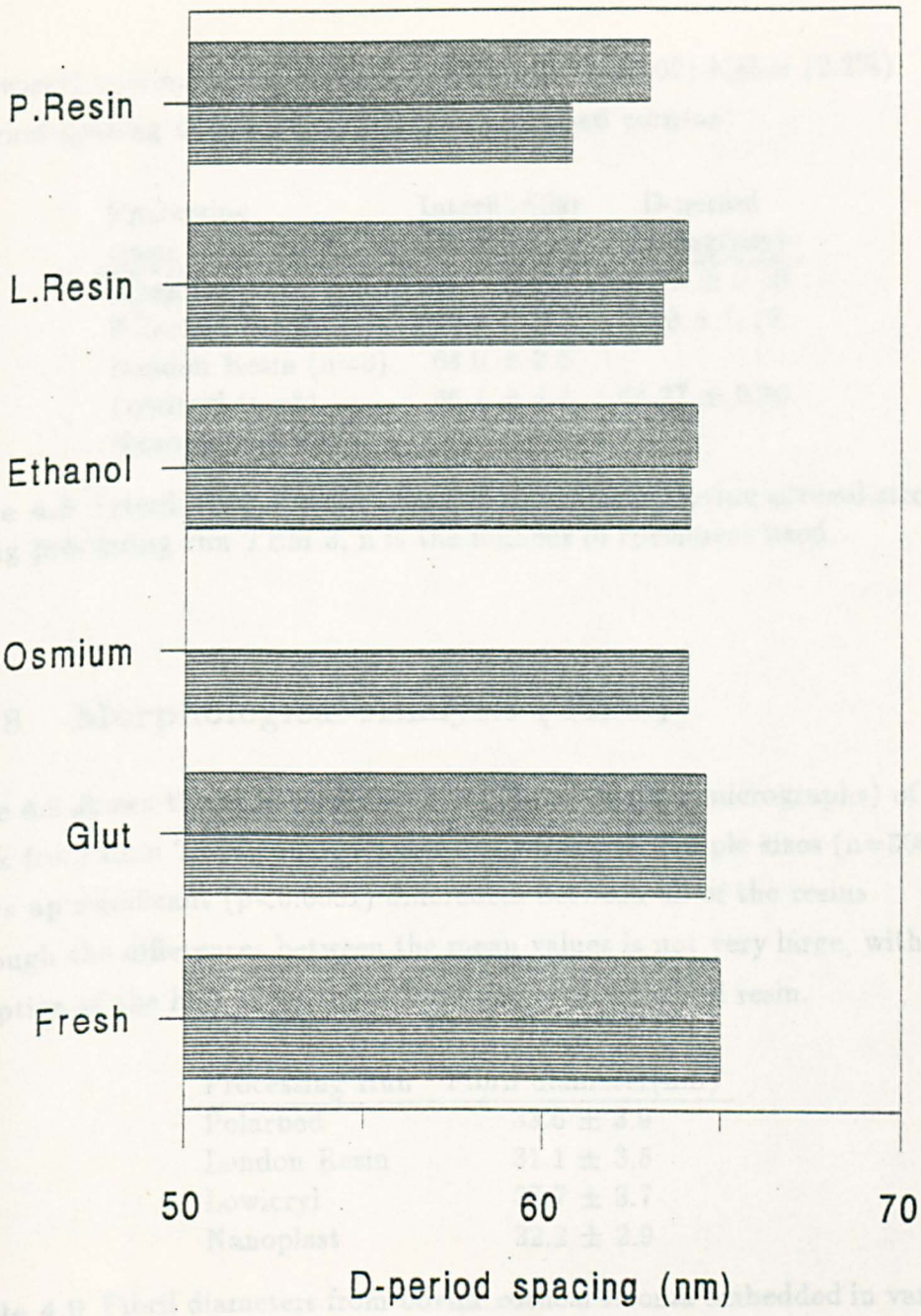

Figure 4.3 Histogram showing the changes that occur in D-period spacing in the bovine cornea during processing runs TEM 1 (lower bars) and TEM 2 (upper bars).

2. Lowicryl processing results in a significantly ($p<0.02$) higher (2.2%) D-period spacing compared to Polarbed processed corneas.

Processing stage	Interfibrillar spacing(nm)	D-period spacing(nm)
Fresh (n=12)	65.9 ± 2.8	64.99 ± 0.10
Polarbed (n=3)	62.9 ± 2.2	62.9 ± 0.10
London Resin (n=3)	64.0 ± 2.8	-
Lowicryl (n=3)	66.1 ± 4.1	64.27 ± 0.30
Nanoplast (n=3)	-	-

Table 4.8 Interfibrillar spacing changes occurring in bovine corneal stroma during processing run TEM 3, n is the number of specimens used.

4.2.8 Morphological Analysis (TEM)

Table 4.9 shows the measured diameters (from electron micrographs) of the fibrils from from TEM run 3. Analysis of very large sample sizes (n=300) shows up significant ($p<0.0001$) differences between all of the resins although the differences between the mean values is not very large, with the exception of the high mean value produced with Lowicryl resin.

Processing Run	Fibril diameter(nm)
Polarbed	33.6 ± 3.9
London Resin	31.1 ± 3.5
Lowicryl	37.7 ± 3.7
Nanoplast	32.2 ± 2.9

Table 4.9 Fibril diameters from bovine corneal stroma embedded in various resins during processing run TEM 3

As well as changes in the interfibrillar spacings and fibril diameters when different resins are used, there are also changes in the appearance of the fibrils under the TEM.

Figure 4.4 shows the conventional arrangement of fibrils as expected under the TEM.

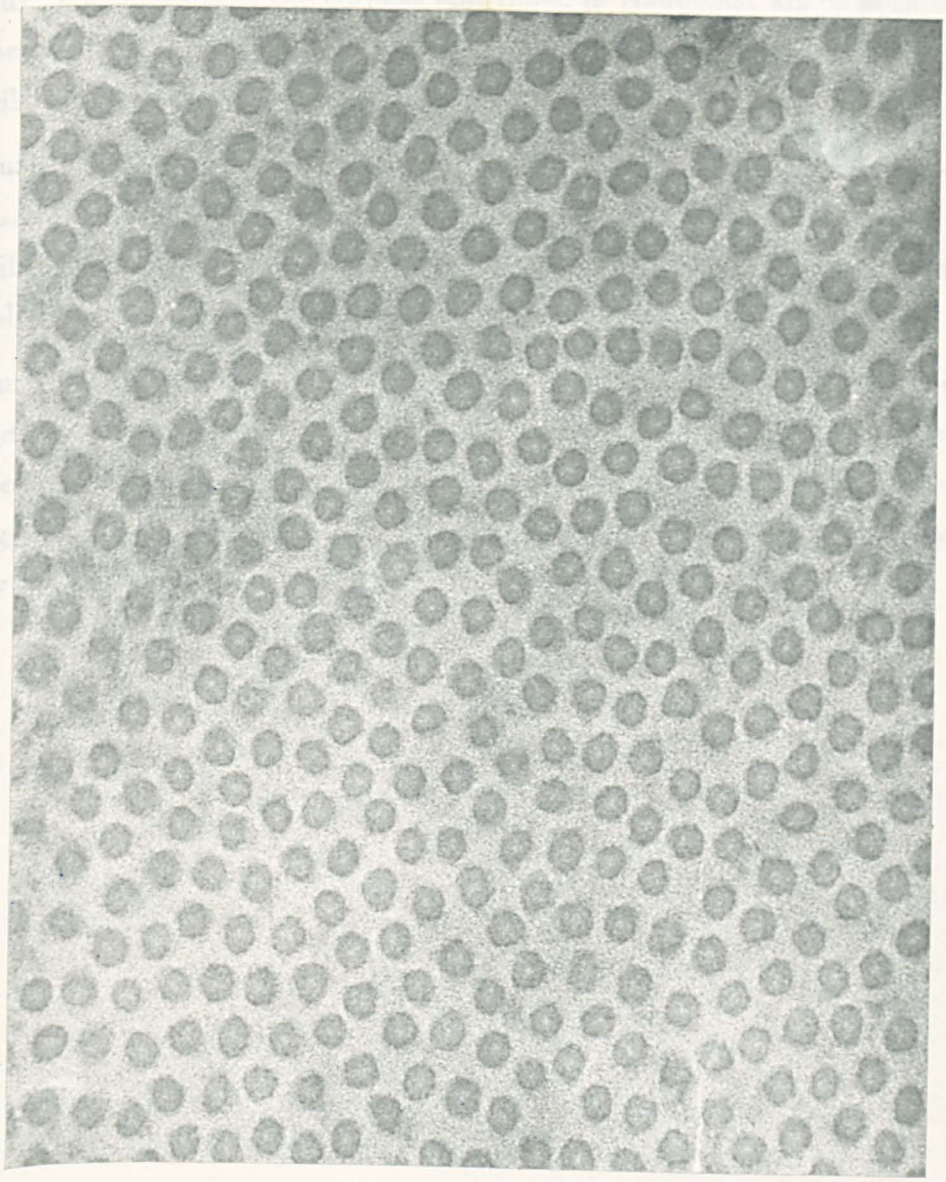

Figure 4.4 TEM micrograph of bovine cornea embedded in Polarbed and stained with uranyl acetate and PTA. This micrograph shows the appearance of the corneal stroma produced by conventional processing. ×151,500 magnification.

Figure 4.5 shows that the corneas embedded in Nanoplast are of normal appearance and spacing, however extra material is also visible between the fibrils.

Figure 4.6 shows that in certain regions of the stroma of corneas embedded in L.R. White resin the fibrils can be seen arranged in long lines where the fibrils in the lines are in contact. Some interfibrillar material is also present in places.

Figure 4.7 shows that the fibrils of corneas embedded in Lowicryl resin have larger diameters than seen in conventional resins. In addition the fibrils appear to have a slightly more irregular outline than normal, with a larger range of spacings. Also, the ground substance between the fibrils appears very dense.

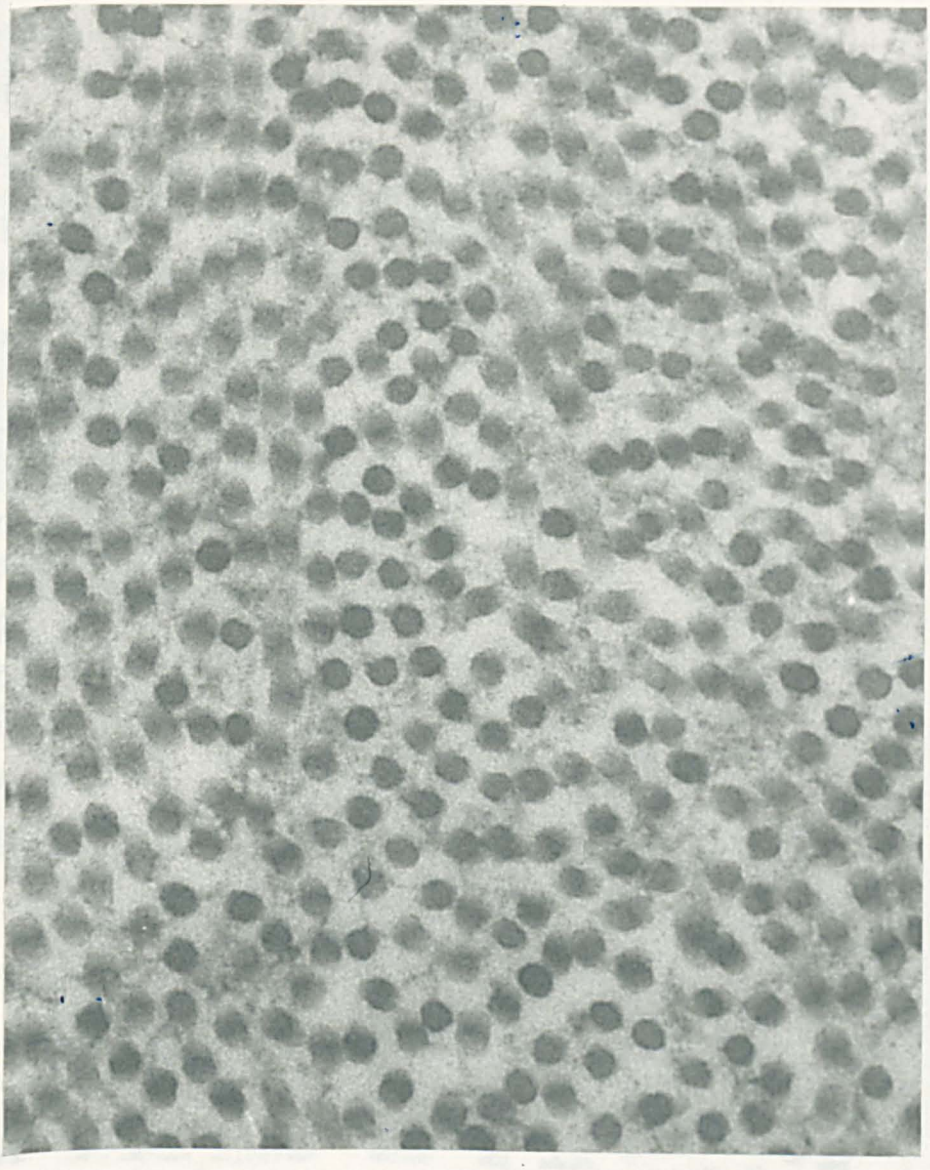

Figure 4.5 TEM micrograph of bovine cornea embedded in Nanoplast and stained with uranyl acetate and PTA. Intrafibrillar material is evident in this micrograph which is not visible in Figure 4.4. ×151,500 magnification.

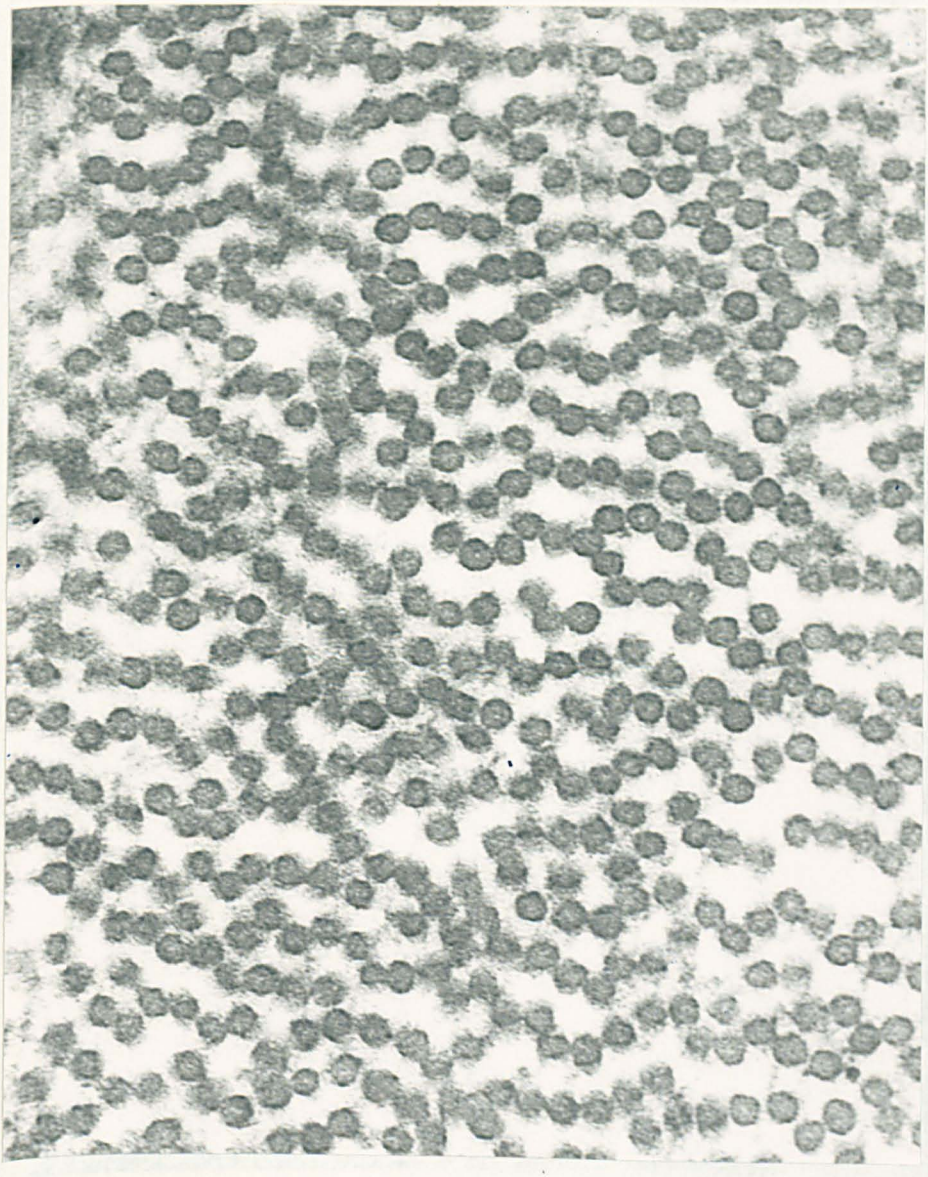

Figure 4.6 TEM micrograph of bovine cornea embedded in L.R. White and stained with uranyl acetate and PTA. Often the fibrils appear to be arranged in lines, the fibrils in the lines are in contact, with spaces between the lines, some interfibrillar material can also be seen. × 151,500 magnification.

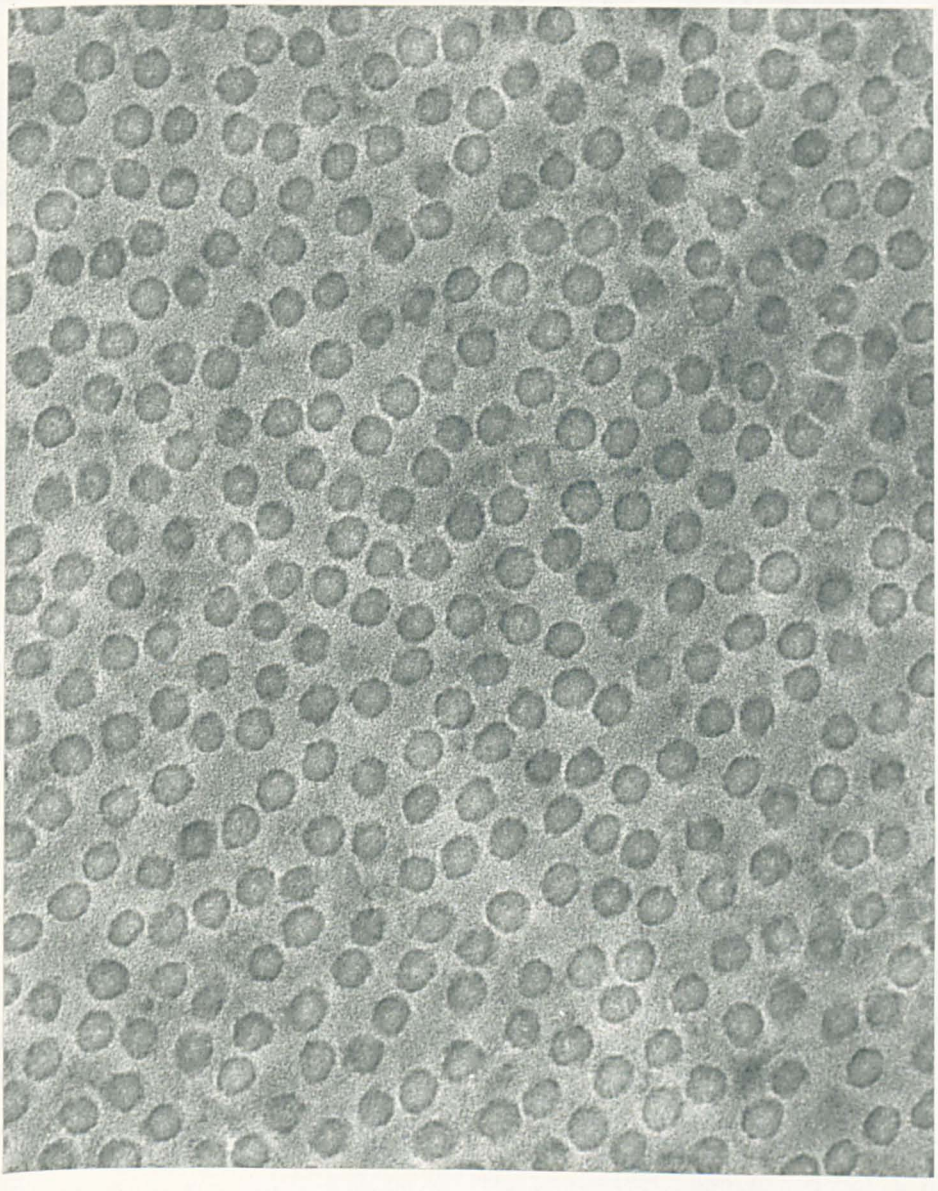

Figure 4.7 TEM micrograph of bovine cornea embedded in Lowicryl and stained with uranyl acetate and PTA. The fibrils have a large range of spacings, and the ground substance between the fibrils appears very dense when compared to Figure 4.4. ×151,500 magnification.

4.3 Scanning Electron Microscopy

As the effects of fixation, post-fixation and ethanol dehydration have been covered in the previous section, this section on SEM preparation will be confined to the effect of critical point drying.

4.3.1 Critical Point Drying

Processing Run SEM 1

Table 4.10 shows the effect of critical point drying on corneas during processing run SEM 1. The conclusions are summarized as follows.

1. There was a significant ($p<0.01$) decrease (23.1%) in interfibrillar spacing.
2. There was a significant ($p<0.0002$) decrease (28.7%) in intermolecular spacing.
3. There was a significant ($p>0.0002$) decrease (18.8%) in D-period spacing.

Processing stage	Interfibrillar spacing(nm)	Intermolecular spacing(nm)	D-period spacing(nm)
100% Ethanol (n=2)	62.3 ± 1.6	1.87 ± 0.13	64.17 ± 0.19
C.P. Dried (n=2)	47.9 ± 2.1	1.29 ± 0.01	52.09 ± 0.57

Table 4.10 Changes occurring in bovine corneal stroma during critical point drying in processing run SEM 1, n is the number of specimens used.

Processing Run SEM 2

Table 4.11 shows the effect of critical point drying on corneas during processing run SEM 2. The changes are summarized as follows.

1. There is a significant ($p<0.05$) decrease (15.1%) in interfibrillar spacing.
2. There is a significant ($p<0.02$) reduction (26%) in intermolecular spacing.
3. There is a significant ($p>0.001$) decrease (10.3%) in D-period spacing.

Processing stage	Interfibrillar spacing(nm)	Intermolecular spacing(nm)	D-period spacing(nm)
100% Ethanol (n=2)	63.6 ± 4.1	1.94 ± 0.20	64.07 ± 0.09
C.P. Dried (n=2)	54.0 ± 1.1	1.43 ± 0.04	57.46 ± 0.08

Table 4.11 Changes occurring in bovine corneal stroma during critical point drying in processing run SEM 2, n is the number of specimens used.

4.3.2 Overall Changes

The changes in the various spacings during processing runs SEM 1 and SEM 2 are represented graphically.

Figure 4.8 compares the changes in interfibrillar spacing that occur during processing runs SEM 1 and SEM 2. Figure 4.9 compares the changes that occur in intermolecular spacing during processing runs SEM 1 and SEM 2. While Figure 4.10 compares the changes that occur in D-period spacing during processing runs SEM 1 and SEM 2.

The overall changes in bovine corneal stroma between the stages of fresh to critically point dried, are also compared statistically is this section.

Processing Run SEM 1

1. There is a significant ($p<0.0001$) decrease (24.9%) in interfibrillar spacing.
2. There is a significant ($p<0.0001$) reduction (25.0%) in intermolecular spacing.
3. There is a significant ($p<0.0001$) decrease (19.8%) in D-period spacing.

Processing Run SEM 2

1. There is a significant ($p<0.0001$) decrease (15.4%) in the interfibrillar spacing.
2. There is a significant ($p<0.0001$) reduction (16.9%) in intermolecular spacing.
3. There is a significant ($p<0.0001$) decrease (11.5%) in D-period spacing.

4.3.3 Comparison of Processing Runs

This section compares the critical point dried bovine corneas from processing runs SEM 1 and SEM 2, the differences are summarized as follows.

1. There is a significantly ($p<0.05$) lower (11.3%) interfibrillar spacing for corneas prepared by processing run SEM 1 compared to those prepared by processing run SEM 2.
2. There is a significantly ($p<0.02$) lower (10.8%) intermolecular spacing for corneas prepared by processing run SEM 1 compared to SEM 2.
3. There is a significantly ($p<0.005$) lower (10.2%) D-period spacing for corneas prepared by processing run SEM 1 compared to SEM 2.

4.3.4 Summary of Processing Changes

It is apparent that virtually every stage in processing for electron microscopy produces significant changes in the cornea. Glutaraldehyde fixation causes a significant increase in intermolecular spacings; while ethanol dehydration, resin infiltration and resin polymerization each cause shrinkage in all of the spacings monitored. Critical point drying for SEM specimens causes massive shrinkage, but is still preferable to air drying which results in total loss of the interfibrillar pattern. Perhaps the most drastic effect is caused by post-fixation in osmium tetroxide which completely destroys the intermolecular pattern, and appears to increase the amount of shrinkage which occurs during later stages of processing.

The processing schedule that produces least changes in spacings for TEM specimens was found to involve extended fixation in glutaraldehyde followed by low-temperature embedding in Lowicryl resin.

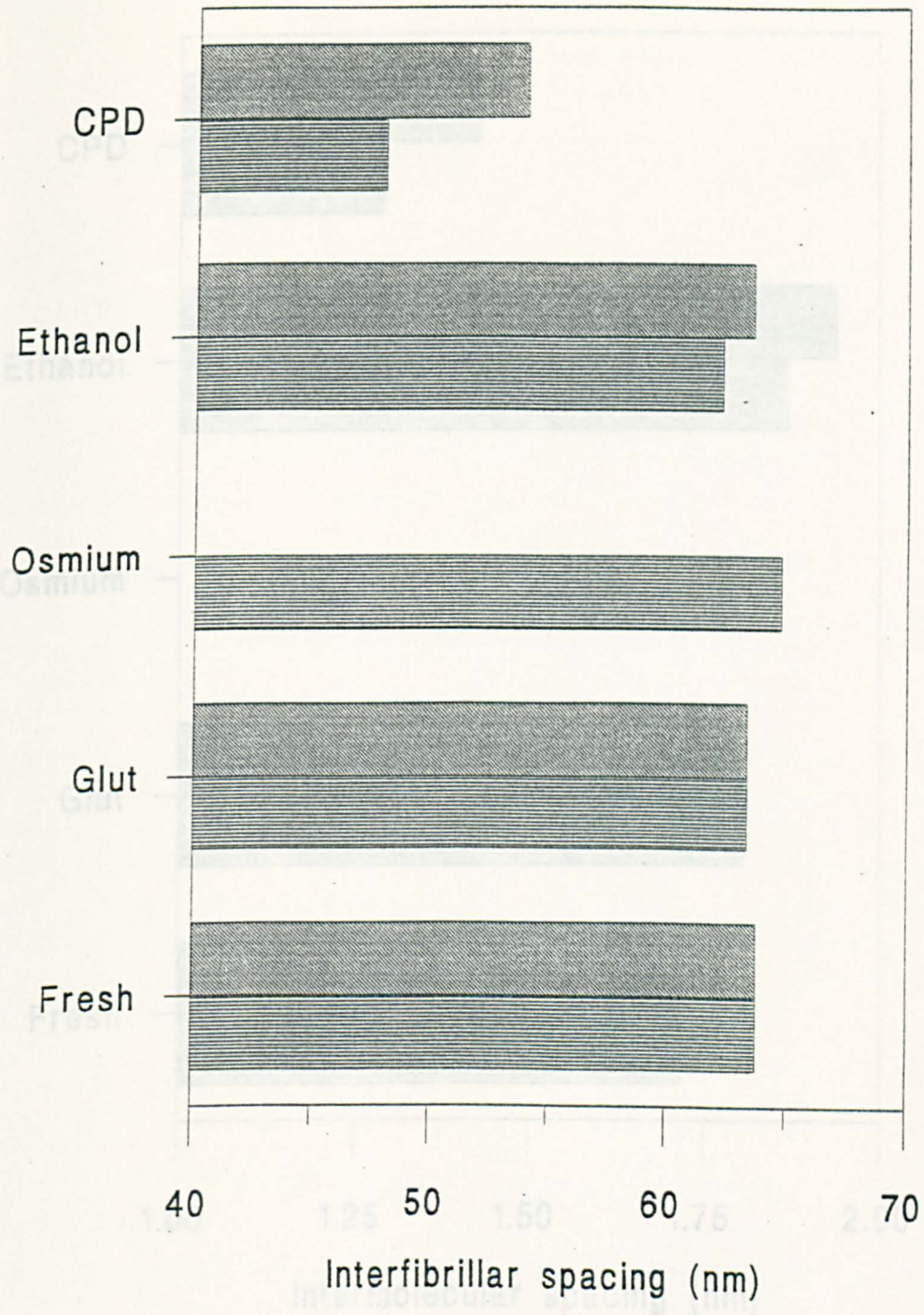

Figure 4.8 Histogram showing the changes that occur in interfibrillar spacing in the bovine cornea during processing runs SEM 1 (lower bars) and SEM 2 (upper bars).

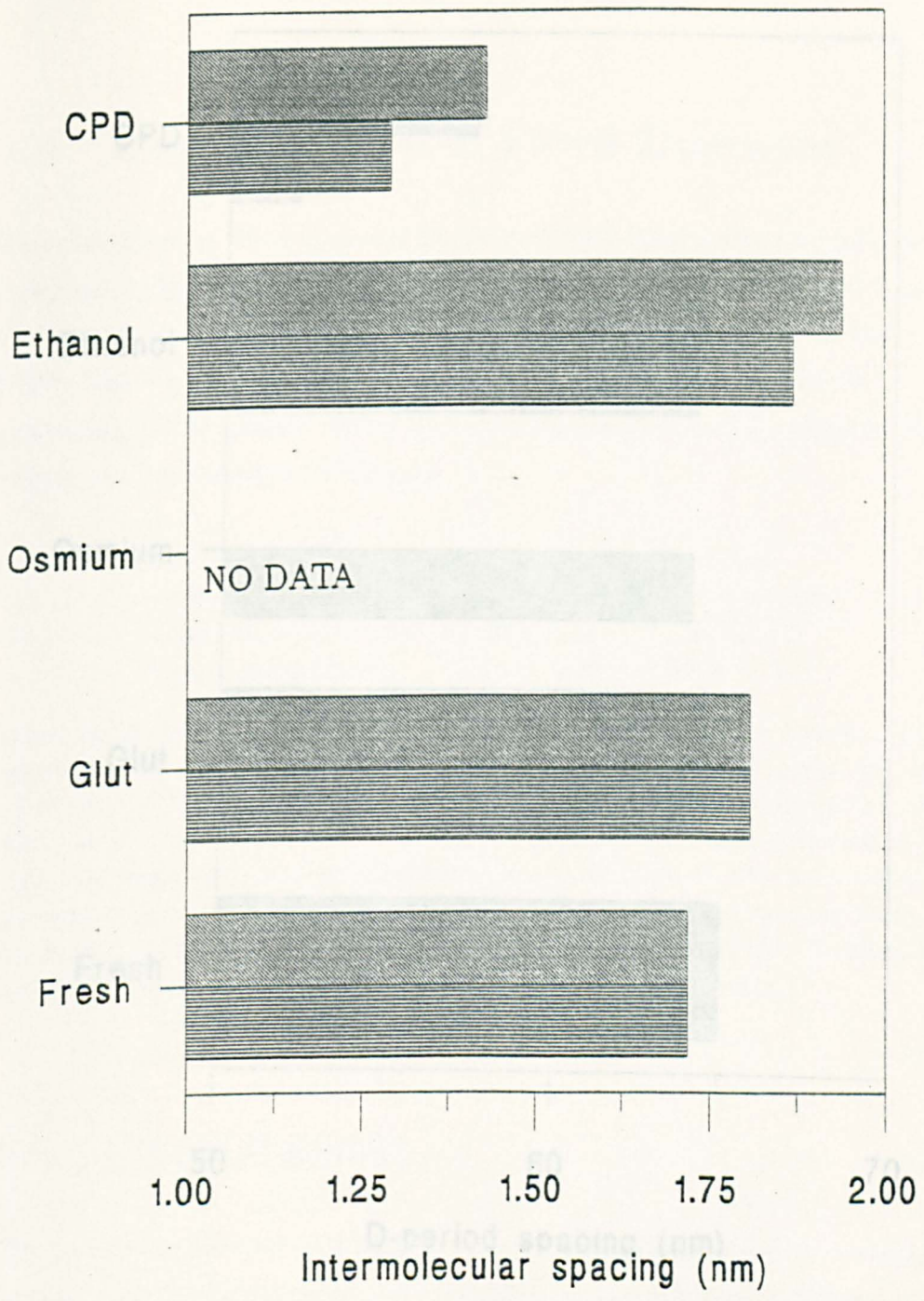

Figure 4.9 Histogram showing the changes that occur in intermolecular spacing in the bovine cornea during processing runs SEM 1 (lower bars) and SEM 2 (upper bars).

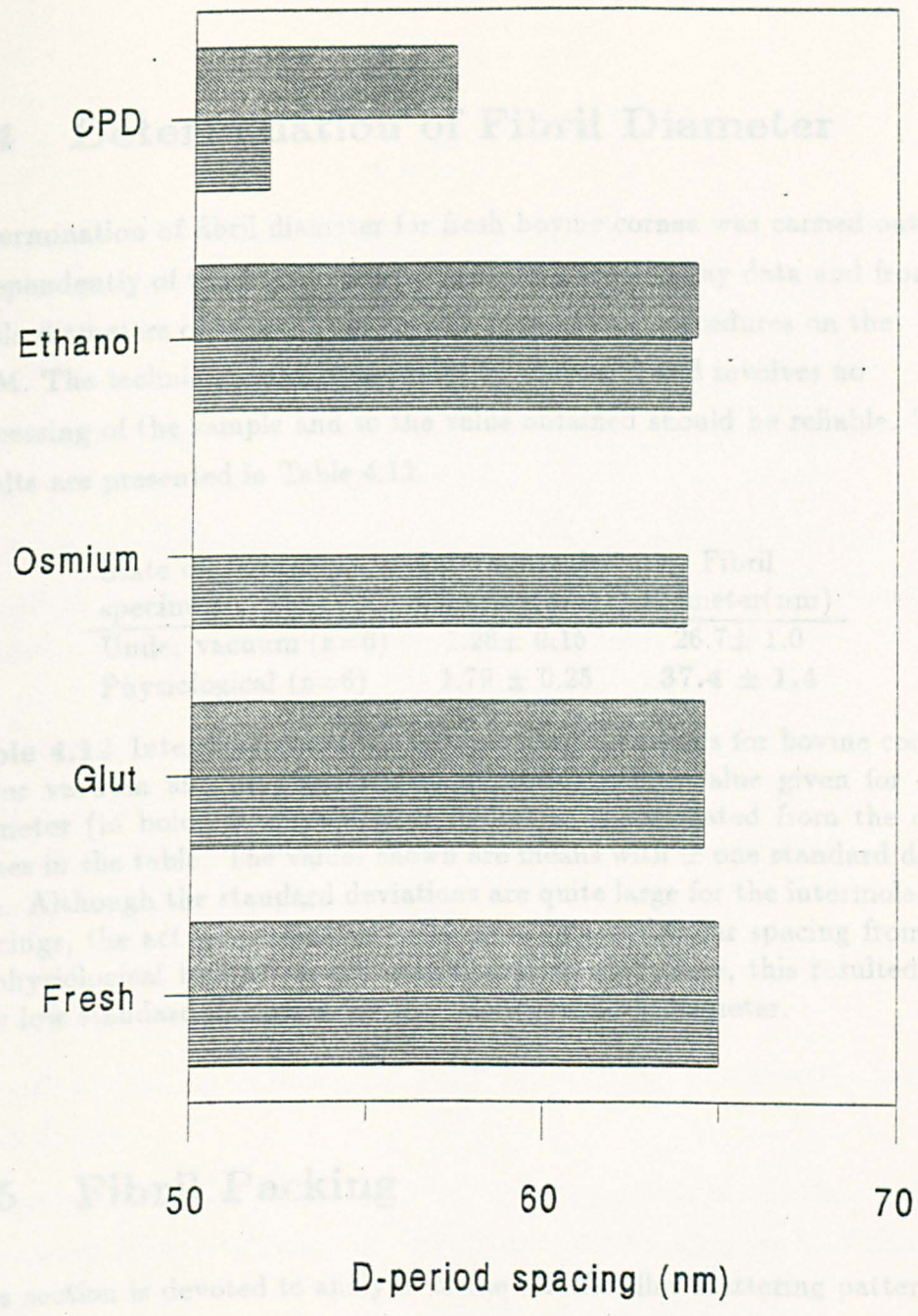

Figure 4.10 Histogram showing the changes that occur in D-period spacing in the bovine cornea during processing runs SEM 1 (lower bars) and SEM 2 (upper bars).

4.4 Determination of Fibril Diameter

Determination of fibril diameter for fresh bovine cornea was carried out independently of the fibril diameter modelling from X-ray data and from fibrils diameters obtained from various preparation procedures on the TEM. The technique used is described in chapter 2 and involves no processing of the sample and so the value obtained should be reliable. The results are presented in Table 4.12.

State of specimen	Intermolecular spacing(nm)	Fibril diameter(nm)
Under vacuum (n=6)	1.28± 0.15	26.7± 1.0
Physiological (n=6)	1.79 ± 0.25	**37.4 ± 1.4**

Table 4.12 Intermolecular spacings and fibril diameters for bovine corneas under vacuum and at physiological hydration. The value given for fibril diameter (in bold) at physiological hydration is calculated from the other values in the table. The values shown are means with ± one standard deviation. Although the standard deviations are quite large for the intermolecular spacings, the actual percentage increase in intermolecular spacing from dry to physiological hydration was very similar in all 6 cases, this resulted in a very low standard deviation for the calculated fibril diameter.

4.5 Fibril Packing

This section is devoted to analysis of the interfibrillar scattering patterns of corneas after being processed for transmission and scanning electron microscopy.

4.5.1 Determination of type of packing

The normalized scattered intensity ($I(kR_f)$) for a system of short range order (such as the cornea) is given as the product as two functions:

$$I(kR_f) = F^2(kR_f)\, T(2\gamma kR_f),$$

where

$$k = \frac{4\pi}{\lambda} \sin\theta,$$

2θ is the scattering angle, λ is the wavelength of the incident X-ray beam, R_f is the collagen fibril radius, and

$$\gamma = \frac{d}{2R_f}$$

is the swelling parameter with d being the centre to centre separation between nearest-neighbour collagen fibrils.

$F(kR_f)$ is the normalized intensity for a single collagen fibril and the normalized scattering intensity for a single fibril ($I(kR_f)$) can be calculated as follows (Bear and Bolduan, 1950; Oster and Riley, 1952):.

$$I(kR_f) = \left(\frac{2J_1(kR_f)}{kR_f}\right)^2,$$

where J_1 is the first-order Bessel function.
This equation is based on the assumptions that the collagen fibrils are infinitely long rods of uniform density.

Figure 4.11 shows the normalized scattering intensity, or fibril transform, calculated for a single fibril.

$T(2\gamma kR_f)$ is the normalized interference function that describes the packing of the fibrils.

The scattered intensity function, $T(u)$, from aggregates of cylinders with short-range order result from the interference from aggregates of N fibrils (Vainshtein 1966).

For $N = 2$

$$T(u) = \frac{1}{2^2}[2 + 2J_0(u)]$$

For $N = 5$

$$T(u) = \frac{1}{5^2}[5 + 14J_0(u) + 4J_0(u\sqrt{3}) + 2J_0(2u)]$$

For $N = 19$

$$\begin{aligned} T(u) \;=\; & \frac{1}{19^2}[19 + 84J_0(u) + 60J_0(u\sqrt{3}) + 54J_0(2u) + 74J_0(u\sqrt{7}) + \\ & 24J_0(3u) + 24J_0(u\sqrt{13}) + 18J_0(2u\sqrt{3}) + 6J_0(4u)] \end{aligned}$$

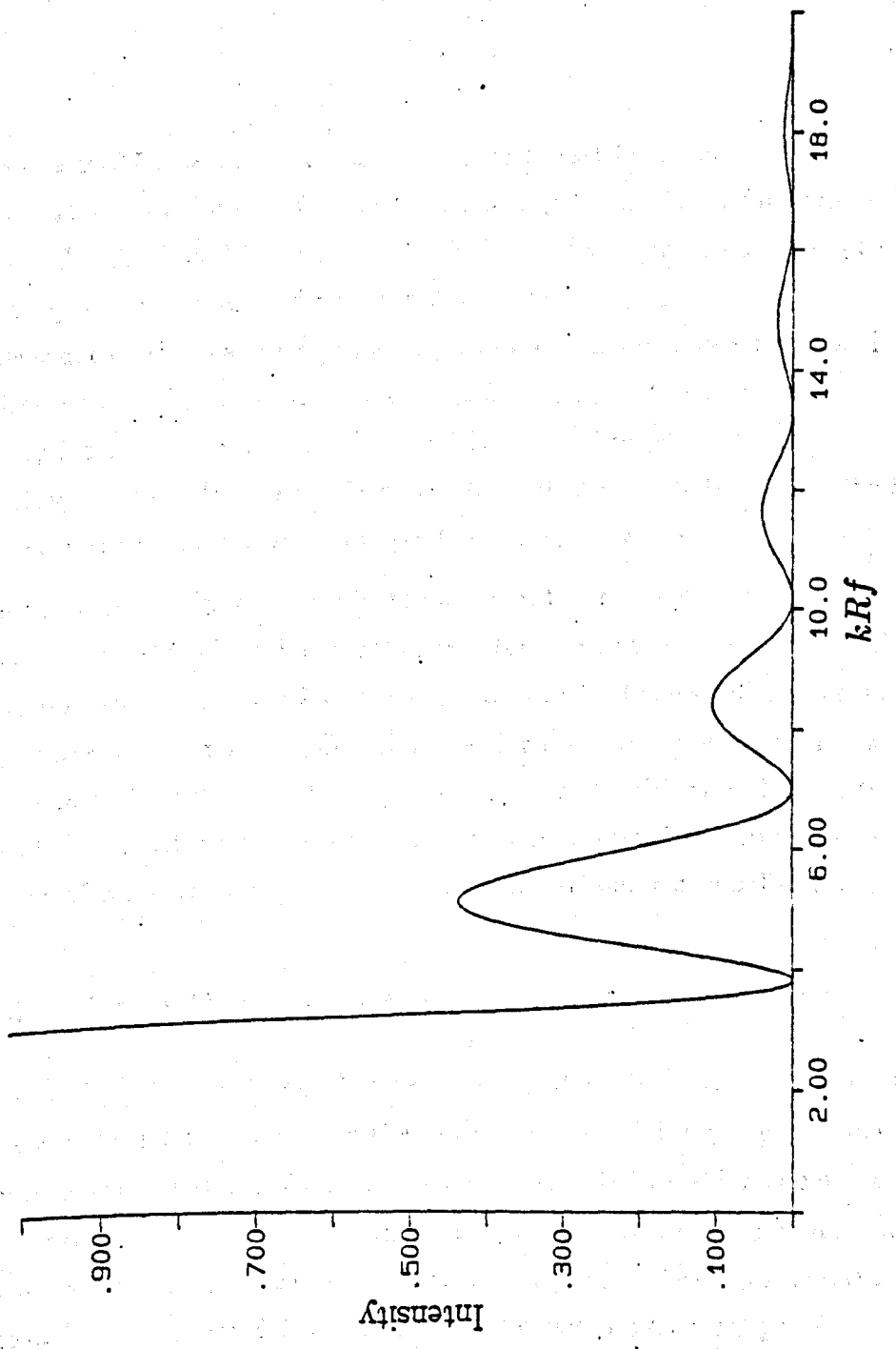

Figure 4.11 Interfibrillar scattering intensity (fibril transform) for a single collagen fibril.

where $u = 2\gamma k R_f$ and J_0 is the zeroth order Bessel function.
Figure 4.12 shows the interference function, $T(u)$, calculated for various values of N. At $N = 19$ the positions of the peaks begin to correspond to scattering by an unbounded hexagonal lattice.
The product of the scattering intensity from a single collagen fibril, and the interference function from the packing of fibrils, gives the scattering intensity for the whole cornea. Figure 4.13 shows the product of the scattering intensity from a single collagen fibril of fibril radius 20nm, and the interference function from the packing of fibrils when N=5.

There are three main variables in the system, the number of fibrils in the packing aggregate, N, which affects the interference function; and the fibril radius, R_f, which affects the scattering intensity, and the swelling parameter γ. By experimenting with different values for these parameters it is possible to produce a theoretical scattering intensity curve which is a close fit to an experimental scattering intensity curve, and consequently derive estimates for order of packing and fibril diameter for a particular corneal sample.

4.5.2 Fresh Bovine Cornea

Sayers et al., (1982) obtained low-angle X-ray data from fresh bovine cornea and found that typically the positions of the 3 intensity maxima occur respectively at 0.017nm^{-1}, 0.042nm^{-1} and 0.074nm^{-1} respectively. These positions do not index exactly on a regular lattice, suggesting that the scattering pattern is caused by short-range order. Using these data, additional data collected from fresh bovine corneas over a range of hydrations (H=0.5 to 13.5), and the equations detailed in the previous section, Sayers et al., (1982) proposed two possible models for fresh bovine cornea at physiological hydration. The first of the models required a fibril diameter of 52nm at physiological hydration; this figure is incompatible with the value of 37.4±1.4nm obtained for fibril diameter during the course of this investigation, consequently this model is rejected. The second model proposed by Sayers et al., has a fibril diameter of ~40nm. This is in close

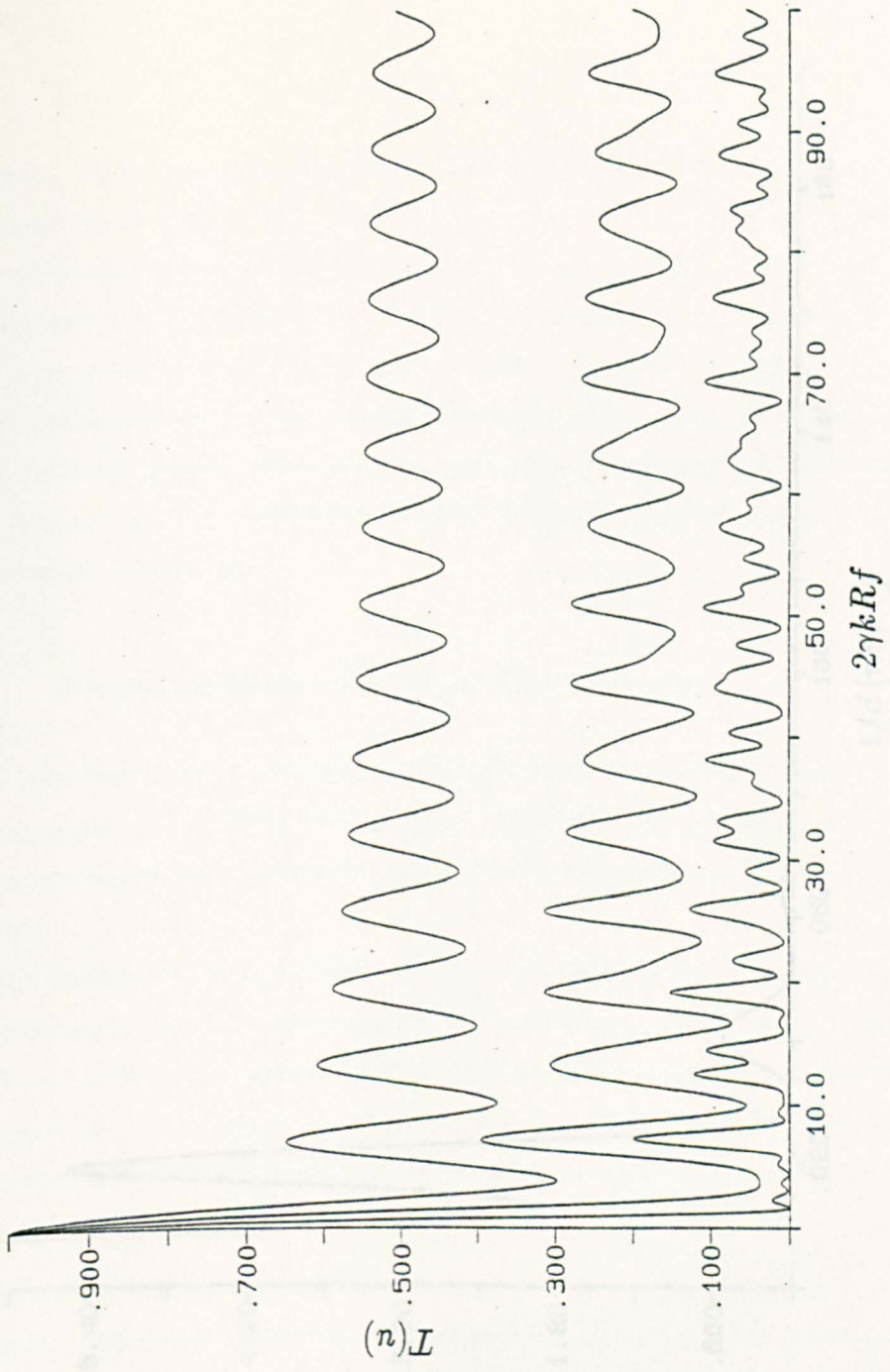

Figure 4.12 Interference function $T(u)$ for $N = 2$ (top), $N = 5$ (middle) and $N = 19$ (bottom).

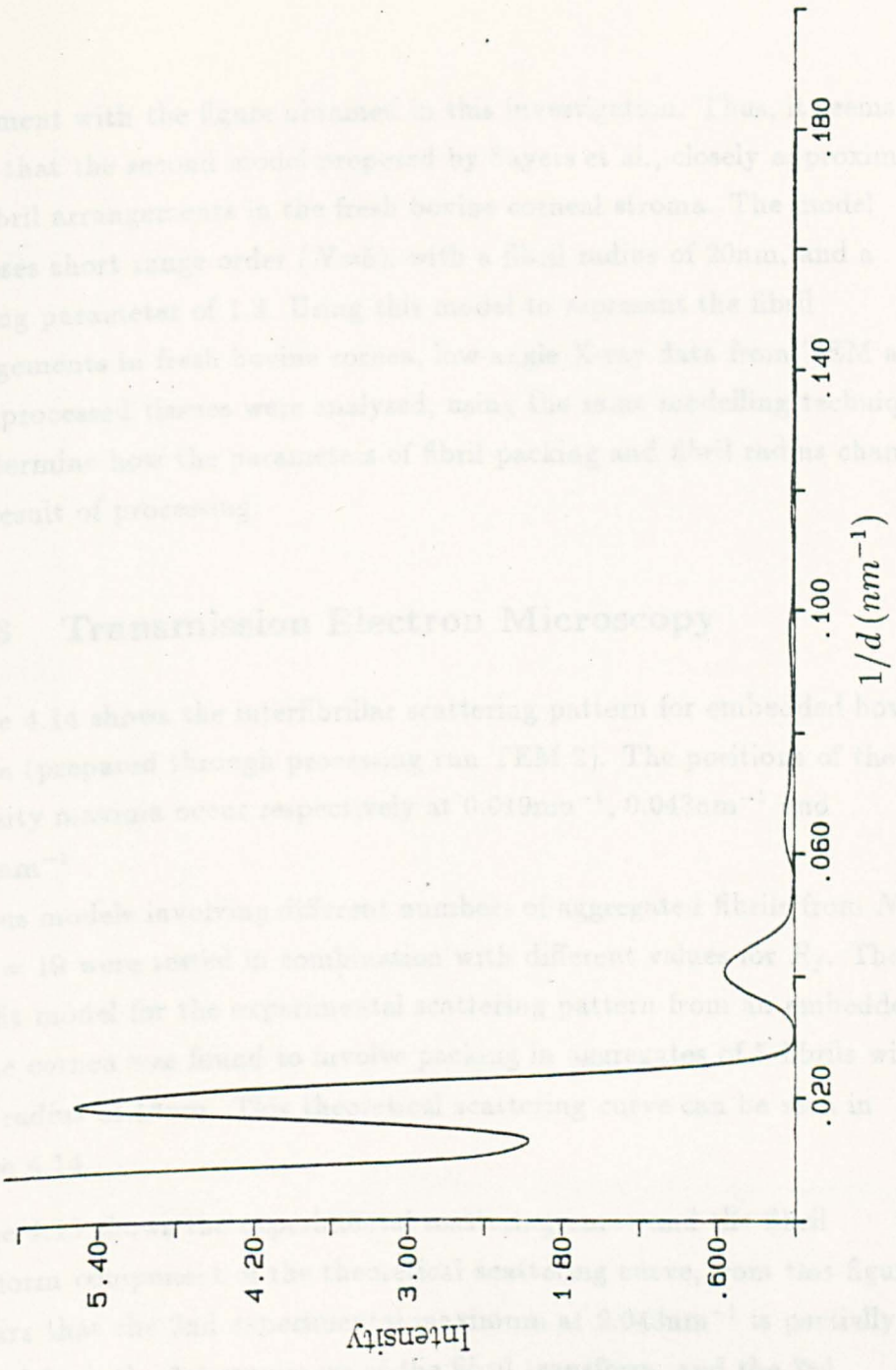

Figure 4.13 Theoretical scattering intensity curve with the values $R_f = 20nm$ and $N = 5$

agreement with the figure obtained in this investigation. Thus, it seems likely that the second model proposed by Sayers et al., closely approximates the fibril arrangements in the fresh bovine corneal stroma. The model proposes short range order (N=5), with a fibril radius of 20nm, and a swelling parameter of 1.3. Using this model to represent the fibril arrangements in fresh bovine cornea, low-angle X-ray data from TEM and SEM processed tissues were analysed, using the same modelling techniques, to determine how the parameters of fibril packing and fibril radius change as a result of processing.

4.5.3 Transmission Electron Microscopy

Figure 4.14 shows the interfibrillar scattering pattern for embedded bovine cornea (prepared through processing run TEM 2). The positions of the 3 intensity maxima occur respectively at 0.019nm^{-1}, 0.043nm^{-1} and 0.076nm^{-1}.
Various models involving different numbers of aggregated fibrils from $N = 2$ to $N = 19$ were tested in combination with different values for R_f. The best-fit model for the experimental scattering pattern from an embedded bovine cornea was found to involve packing in aggregates of 5 fibrils with a fibril radius of 18nm. This theoretical scattering curve can be seen in Figure 4.14.

Figure 4.15 shows the experimental scattering curve and the fibril transform component of the theoretical scattering curve, from this figure it appears that the 2nd experimental maximum at 0.043nm^{-1} is partially derived from the 1st maximum of the fibril transform, and the 3rd experimental maximum at 0.076nm^{-1} is mostly derived from the 2nd maximum of the fibril transform.

Figure 4.16 shows the experimental scattering curve and the packing ($N = 5$) component of the theoretical scattering curve from this figure it is clear that the 1st experimental maximum at 0.019nm^{-1} is derived from the 1st maximum of the interference function, although this is shifted slightly

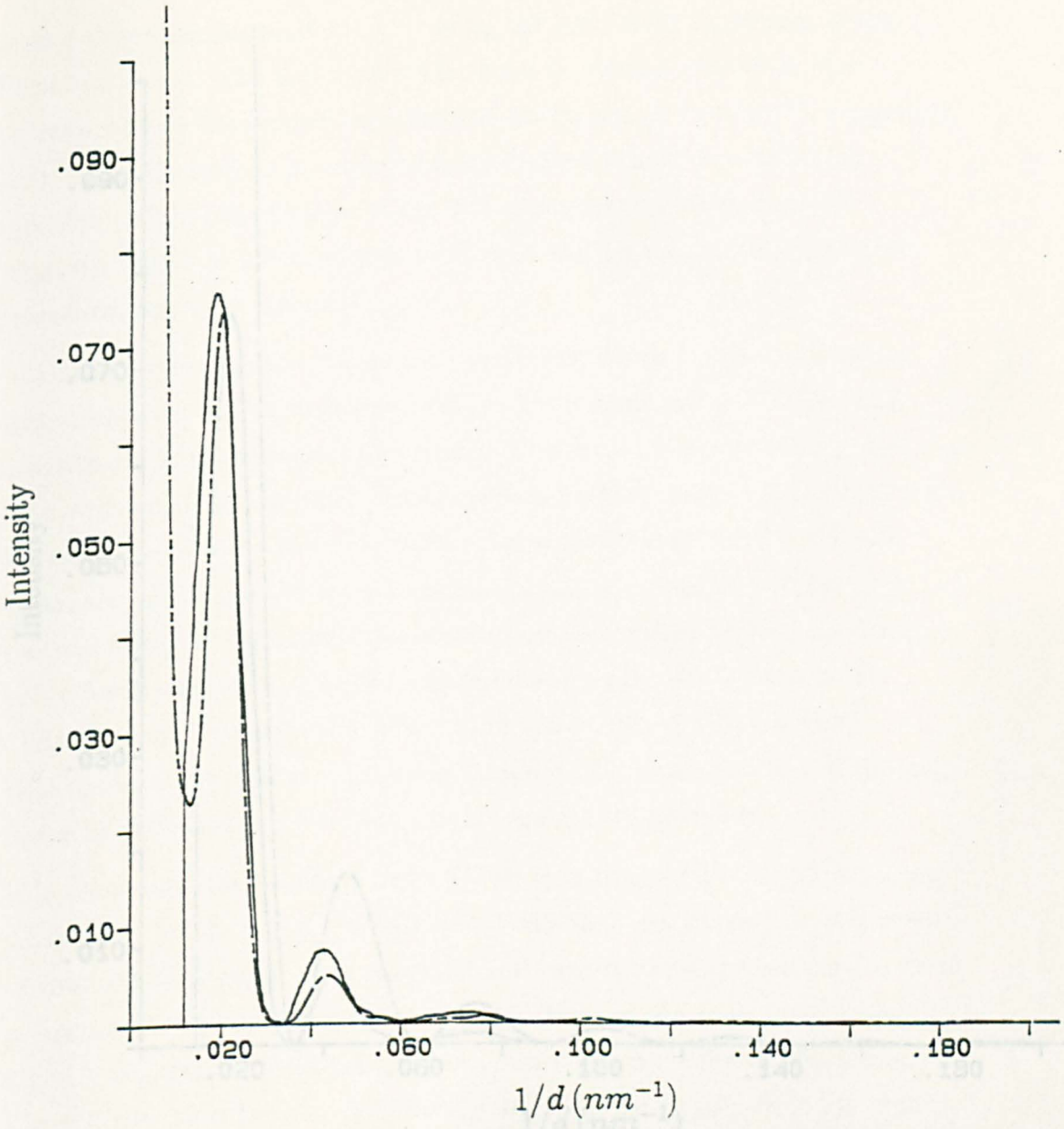

Figure 4.14 Experimental (solid line) and best-fit theoretical (dotted line) scattering curves for embedded cornea. The best-fit model has values of $R_f = 18nm$ and $N = 5$

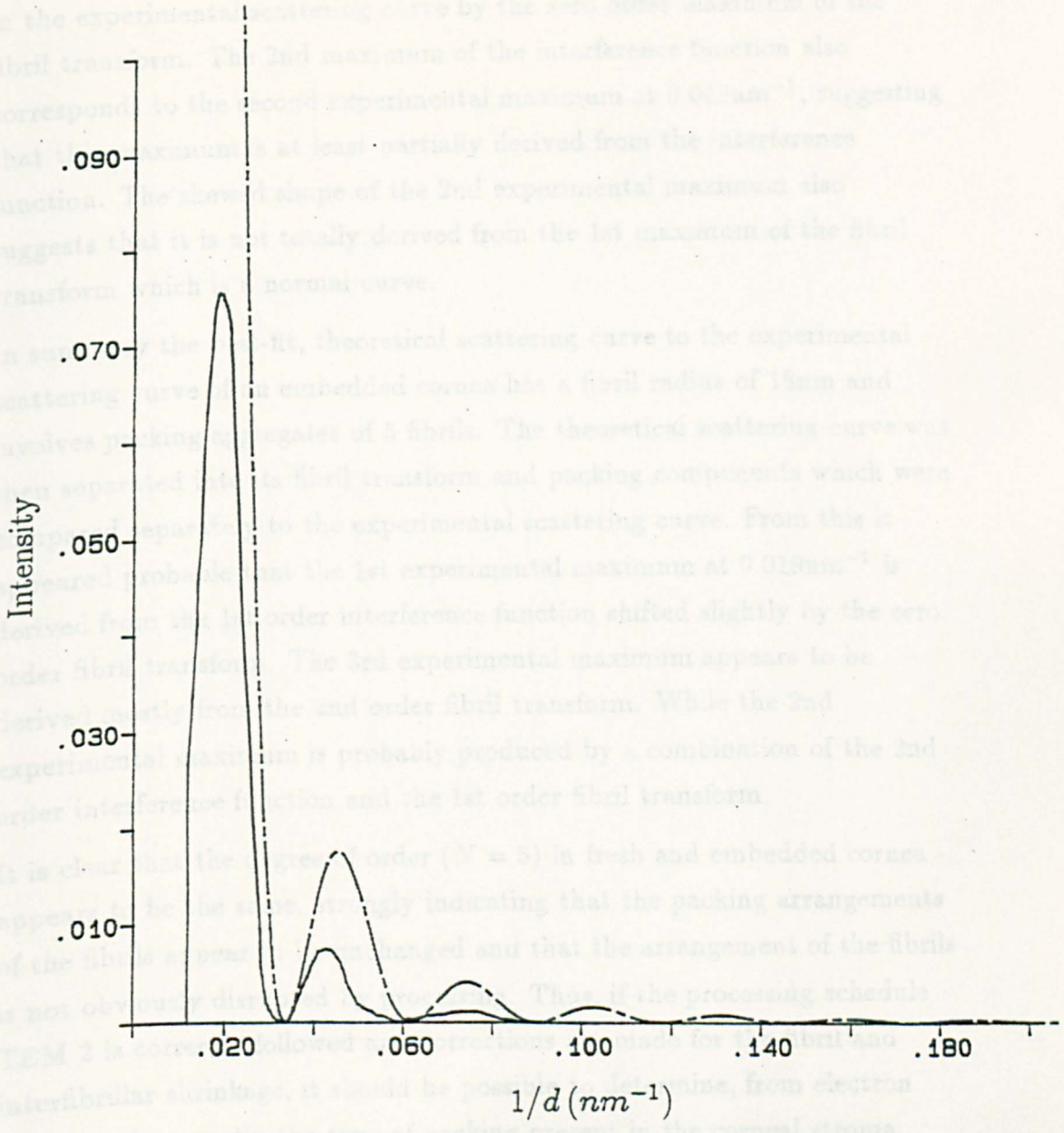

Figure 4.15 Experimental scattering curve (solid line) for embedded cornea and theoretical fibril transform (dotted line) for $R_f = 18nm$

in the experimental scattering curve by the zero order maximum of the fibril transform. The 2nd maximum of the interference function also corresponds to the second experimental maximum at 0.043nm^{-1}, suggesting that this maximum is at least partially derived from the interference function. The skewed shape of the 2nd experimental maximum also suggests that it is not totally derived from the 1st maximum of the fibril transform which is a normal curve.

In summary the best-fit, theoretical scattering curve to the experimental scattering curve of an embedded cornea has a fibril radius of 18nm and involves packing aggregates of 5 fibrils. The theoretical scattering curve was then separated into its fibril transform and packing components which were compared separately to the experimental scattering curve. From this it appeared probable that the 1st experimental maximum at 0.019nm^{-1} is derived from the 1st order interference function shifted slightly by the zero order fibril transform. The 3rd experimental maximum appears to be derived mostly from the 2nd order fibril transform. While the 2nd experimental maximum is probably produced by a combination of the 2nd order interference function and the 1st order fibril transform.

It is clear that the degree of order ($N = 5$) in fresh and embedded cornea appears to be the same, strongly indicating that the packing arrangements of the fibrils appear to be unchanged and that the arrangement of the fibrils is not obviously disrupted by processing. Thus, if the processing schedule TEM 2 is correctly followed and corrections are made for the fibril and interfibrillar shrinkage, it should be possible to determine, from electron micrographs, exactly the type of packing present in the corneal stroma.

This finding of short-range order with $\sim$4 nearest neighbours in embedded material can be interpretated two ways. It is possible that the fibrils are packed in aggregates of $N = 5$ and that the aggregates are distinctly separated from each other. Alternatively, the fibrils could be uniformly distributed in the stroma, but in a relatively disordered arrangement, so that on average the order does not extend beyond groups of $\sim$5 fibrils. It is

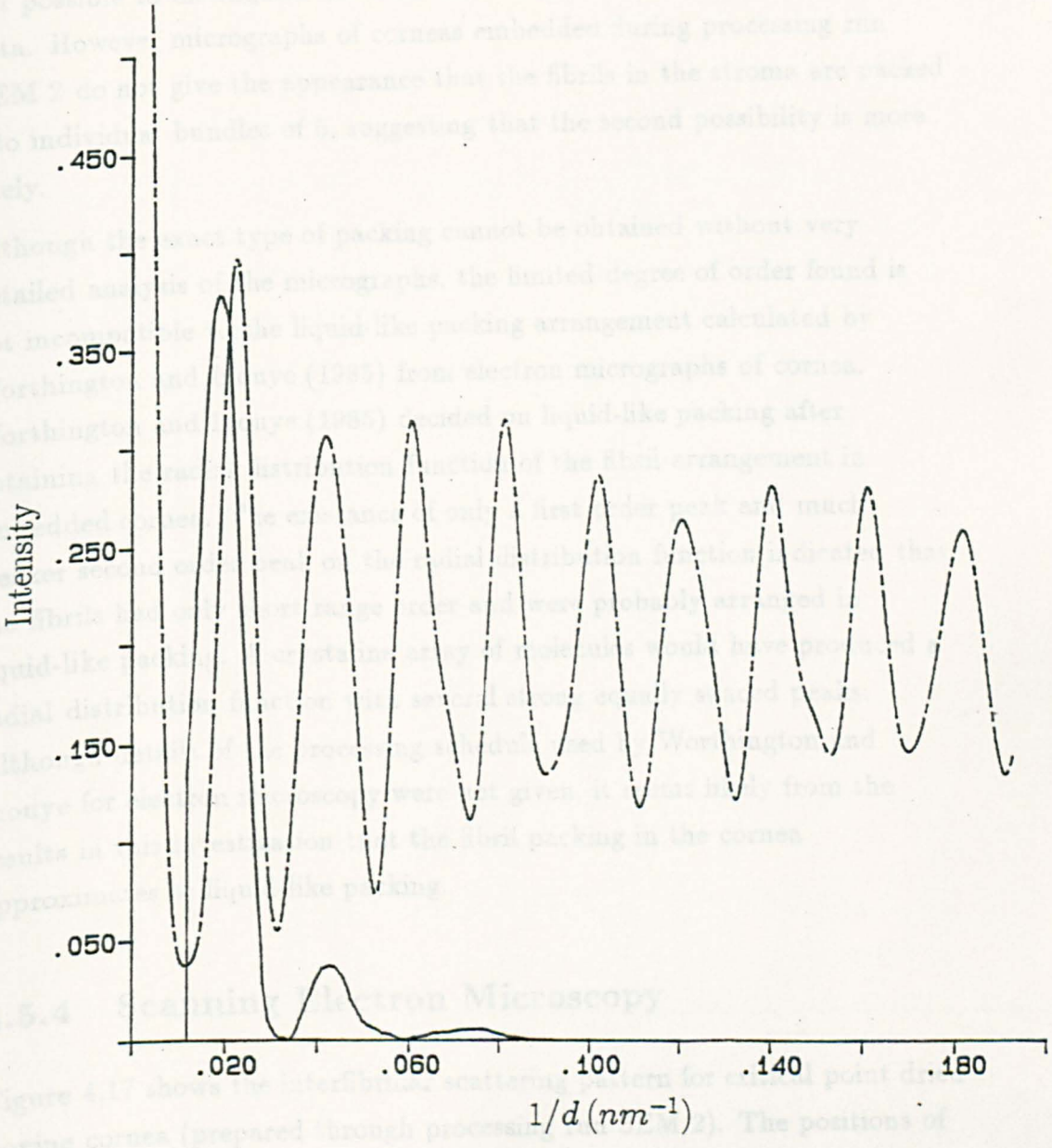

Figure 4.16 Experimental scattering curve (solid line) for embedded cornea and theoretical scattering curve (dotted line) for packing aggregates of $N = 5$

not possible to distinguish between the two possibilities with just the X-ray data. However micrographs of corneas embedded during processing run TEM 2 do not give the appearance that the fibrils in the stroma are packed into individual bundles of 5, suggesting that the second possibility is more likely.

Although the exact type of packing cannot be obtained without very detailed analysis of the micrographs, the limited degree of order found is not incompatible to the liquid-like packing arrangement calculated by Worthington and Inouye (1985) from electron micrographs of cornea. Worthington and Inouye (1985) decided on liquid-like packing after obtaining the radial distribution function of the fibril arrangement in embedded cornea. The existance of only a first order peak and much weaker second order peak on the radial distribution function indicated that the fibrils had only short range order and were probably arranged in liquid-like packing. A crystaline array of molecules would have produced a radial distribution function with several strong equally spaced peaks. Although details of the processing schedule used by Worthington and Inouye for electron microscopy were not given, it seems likely from the results in this investigation that the fibril packing in the cornea approximates to liquid-like packing.

4.5.4 Scanning Electron Microscopy

Figure 4.17 shows the interfibrillar scattering pattern for critical point dried bovine cornea (prepared through processing run SEM 2). The positions of the 3 intensity maxima occur respectively at 0.23nm^{-1}, 0.054nm^{-1} and 0.094nm^{-1}.

Various models involving different numbers of aggregated fibrils from $N = 2$ to $N = 19$ were tested in combination with different values for R_f. The best-fit model for the experimental scattering pattern from a critical point dried bovine cornea was found to involve packing in aggregates of 5 fibrils with a fibril radius of 15nm. This theoretical scattering curve can be seen

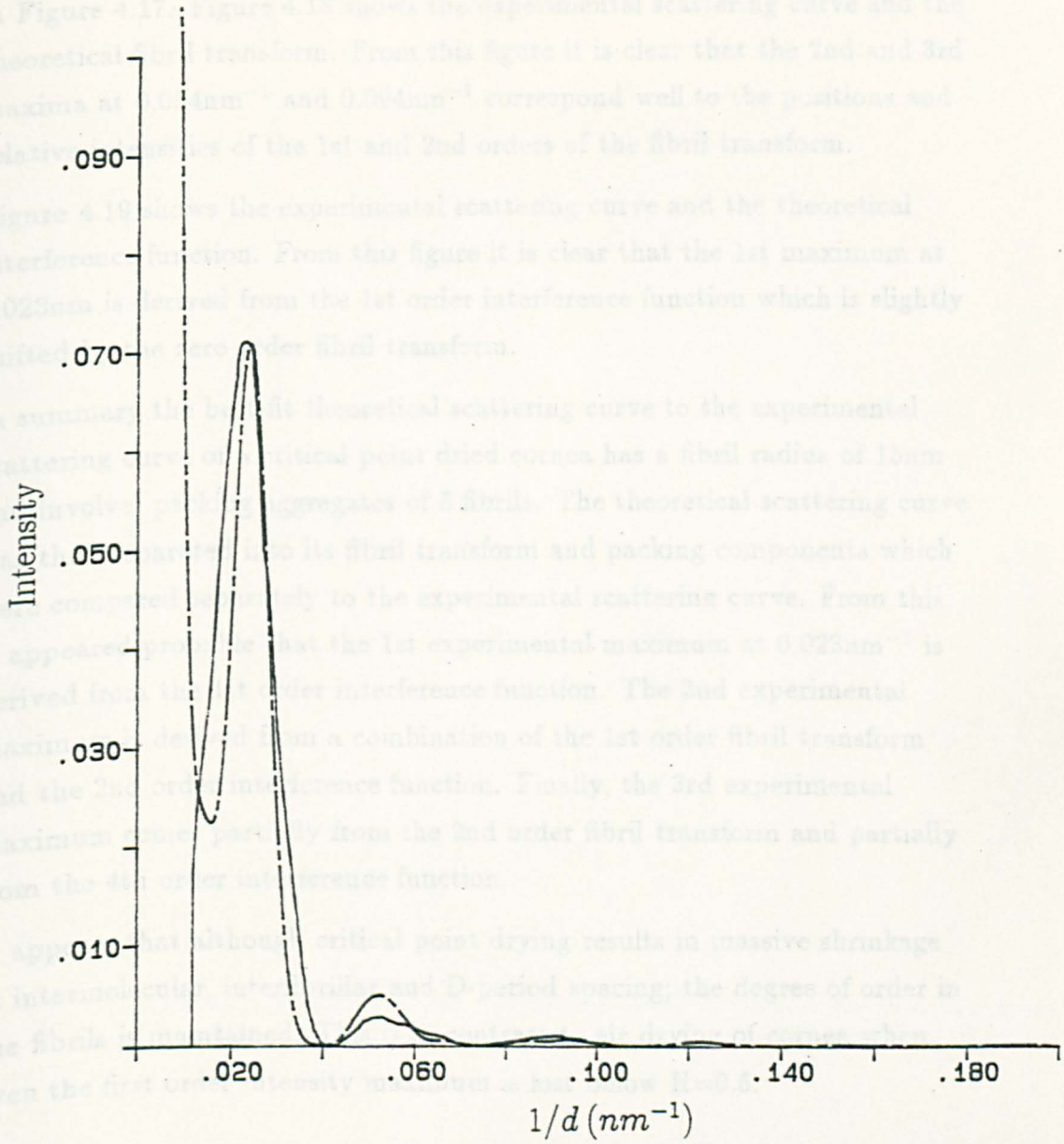

Figure 4.17 Experimental (solid line) and best-fit theoretical (dotted line) scattering curves for critically point dried bovine cornea, the best-fit model has values of $R_f = 15nm$ and $N = 5$

in Figure 4.17. Figure 4.18 shows the experimental scattering curve and the theoretical fibril transform. From this figure it is clear that the 2nd and 3rd maxima at $0.054nm^{-1}$ and $0.094nm^{-1}$ correspond well to the positions and relative intensities of the 1st and 2nd orders of the fibril transform.

Figure 4.19 shows the experimental scattering curve and the theoretical interference function. From this figure it is clear that the 1st maximum at 0.023nm is derived from the 1st order interference function which is slightly shifted by the zero order fibril transform.

In summary the best-fit theoretical scattering curve to the experimental scattering curve of a critical point dried cornea has a fibril radius of 15nm and involves packing aggregates of 5 fibrils. The theoretical scattering curve was then separated into its fibril transform and packing components which were compared separately to the experimental scattering curve. From this it appeared probable that the 1st experimental maximum at $0.023nm^{-1}$ is derived from the 1st order interference function. The 2nd experimental maximum is derived from a combination of the 1st order fibril transform and the 2nd order interference function. Finally, the 3rd experimental maximum comes partially from the 2nd order fibril transform and partially from the 4th order interference function.

It appears that although critical point drying results in massive shrinkage in intermolecular, interfibrillar and D-period spacing; the degree of order in the fibrils is maintained. This is in contrast to air drying of cornea when even the first order intensity maximum is lost below H=0.5.

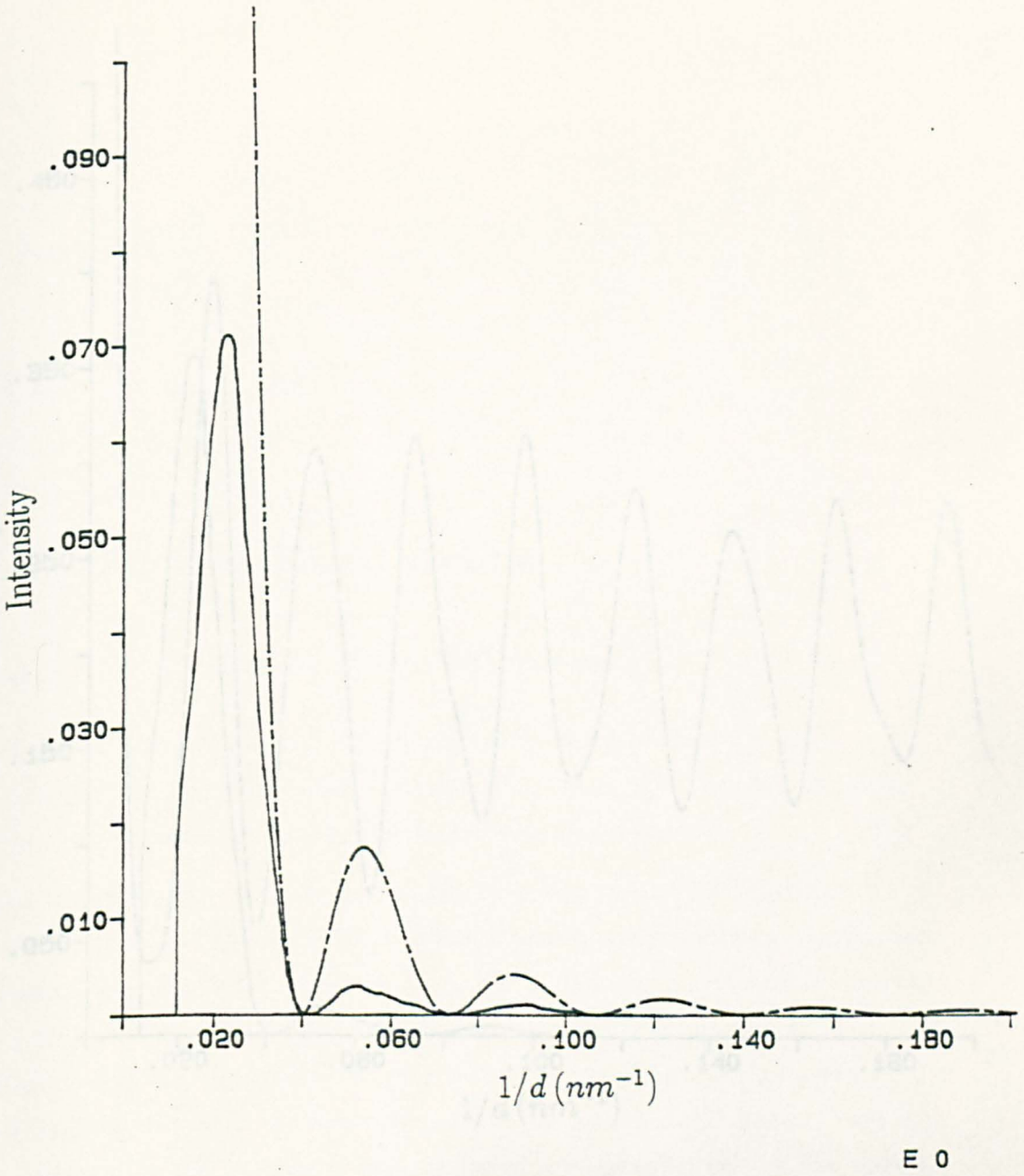

Figure 4.18 Experimental scattering curve (solid line) for critical point dried cornea and theoretical fibril transform (dotted line) for $R_f = 15nm$

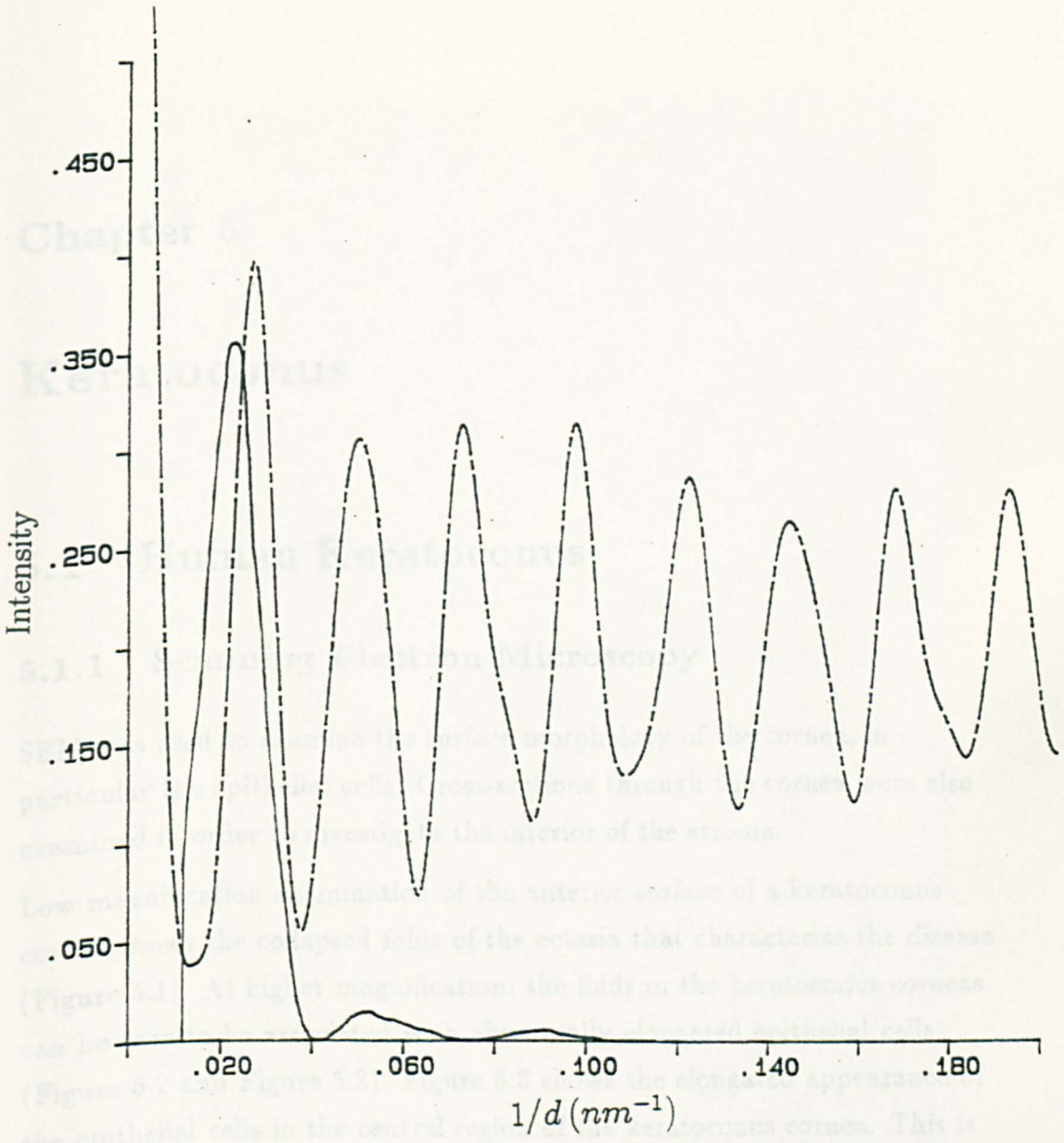

Figure 4.19 Experimental scattering curve (solid line) for critical point dried cornea and theoretical scattering curve (dotted line) for packing aggregates of $N = 5$

Chapter 5

Keratoconus

5.1 Human Keratoconus

5.1.1 Scanning Electron Microscopy

SEM was used to examine the surface morphology of the cornea, in particular the epithelial cells. Cross-sections through the cornea were also examined in order to investigate the interior of the stroma.

Low magnification examination of the anterior surface of a keratoconus cornea shows the collapsed folds of the ectasia that characterize the disease (Figure 5.1). At higher magnification, the folds in the keratoconus corneas can be seen to be associated with abnormally elongated epithelial cells (Figure 5.2 and Figure 5.3). Figure 5.3 shows the elongated appearance of the epithelial cells in the central region of the keratoconus cornea. This is in contrast to the hexagonal appearance of the epithelial cells of the normal cornea seen in Figure 5.4.

The central region of the keratoconus cornea also exhibits considerable thinning as seen in Figure 5.5. Examined in cross-section, it is clear that there are fewer lamellae in this central region. These are formed into Z-shaped folds as seen in Figure 5.6 in contrast to the flat, parallel lamellae seen in normal cornea (Figure 5.7).

Figure 5.1 Low magnification SEM micrograph of ectasia in the central region of a keratoconus cornea. $\times 120$ magnification.

Figure 5.2 SEM micrograph of the ectasia and epithelial cells in the central region of a keratoconus cornea. The cells associated with the ectasia appear abnormally elongated. ×1,800 magnification.

Figure 5.3 SEM micrograph of the epithelial cells from the central region of a keratoconus cornea, the epithelial cells appear abnormally elongated. $\times 3{,}500$ magnification.

Figure 5.4 SEM micrograph of the epithelial cells from the central region of a normal cornea. The epithelial cells have a normal hexagonal appearance. $\times$3,500 magnification.

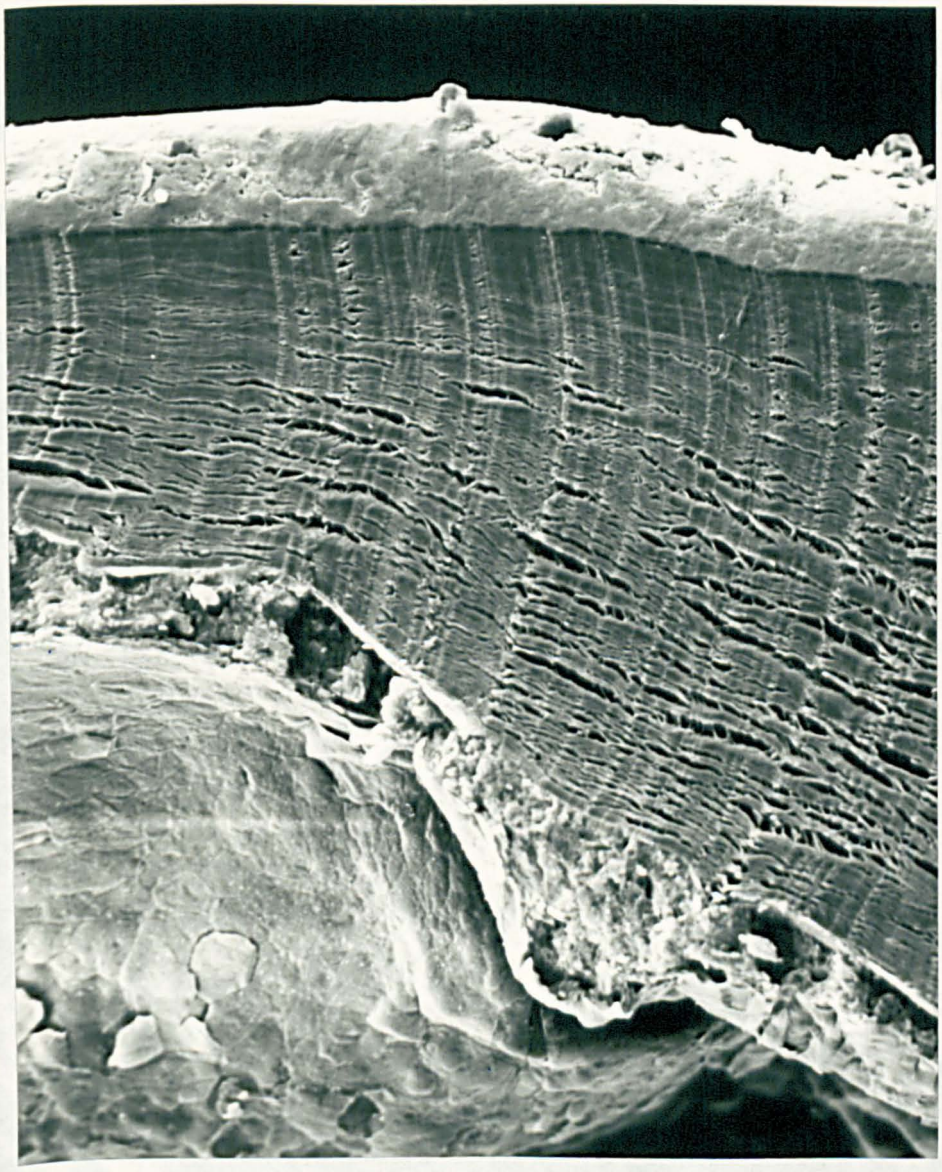

Figure 5.5 SEM micrograph of a transverse section through the stroma of a keratoconus cornea. The thinning of the stroma towards the centre of the cornea is clearly evident. $\times 50$ magnification.

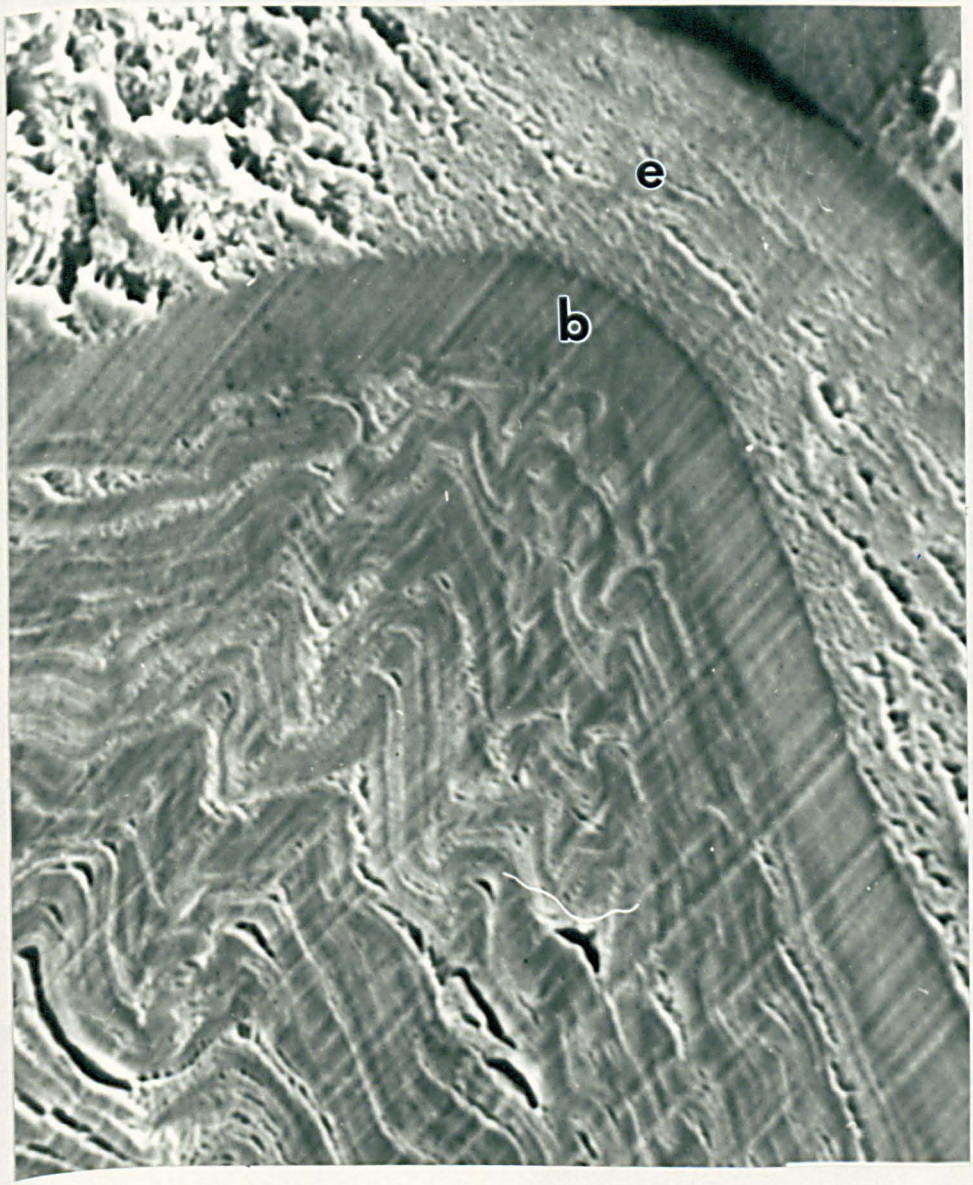

Figure 5.6 SEM micrograph of a transverse section through the central stroma of a keratoconus cornea. The epithelial layer (e) and Bowman's layer (b) can be seen at the top of the micrograph, and the abnormally 'Z' shaped lamellae are clearly visible. ×600 magnification.

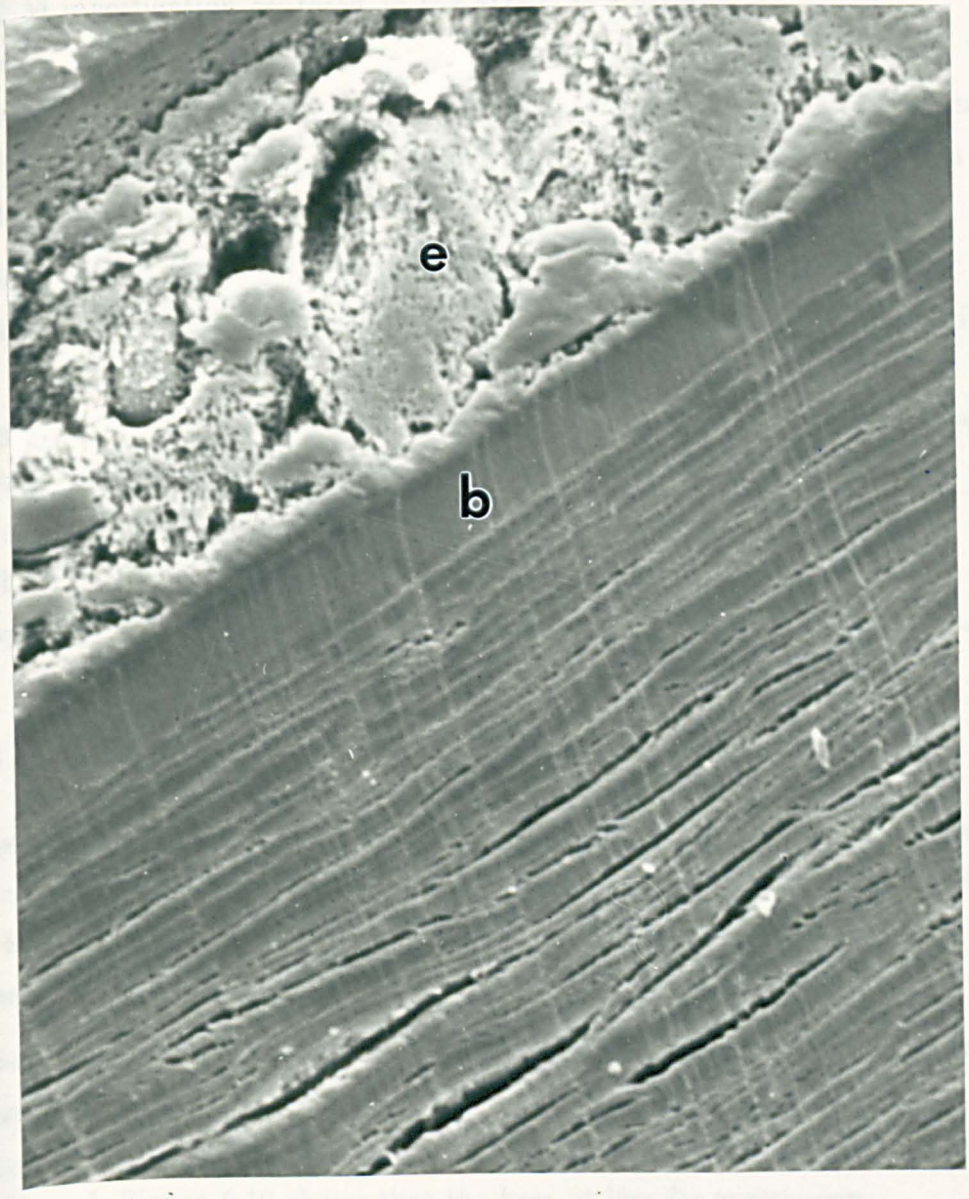

Figure 5.7 SEM micrograph of a transverse section through the central lamellae of a normal cornea. the epithelial layer (e) and Bowmans layer (b) can be seen at the top of the micrograph, and the lamellae can be seen to run parallel to the surface of the cornea. ×600 magnification.

5.1.2 Transmission Electron Microscopy

TEM investigation centered on the nature and distribution of the proteoglycans relative to the collagen fibrils within the corneal stroma. The proteoglycans within keratoconus and normal human corneas were stained with cuprolinic blue using the 'critical electrolyte' method, described in Chapter 2.

The normal arrangement of proteoglycans orientated crosswise to the collagen fibrils, as demonstrated in Figure 5.8, was seen over the majority of the stroma in keratoconus corneas. However, in parts of the central regions, keratoconus corneas had abnormal arrangements of proteoglycans. These abnormalities took the form of larger than normal proteoglycans arranged irregularly, often parallel, rather than perpendicular to the collagen fibrils, as seen in Figure 5.9. In general keratoconus specimens appear to have less densely staining proteoglycans than normal corneas.

5.1.3 X-ray diffraction

Figure 5.10 shows the *interfibrillar* spacings from normal and keratoconus corneas as a function of tissue hydration. The line-fitting can be justified as it has been demonstrated that interfibrillar spacing squared is a linear function of hydration (Sayers et al., 1982, Goodfellow at al., 1978).

The slope of the lines appears to be the same for keratoconus and control corneas. The interfibrillar spacing at H=3.2 has been calculated from Figure 5.10 for control and keratoconus corneas and is shown in Table 5.1. Although Figure 5.10 shows that the best-fit line for keratoconus interfibrillar spacing is lower than that for normal, the high level of scatter in the data does not allow us to decide whether or not this is significant.

By equilibrating corneas to a specific hydration (H=2.4), it was possible to carry out a t-test on large numbers of samples (Table 5.2). No significant difference ($p>0.2$) in interfibrillar spacing was observed between

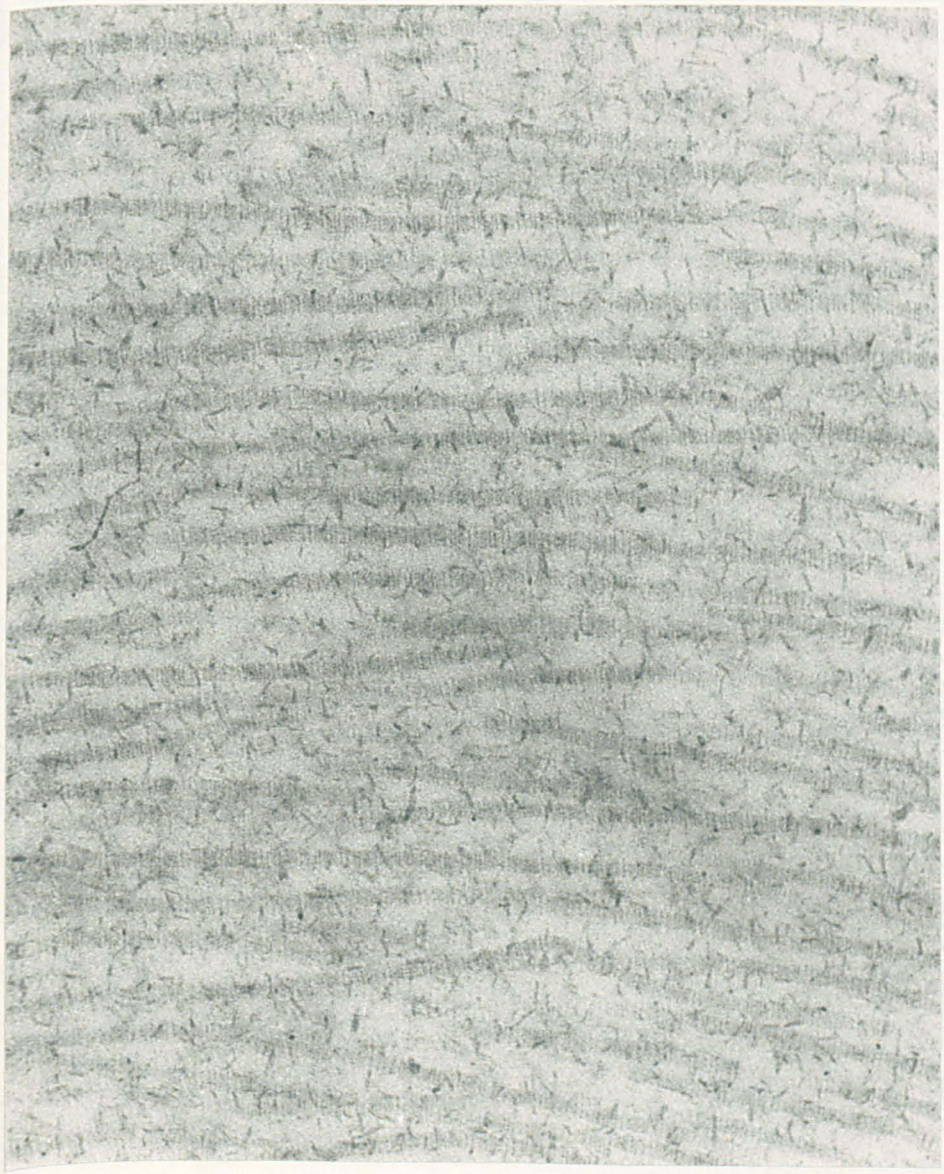

Figure 5.8 TEM micrograph of the stroma of a cuprolinic blue-stained human normal cornea. The proteoglycans are visible as fine filaments orientated mostly cross-wise to the collagen fibrils. ×82,000 magnification.

Figure 5.9 TEM micrograph of the stroma of a cuprolinic blue-stained human keratoconus cornea. Many of the proteoglycans visible are much larger that those seen in Figure 5.8, and are nearly all orientated parallel to the collagen fibrils. ×82,000 magnification.

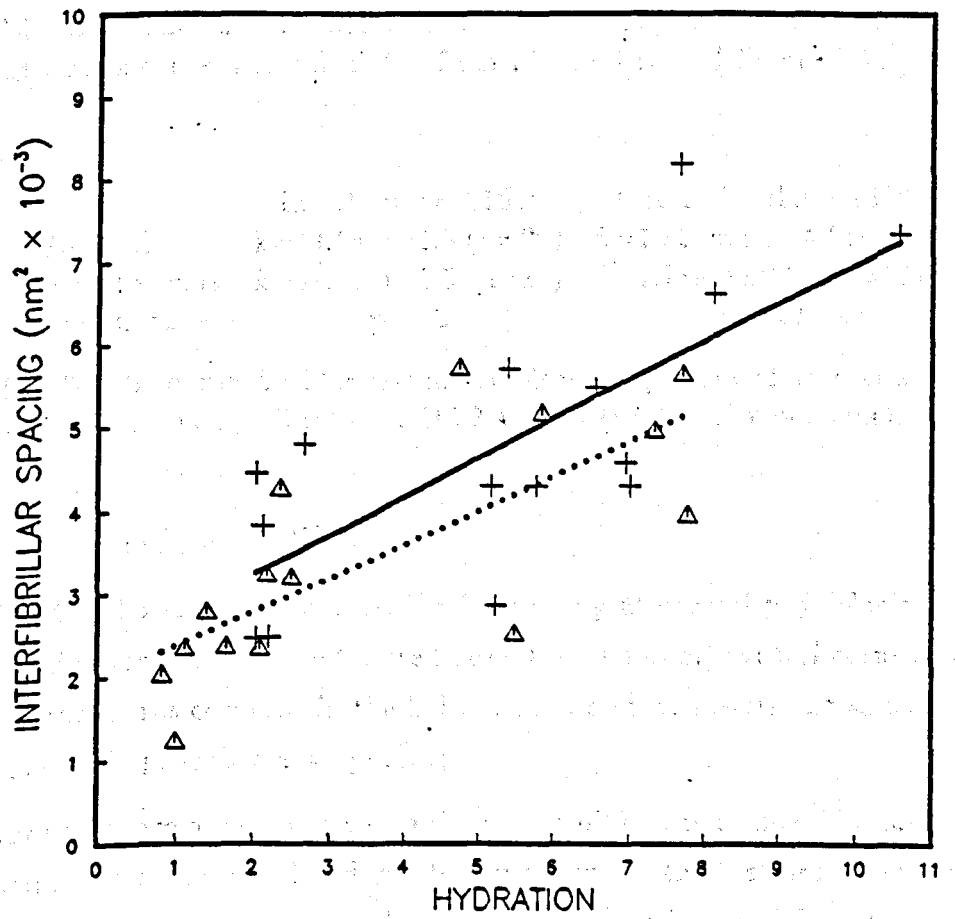

Figure 5.10 The interfibrillar spacings[2] of normal corneas (crosses) and keratoconus corneas (triangles) plotted against hydration. The solid (normal) and broken (keratoconus) lines represent the best fit linear regression to the data.

	Interfibrillar ±1SD	Intermolecular ±1SD
Normal	61.7nm±5.3	1.82nm±0.07
Keratoconus	57.3nm±4.6	1.74nm±0.04

Table 5.1 The interfibrillar and intermolecular spacings for normal and keratoconus corneas as calculated from Figure 5.10 and Figure 5.12

	Interfibrillar ±1SD	Intermolecular ±1SD
Normal	$\bar{x}$=49.5nm±1.8 (n=20)	$\bar{x}$=1.82nm±0.04 (n=23)
Keratoconus	$\bar{x}$=49.6nm±2.3 (n=13)	$\bar{x}$=1.78nm±0.03 (n=16)
Significance	p>0.2	p<0.01

Table 5.2 The interfibrillar and intermolecular spacings of normal and keratoconus corneas equilibrated to H=2.4±0.24 (n=no. of specimens).

keratoconus and control corneas.

Table 5.3 shows the mean interfibrillar spacing at normal physiological hydration for fresh (i.e. not stored in culture medium) control corneas and for keratoconus corneas. In the light of the previous results the small difference is probably not significant.

Although there appears to be no significant difference in interfibrillar spacing between normal and keratoconus corneas, the first-order reflection in keratoconus corneas is usually much broader and more diffuse than seen in normal corneas (Figure 5.11), indicating a wider range of interfibrillar

	Interfibrillar ±1SD	Intermolecular ±1SD
Normal	$\bar{x}$=61.9nm±4.5 (n=4)	$\bar{x}$=1.85nm±0.07 (n=8)
Keratoconus	$\bar{x}$=57.3nm±4.6 (n=15)	$\bar{x}$=1.73nm±0.03 (n=6)
Significance	*	p<0.001

Table 5.3 Interfibrillar and intermolecular spacings of normal and keratoconus corneas at physiological hydration. n=no. of specimens. * t-test not possible as keratoconus interfibrillar value is calculated from linear regression line in Figure 5.10

spacings in keratoconus corneas. The ratio of peak height to peak width (at half height), gives an inverse measure of range of spacing irrespective of relative exposure time. Typically for keratoconus this ratio is 2.0 whereas for normal corneas it is closer to 2.9.

Figure 5.12 shows the *intermolecular* spacings of normal and keratoconus corneas as a function of hydration. The results on bovine corneas in Chapter 3 and human corneas (personal communication, N.S.Malik), has demonstrated that above H=2 there is little change in intermolecular spacing with increasing hydration, Figure 5.12 shows that this appears to be true for keratoconus corneas as well.

Values for intermolecular spacings at H=3.2 were calculated from the X-ray data in Figure 5.12 (by averaging the values above H=2) and are presented in Table 5.1. Equilibrated corneas were used to measure the intermolecular spacings of large numbers of control and keratoconus corneas at a specific hydration. These results are presented in Table 5.2, where it can be seen that keratoconus corneas have significantly ($p<0.01$) lower intermolecular spacings than the controls.

Table 5.3 gives the mean intermolecular spacings for fresh control and keratoconus corneas at normal physiological hydration. There is a highly significant ($p<0.001$) decrease in intermolecular spacing in keratoconus corneas.

The results from the low-angle meridional X-ray pattern for untreated control and keratoconus corneas are presented in Table 5.4.

The second and third columns of the table show the first nine integrated intensities from the low-angle X-ray patterns of untreated control and keratoconus corneas. The data have been arbitrarily scaled so as to equate the fifth-order intensities. A number of normalization techniques were used to scale the 'control' data to the keratoconus intensities. The success of the normalization technique was assessed by calculating the R-factor between the two sets of data which is defined as

$$R = \Sigma \parallel F_{keratoconus} \mid - \mid F_{control} \parallel / \Sigma \mid F_{keratoconus} \mid$$

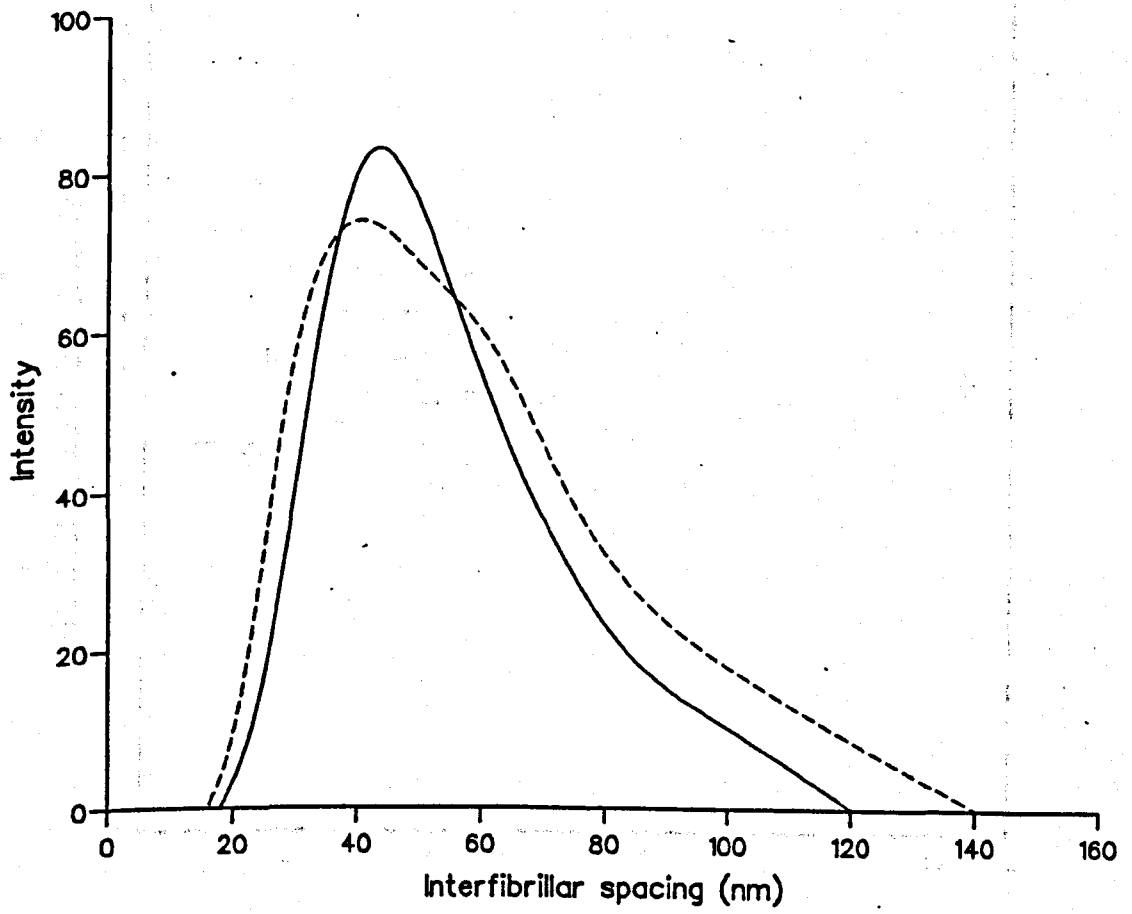

Figure 5.11 The peak profiles of the first-order interfibrillar reflections from control cornea (solid line) and a keratoconus cornea (dotted line) at normal physiological hydration. The background has been subtracted and the peaks are shown in real space.

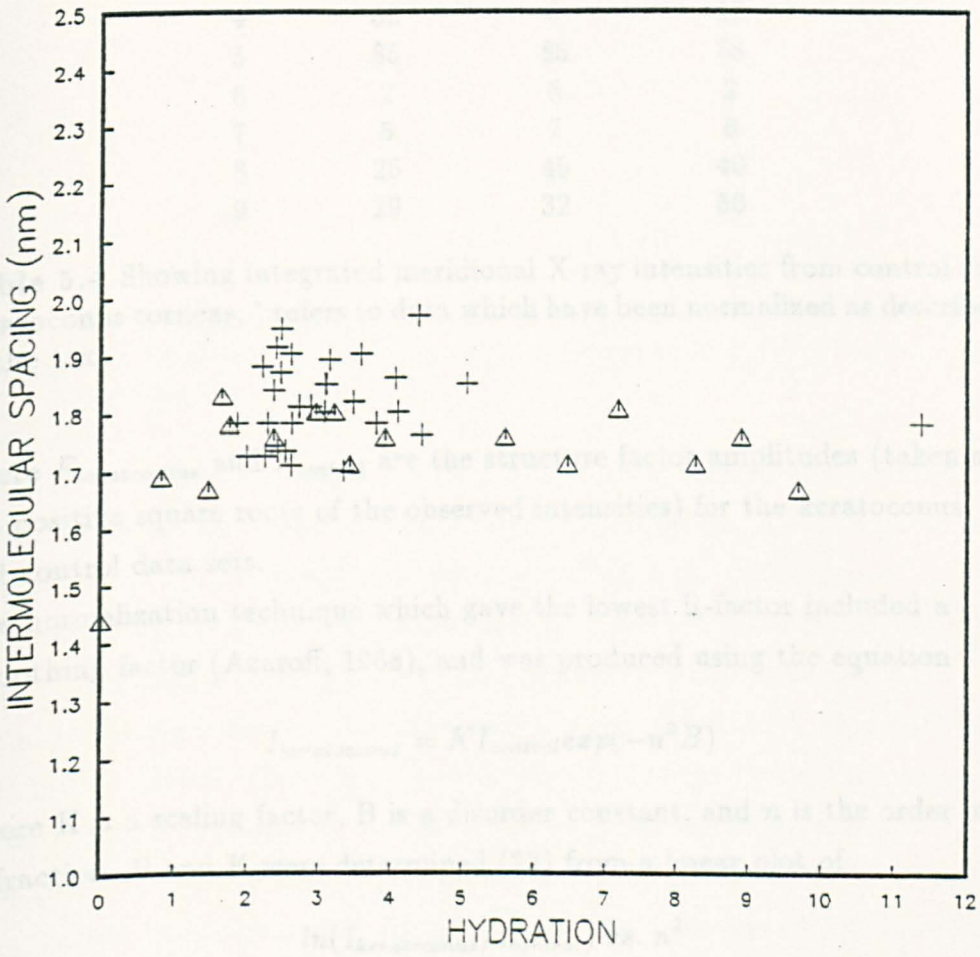

Figure 5.12 The intermolecular spacings of unequilibrated normal corneas (crosses) and keratoconus corneas (triangles) plotted against hydration.

Order(n)	Control	Keratoconus	Control*
1	135	83	90
2	21	21	15
3	275	228	204
4	52	9	42
5	85	85	78
6	2	8	2
7	5	7	6
8	26	49	40
9	29	32	56

Table 5.4 Showing integrated meridional X-ray intensities from control and keratoconus corneas, * refers to data which have been normalized as described in the text

where $F_{keratoconus}$ and $F_{control}$ are the structure factor amplitudes (taken as the positive square roots of the observed intensities) for the keratoconus and control data sets.

The normalization technique which gave the lowest R-factor included a smoothing factor (Azaroff, 1968), and was produced using the equation

$$I_{keratoconus} = K I_{control} exp(-n^2 B)$$

where K is a scaling factor, B is a disorder constant, and n is the order of diffraction. B and K were determined (23) from a linear plot of

$$ln(I_{keratoconus}/I_{control})\ vs.\ n^2$$

The normalized intensities are listed in the fourth column of Table 5.4 (Control*) and give an R-factor of 0.17. This very low value indicates that the axial distribution of electron density along the collagen fibril is not much altered in keratoconus corneas.

The integrated meridional intensities from the control and keratoconus Cupromeronic blue-stained corneas are presented in Table 5.5.

The measured control and keratoconus data have again been scaled to equate the fifth order intensities and the normalization has been carried out as described above and is listed under Control†.

Order(*n*)	Control	Keratoconus	Control†
1	129	9	37
2	129	18	39
3	193	195	63
4	83	53	30
5	85	85	36
6	75	23	38
7	18	35	11
8	91	37	72
9	142	91	147

Table 5.5 Showing integrated meridional X-ray intensities from control and keratoconus corneas after staining with cupromeronic blue, †refers to data which have been normalized as described in the text.

An R-factor of R=0.39 was calculated from the cupromeronic blue-stained keratoconus and modelled control (Control†) intensities. A significance test (Hamilton, 1964) between the R values obtained from the unstained material (R=0.17) and the cupromeronic blue-stained material (R=0.39) gives a significance level of $p<0.01$ that in cupromeronic blue-stained material the axial electron density along the collagen fibril is different from that of the control. Since the cupromeronic blue in the corneal stroma is thought to bind exclusively to the sulphated glycosaminoglycans, it is reasonable to assume that the difference in intensities in Table 5.5 is caused by a change in the nature or distribution of proteoglycans in keratoconus corneas.

Further analysis of the measured intensities of the normal and keratoconus corneas was carried out by means of a Patterson function as described in Chapter 1. This gives information on the relative frequency of occurrence of intraperiod electron density vectors within the D-period.

The Patterson functions calculated from the unstained control and keratoconus intensities are shown in Figure 5.13, which shows the patterns for control (solid line) and keratoconus (broken line) to be very similar. The figure shows three peaks which occur in the same positions for the

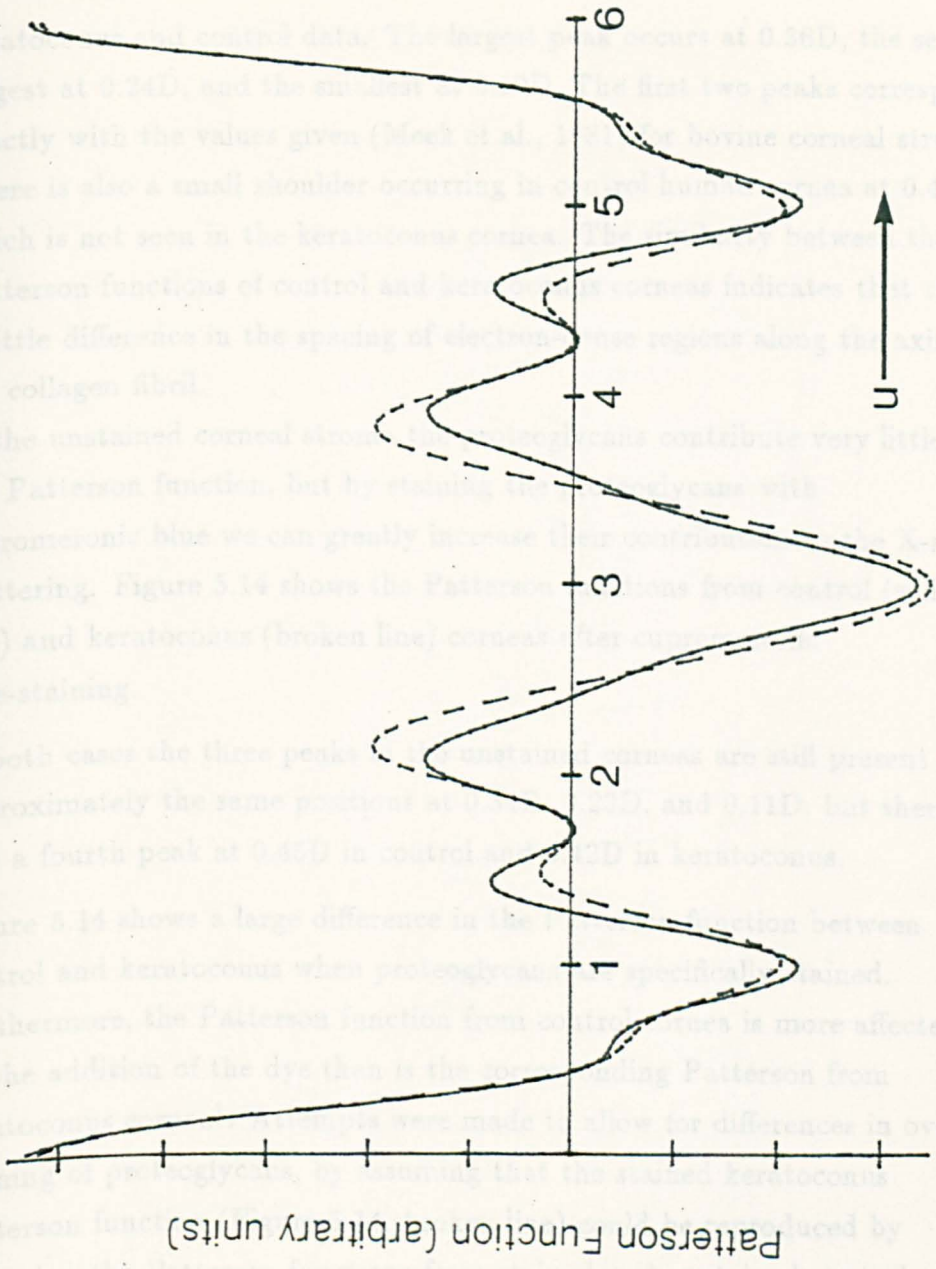

Figure 5.13 Patterson functions from unstained control corneas (solid line) and keratoconus corneas (broken line). The abscissa (u) is marked in units of D/6.

keratoconus and control data. The largest peak occurs at 0.36D, the second largest at 0.24D, and the smallest at 0.10D. The first two peaks correspond exactly with the values given (Meek et al., 1981) for bovine corneal stroma. There is also a small shoulder occurring in control human cornea at 0.42D which is not seen in the keratoconus cornea. The similarity between the Patterson functions of control and keratoconus corneas indicates that there is little difference in the spacing of electron-dense regions along the axis of the collagen fibril.

In the unstained corneal stroma the proteoglycans contribute very little to the Patterson function, but by staining the proteoglycans with cupromeronic blue we can greatly increase their contribution to the X-ray scattering. Figure 5.14 shows the Patterson functions from control (solid line) and keratoconus (broken line) corneas after cupromeronic blue-staining.

In both cases the three peaks in the unstained corneas are still present in approximately the same positions at 0.34D, 0.23D, and 0.11D, but there is also a fourth peak at 0.45D in control and 0.42D in keratoconus.

Figure 5.14 shows a large difference in the Patterson function between control and keratoconus when proteoglycans are specifically stained. Furthermore, the Patterson function from control cornea is more affected by the addition of the dye than is the corresponding Patterson from keratoconus cornea[1]. Attempts were made to allow for differences in overall staining of proteoglycans, by assuming that the stained keratoconus Patterson function (Figure 5.14, broken line) could be reproduced by averaging the Patterson functions from stained and unstained control corneas (Figures 5.13 and 5.14, solid lines), using different relative weightings. Although the fit was improved, it was found impossible to obtain a precise fit to the stained keratoconus Patterson function using this method.

[1]Compare the broken lines in Figure 5.13 and Figure 5.14 with each other, then compare the solid lines in these figures

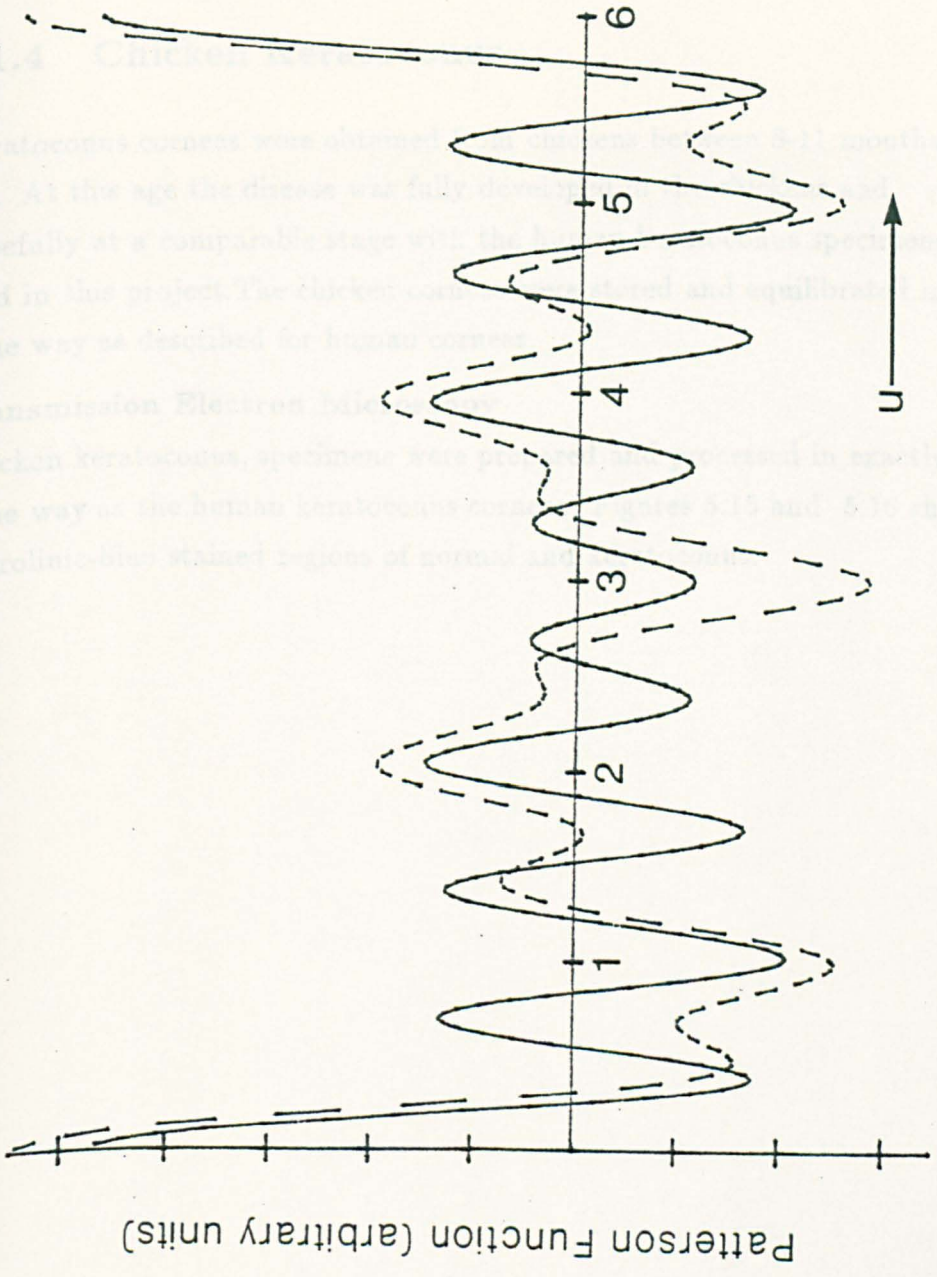

Figure 5.14 Patterson functions from cupromeronic blue-stained control corneas (solid line) and keratoconus corneas (broken line). The abscissa (u) is marked in units of D/6.

5.1.4 Chicken Keratoconus

Keratoconus corneas were obtained from chickens between 8-11 months of age. At this age the disease was fully developed in the chickens and hopefully at a comparable stage with the human keratoconus specimens used in this project.The chicken corneas were stored and equilibrated in the same way as described for human corneas.

Transmission Electron Microscopy

Chicken keratoconus, specimens were prepared and processed in exactly the same way as the human keratoconus corneas. Figures 5.15 and 5.16 show cuprolinic-blue stained regions of normal and keratoconus.

Figure 5.15 A normal chicken corneal stroma showing the collagen fibrils with the densely stained proteoglycans orientated crosswise to the fibrils. $\times 62{,}000$ magnification.

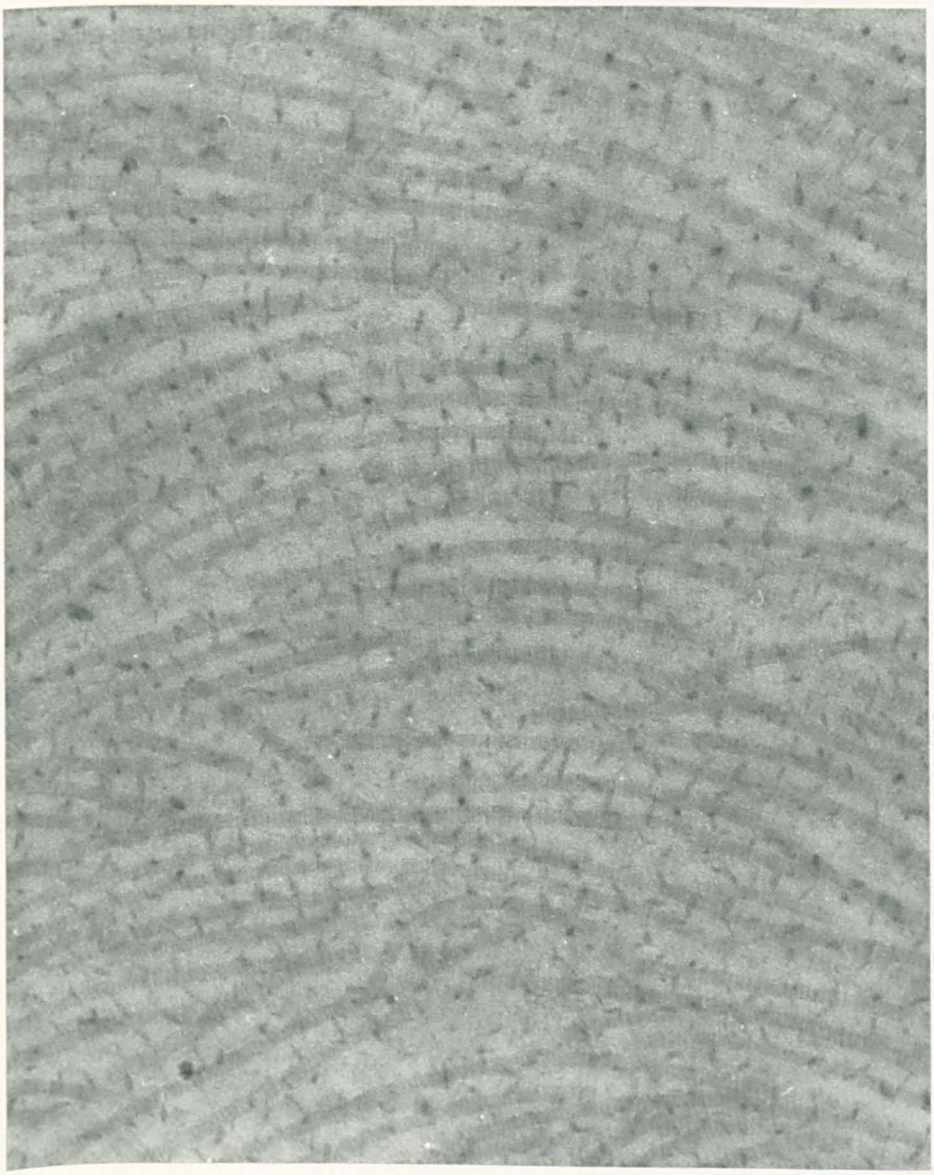

Figure 5.16 A chicken keratoconus corneal stroma showing the collagen fibrils with the densely stained proteoglycans orientated crosswise to the fibrils. ×62,000 magnification.

The results from the investigation of the keratoconus chicken corneas with the TEM appear to show that there is no apparent difference in the proteoglycans present in chicken keratoconus corneas (Figure 5.16) compared to normal corneas (Figure 5.15). The collagen fibrils also have the same distribution and appearance in both tissues.

X-ray diffraction

The results from the low-angle X-ray work give a very high probability ($p<0.01$) that the interfibrillar spacing is significantly different between keratoconus and normal corneas. The mean interfibrillar spacings at $H=2.3\pm0.3$ are 63.8 ± 2.0nm for keratoconus corneas and 58.4 ± 0.6nm for normal corneas. The wide-angle data show that there is no significant difference ($p>0.1$), in intermolecular spacing between normal and keratoconus corneas. The mean intermolecular spacings at $H=2.6\pm0.3$ are 1.54 ± 0.28nm for normal corneas and 1.57 ± 0.28nm for keratoconus corneas. These findings are in direct contrast to the results on human keratoconus, where a significant difference in intermolecular spacing was found but no significant difference in interfibrillar spacing. The implications of this are discussed in the final chapter.

Chapter 6

Myopia

6.1 Introduction

This chapter details the results obtained from an ultrastructural and X-ray investigation in to form-deprivation myopia in 6 week old chicks. Both the cornea and sclera were investigated, although the major changes were expected to occur in the sclera since this is where the elongation of the eyeball occurs in myopic chicks.

6.1.1 Specimen Details

Table 6.1.1 gives the details on corneal curvature and the power of the correcting lens in diopters for the normal and experimental chickens used in this investigation.

6.2 X-ray Diffraction

The low and high-angle X-ray results from cornea and sclera from control and normal chicks are summarized in Table 6.2. There are no low-angle results for sclera because the distribution of fibril diameters and spacings is too disordered to produce an X-ray pattern.

Chick No.	Eye	Corneal curvature (mm)	Lens power (diopters)
1	R-Con.	4.09	1.29
1	L-Exp.	4.01	-20.77
2	R-Exp.	4.05	-13.40
2	L-Con.	4.00	-0.28
3	R-Con.	3.85	2.00
3	L-Exp.	3.25	-36.27
4	R-Con.	4.04	0.06
4	L-Exp.	3.96	-32.78
5	R-Con.	3.96	2.17
5	L-Exp.	3.73	-26.76

Table 6.1 Refractometry and keratometry data on six week old chicks, each chick had one eye fitted with a full occluder to produce myopia, the other eye acted as a control. The lens power refers to the strength of the lens needed to restore normal vision. These data and the original samples were supplied by David Troilo, University of Oxford.

6.2.1 Low-angle results

The results from low-angle X-ray diffraction gave a mean interfibrillar spacing of 54.6 $\pm$5.9nm for control corneas, and a mean interfibrillar spacing of 58.3 $\pm$5.3nm for myopic corneas. No significant difference ($p>0.2$) was found between the two types of cornea.

6.2.2 High-angle results

The results from high-angle X-ray diffraction give a mean intermolecular spacing of 1.10 $\pm$0.05nm for control corneas, and a mean intermolecular spacing of 1.14 $\pm$0.06nm for myopic corneas. No significant difference ($p>0.05$) was found in this spacing between the two types of cornea. High-angle X-ray patterns were also obtained from the intermolecular spacing of collagen molecules within the collagen fibrils in the scleral stroma. A mean intermolecular spacing of 1.16 $\pm$ 0.03nm was obtained for normal sclera, and a mean intermolecular spacing of 1.20 $\pm$0.02nm. Myopic sclera was found to have a significantly ($p<0.0005$) higher intermolecular spacing than the control sclera.

Chick No.	Eye	Interfib. Spa. Cornea(nm)	Intermol. Spa. Cornea(nm)	Intermol. Spa. Sclera(nm)
1	R-Con.	60.0	1.13	1.15
1	L-Exp.	60.0	1.13	1.19
2	R-Exp.	61.4	1.17	1.20
2	L-Con.	52.5	1.09	1.17
3	R-Con.	47.2	1.02	1.12
3	L-Exp.	50.3	1.05	1.18
4	R-Con.	61.4	1.13	1.14
4	L-Exp.	56.2	1.11	1.19
5	R-Con.	52.1	1.10	1.21
5	L-Exp.	63.8	1.22	1.24

Table 6.2 Interfibrillar and intermolecular spacings from cornea and posterior sclera of normal and myopic eyes of six week old chicks.

In addition to a higher intermolecular spacing, myopic sclera also had a wider *range* of intermolecular spacings than control sclera. Figure 6.1 shows the peak profiles from the high-angle patterns of a typical control (solid line) and myopic (dotted line) chick scleras. The first-order reflection from myopic sclera is broader and more diffuse than that from normal sclera, indicating a wider range of interfibrillar spacings in myopic sclera. Typically for myopic sclera the ratio of peak height to peak width (at half height) is ~4 compared to a value of ~6 for normal sclera.

6.3 Electron Microscopy

6.3.1 Cornea

Figure 6.2 shows the central region from the cornea of control chicks, and Figure 6.3 the same region from myopic chick cornea; these appeared to be very similar to each other. The collagen fibrils in both types of cornea were regular in appearance and approximately 25nm in diameter. The cuprolinic blue-stained proteoglycans appeared to be of similar size and numbers in both tissues, morphologically there appeared to be only one type. It was impossible to localize where along the collagen fibril the proteoglycans were

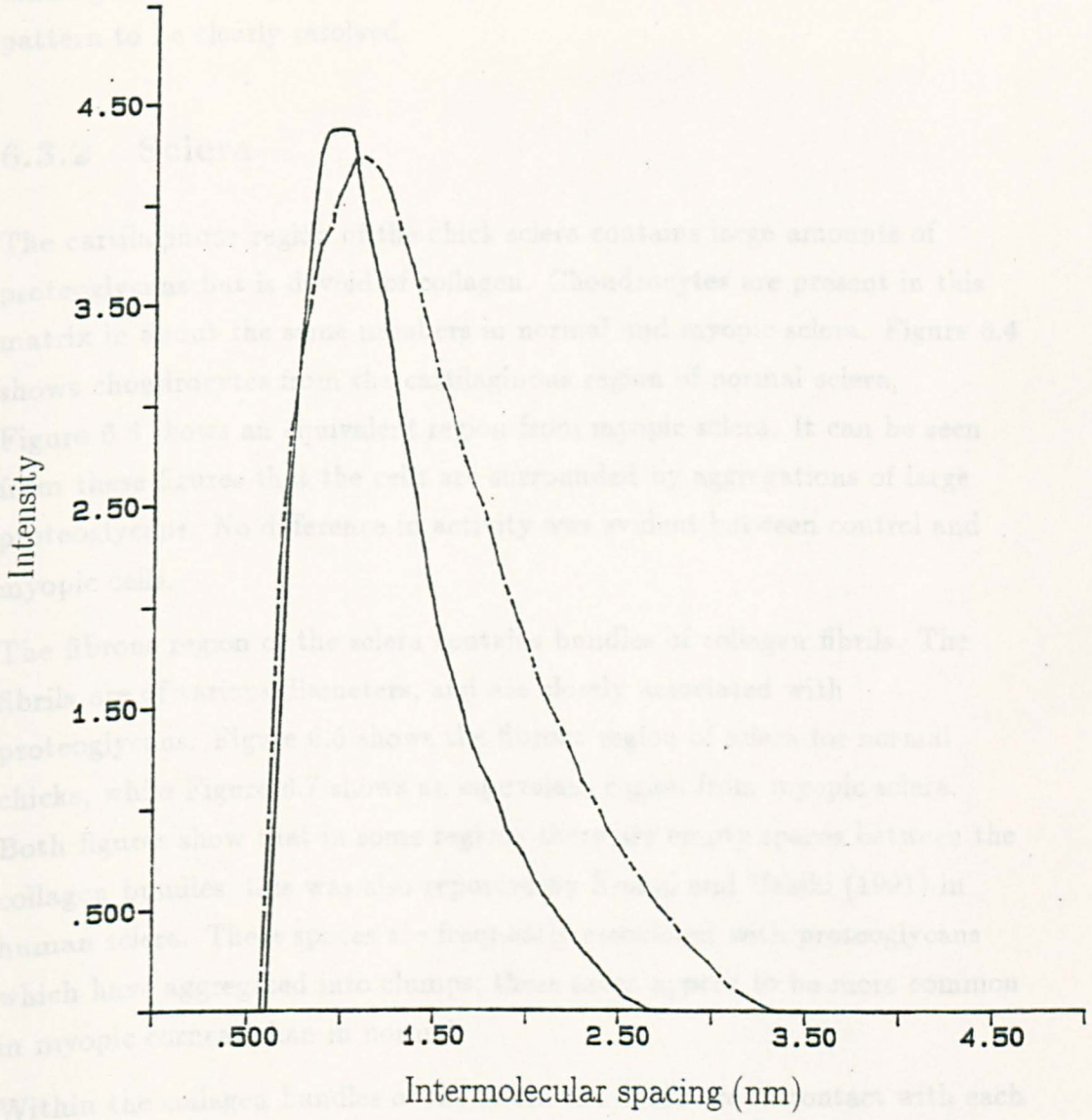

Figure 6.1 Shows the peak profiles of the intermolecular spacing of control (solid line) and myopic (dotted line) sclera. The profiles have been obtained from densitometer traces of representative high-angle patterns which have had their backgrounds subtracted, been converted into real space and smoothed.

binding as the collagen fibrils were of too narrow to allow the banding pattern to be clearly resolved.

6.3.2 Sclera

The cartilaginous region of the chick sclera contains large amounts of proteoglycans but is devoid of collagen. Chondrocytes are present in this matrix in about the same numbers in normal and myopic sclera. Figure 6.4 shows chondrocytes from the cartilaginous region of normal sclera, Figure 6.5 shows an equivalent region from myopic sclera. It can be seen from these figures that the cells are surrounded by aggregations of large proteoglycans. No difference in activity was evident between control and myopic cells.

The fibrous region of the sclera contains bundles of collagen fibrils. The fibrils are of various diameters, and are closely associated with proteoglycans. Figure 6.6 shows the fibrous region of sclera for normal chicks, while Figure 6.7 shows an equivalent region from myopic sclera. Both figures show that in some regions there are empty spaces between the collagen bundles, this was also reported by Komai and Ushiki (1991) in human sclera. These spaces are frequently associated with proteoglycans which have aggregated into clumps; these areas appear to be more common in myopic corneas than in normal.

Within the collagen bundles of the sclera the fibrils are in contact with each other. Some adjacent fibres were observed running in opposite directions with others running in the same direction. Two sizes of proteoglycan were observed in the stroma The first were small (~25nm long) elongated proteoglycans which were commonly observed bound to collagen fibrils. Larger proteoglycans, fairly irregular in shape, are also present in quantity. These proteoglycans are also usually observed attached to the collagen fibrils, they are also seen aggregated in clumps. Figure 6.8 shows proteoglycans attached to specific regions of the collagen fibril in control sclera, and Figure 6.9 indicates a similar picture in myopic sclera. In both

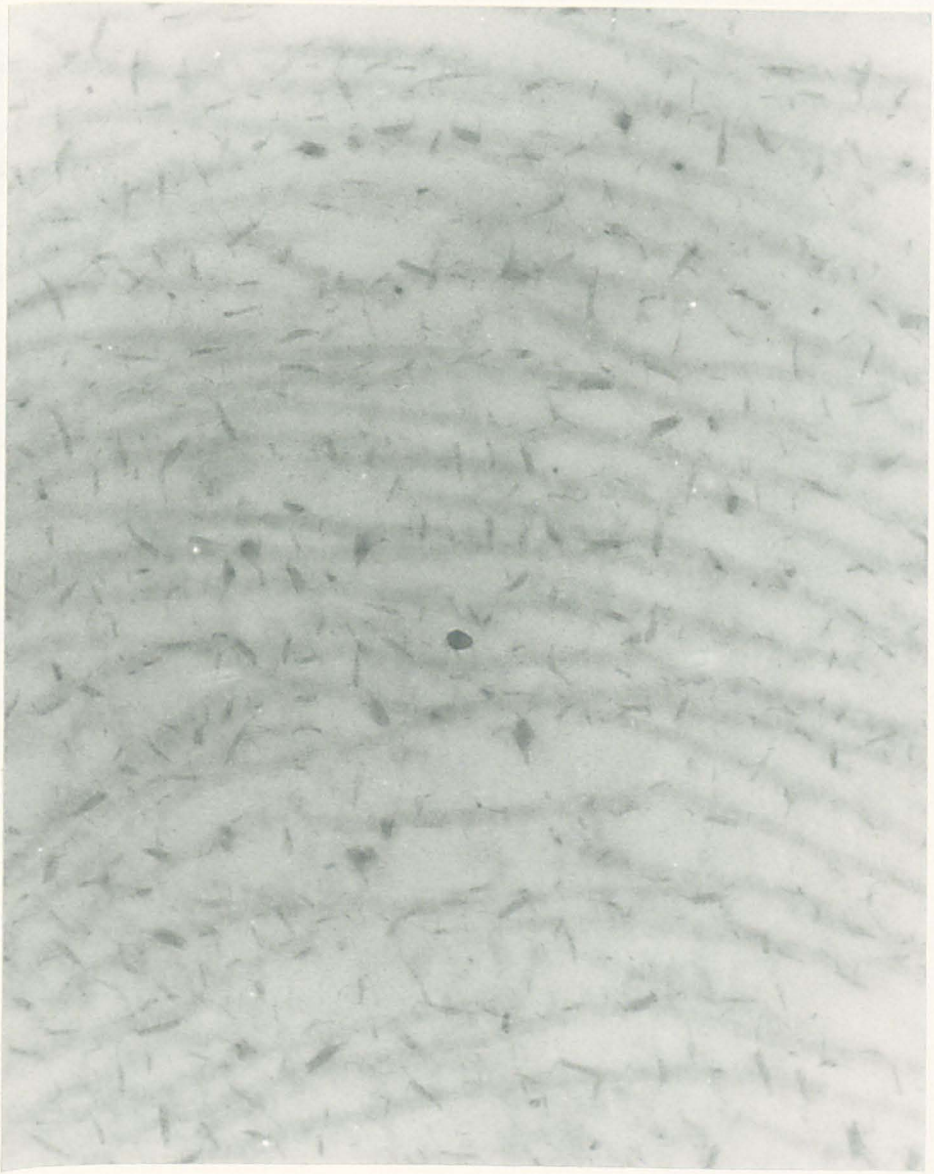

Figure 6.2 Shows the central region of the corneal stroma of a normal chick. The cuprolinic blue-stained proteoglycans are orientated mostly crosswise to the fibrils. ×111,000 magnification.

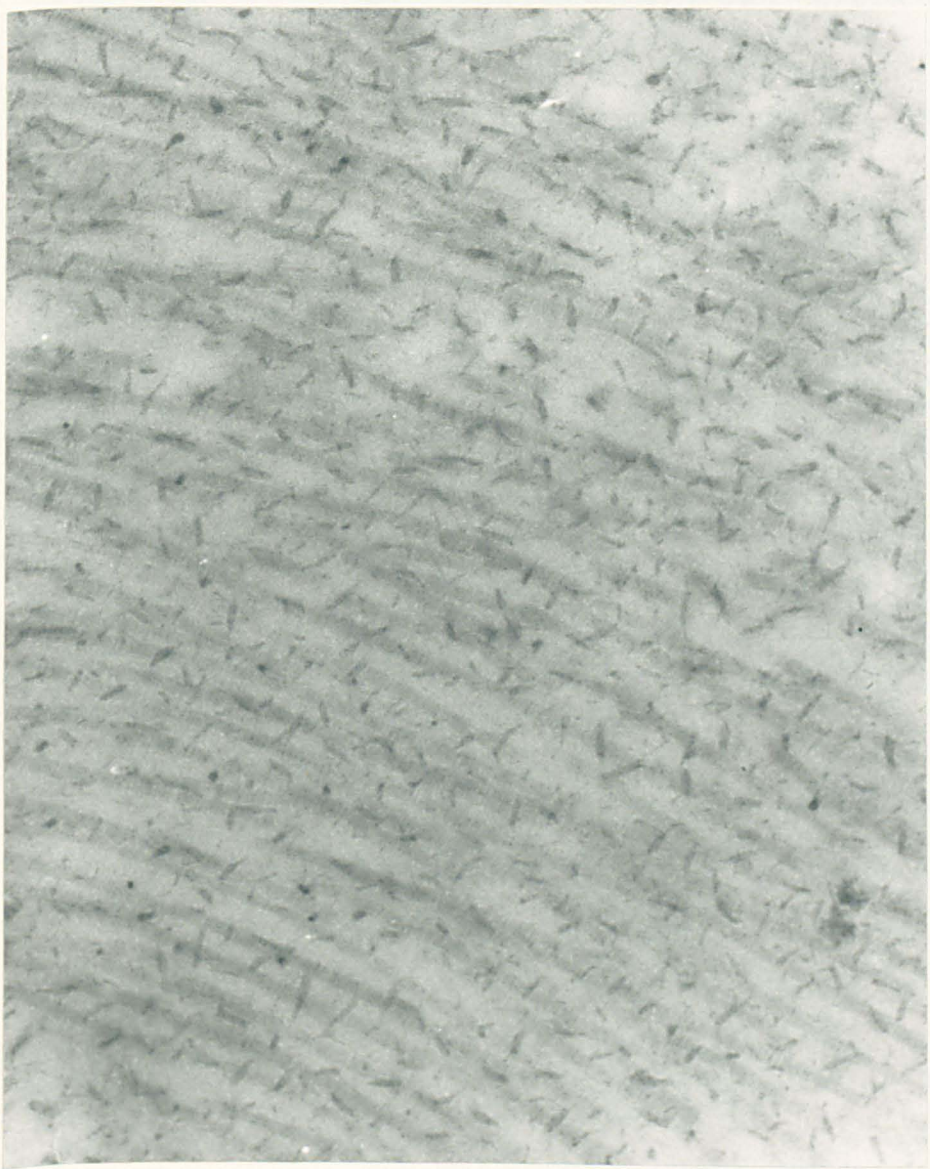

Figure 6.3 Shows the central region of the corneal stroma of a myopic chick. The cuprolinic blue-stained proteoglycans are orientated mostly crosswise to the fibrils. ×111,000 magnification.

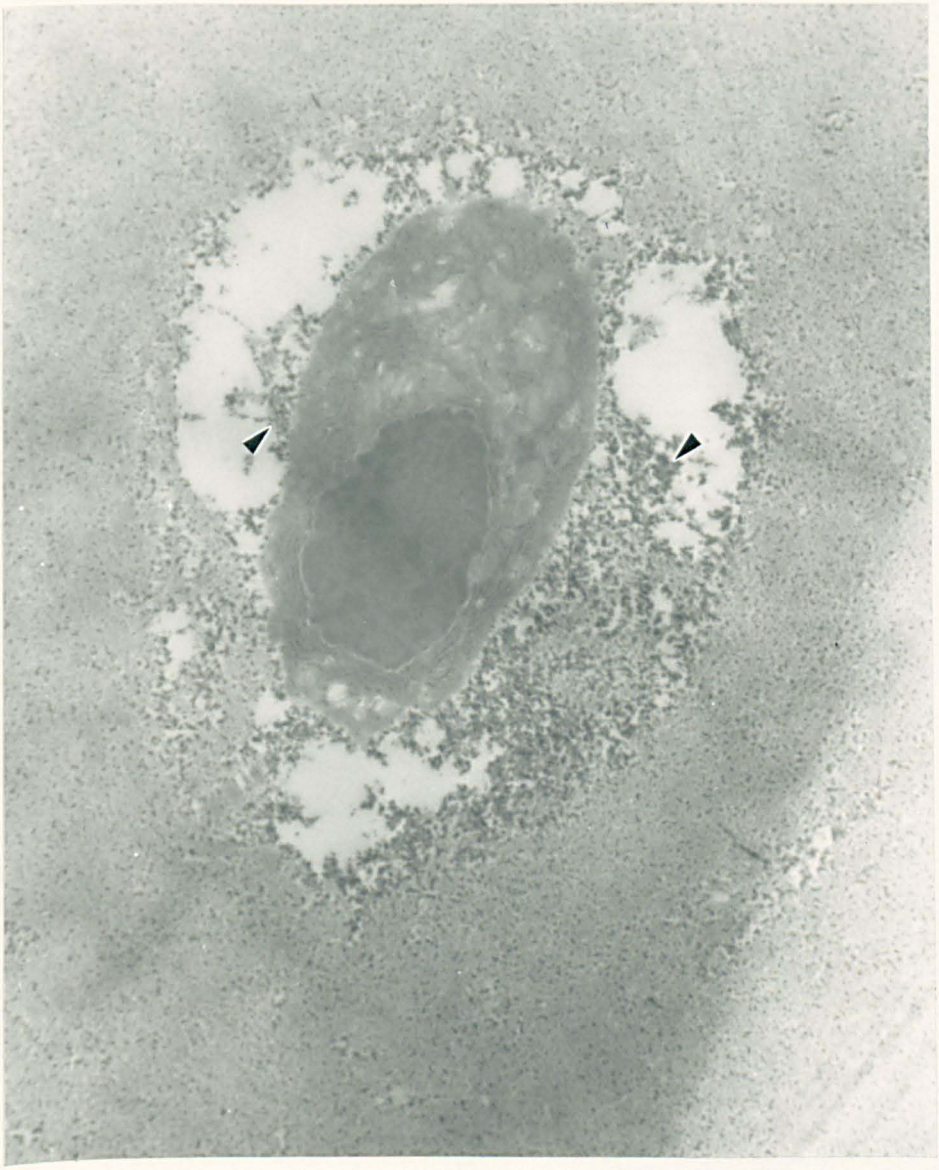

Figure 6.4 Chondrocyte in the cartilaginous sclera of a normal chick. The micrograph shows that the chondrocyte is surrounded by aggregations of large proteoglycans (arrows). The empty space around the chondrocyte is probably an artifact caused by the unavoidably low osmolarity of the 'critical electrolyte' fixing solution. ×14,000 magnification.

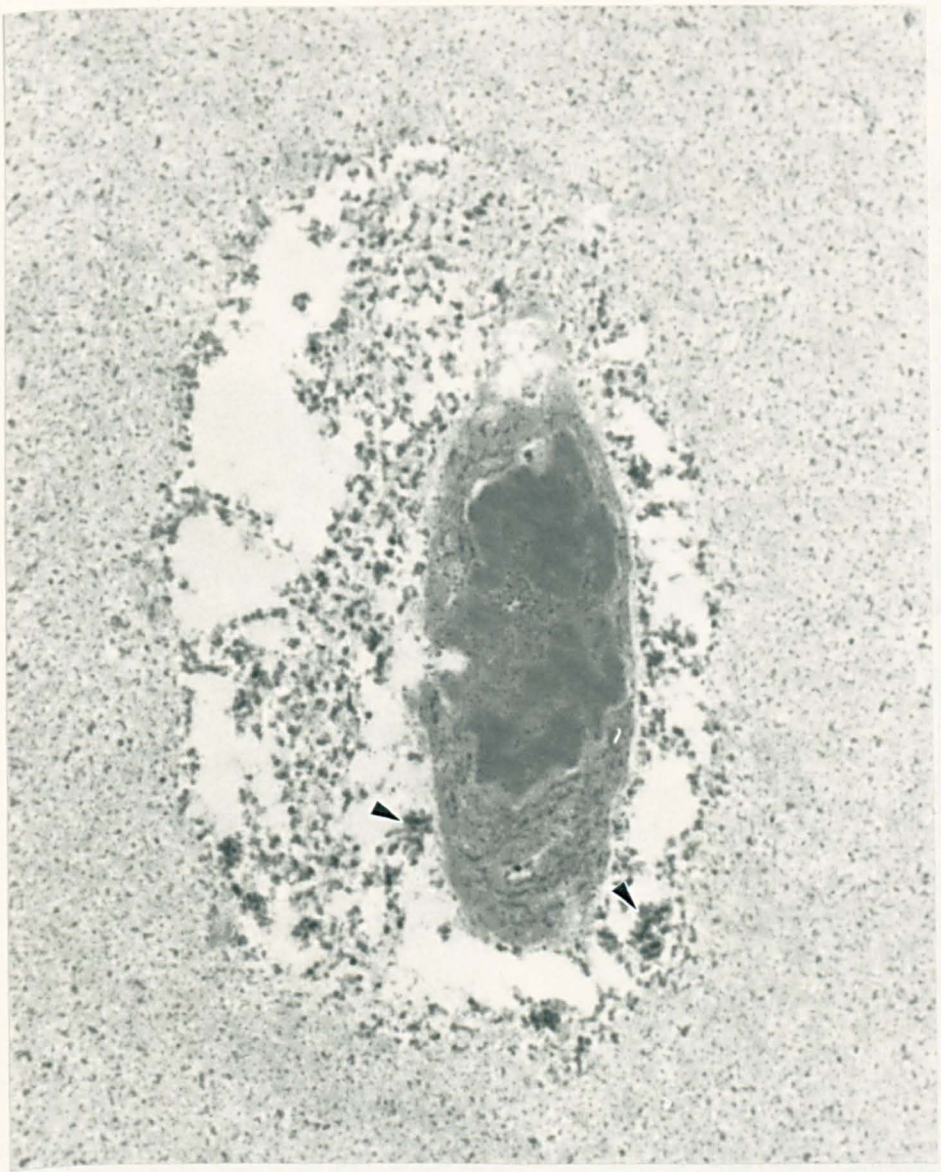

Figure 6.5 Chondrocyte in the cartilaginous sclera of a myopic chick. The micrograph shows that the chondrocyte is surrounded by aggregations of large proteoglycans (arrows). The empty space around the chondrocyte is probably an artifact caused by the unavoidably low osmolarity of the 'critical electrolyte' fixing solution. ×14,000 magnification.

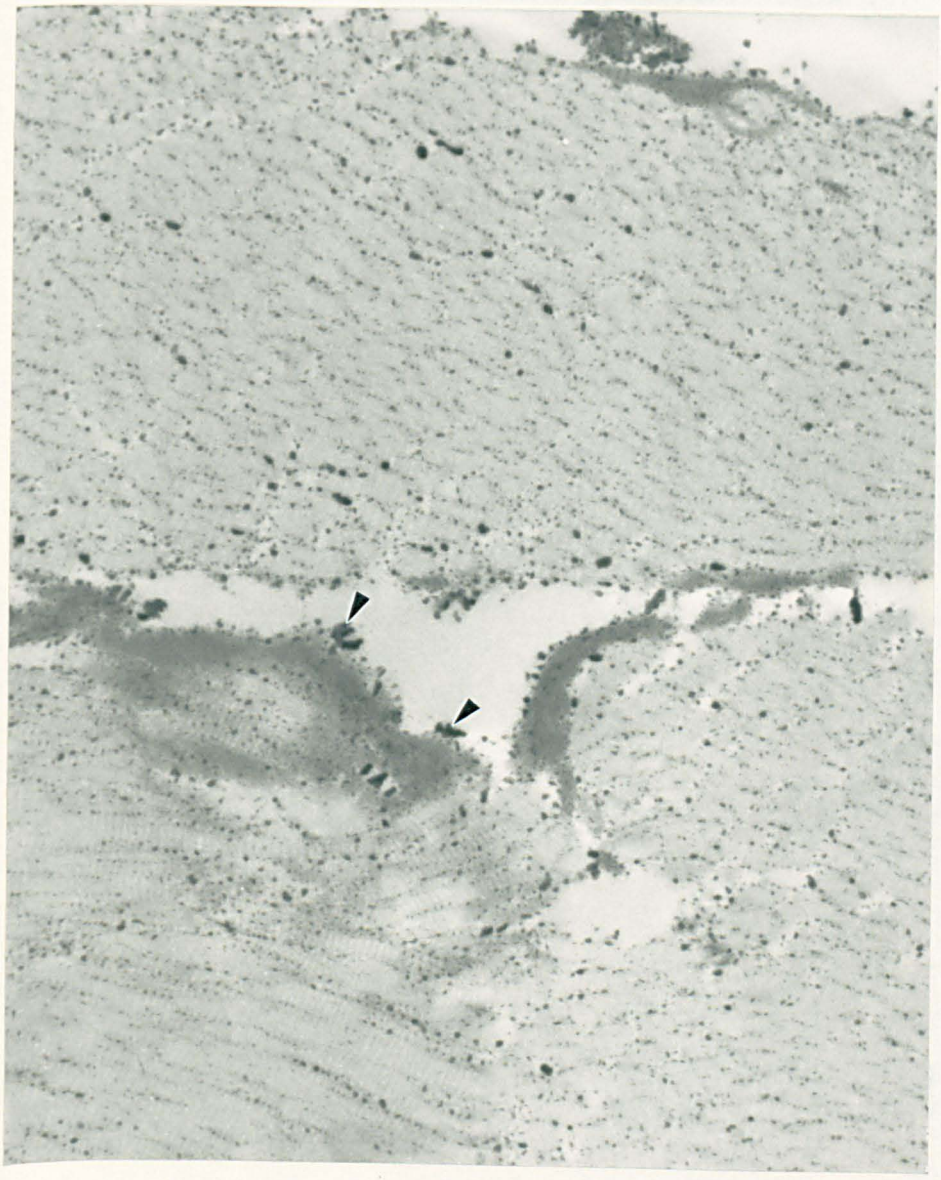

Figure 6.6 Shows the fibrous sclera from a normal chick. Numerous large proteoglycans are associated with the collagen bundles. Aggregations of proteoglycans are also sometimes evident in spaces between the collagen bundles (arrows). $\times 12{,}000$ magnification.

Figure 6.7 Shows the fibrous sclera from a myopic chick. Numerous large proteoglycans are visible associated with the collagen bundles. Aggregations of proteoglycans are also sometimes evident in spaces between the collagen bundles (arrows), these appear more common in myopic sclera than in normal sclera. $\times 12{,}000$ magnification.

samples proteoglycans were observed bound at all points along the D-period of the collagen fibril, however the most commonly observed binding was to the 'd' and 'e' bands of the collagen fibrils.

As well as both large and small proteoglycans which bind to the exterior of the collagen fibril there are also small proteoglycans present *within* the collagen fibrils of both normal and myopic sclera. These small proteoglycans are always orientated parallel to the axis of the collagen fibril. Figure 6.10 shows small proteoglycans present within the collagen fibrils from control sclera, while Figure 6.11 shows that these intrafibrillar proteoglycans also occur in myopic sclera. In both cases the proteoglycans appear to be preferentially located along the gap region (double arrow) of the D-period; the gap region is located between the 'c_2' and 'a_3' bands along the collagen fibril.

Figure 6.12 shows a transverse section through the fibrous sclera of a normal chick, Figure 6.13 is an equivalent region from myopic sclera. Both figures clearly show the presence of intrafibrillar proteoglycans. A few of the intrafibrillar proteoglycans observed were quite large (up to 40nm in diameter) although the majority were approximately 10nm in diameter. The intrafibrillar proteoglycans tended to be more common towards the outer surface of the sclera, and were occasionally associated with what appeared to be holes in the collagen fibrils.

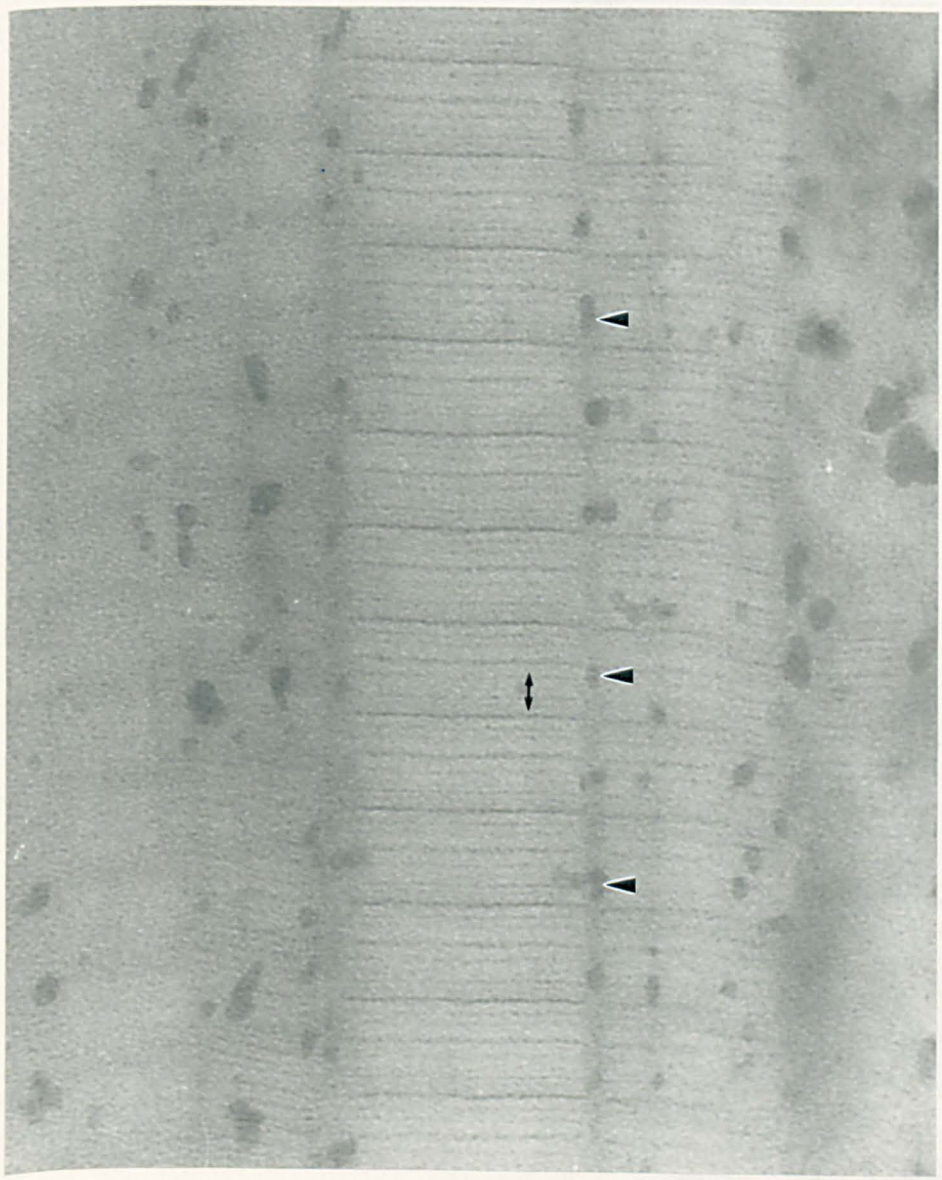

Figure 6.8 Shows the fibrous sclera of a normal chick. It is evident that the small proteoglycans (arrows) are attached preferentially to the 'd' and 'e'bands in the gap region (double arrow) of the collagen fibrils. ×205,000 magnification.

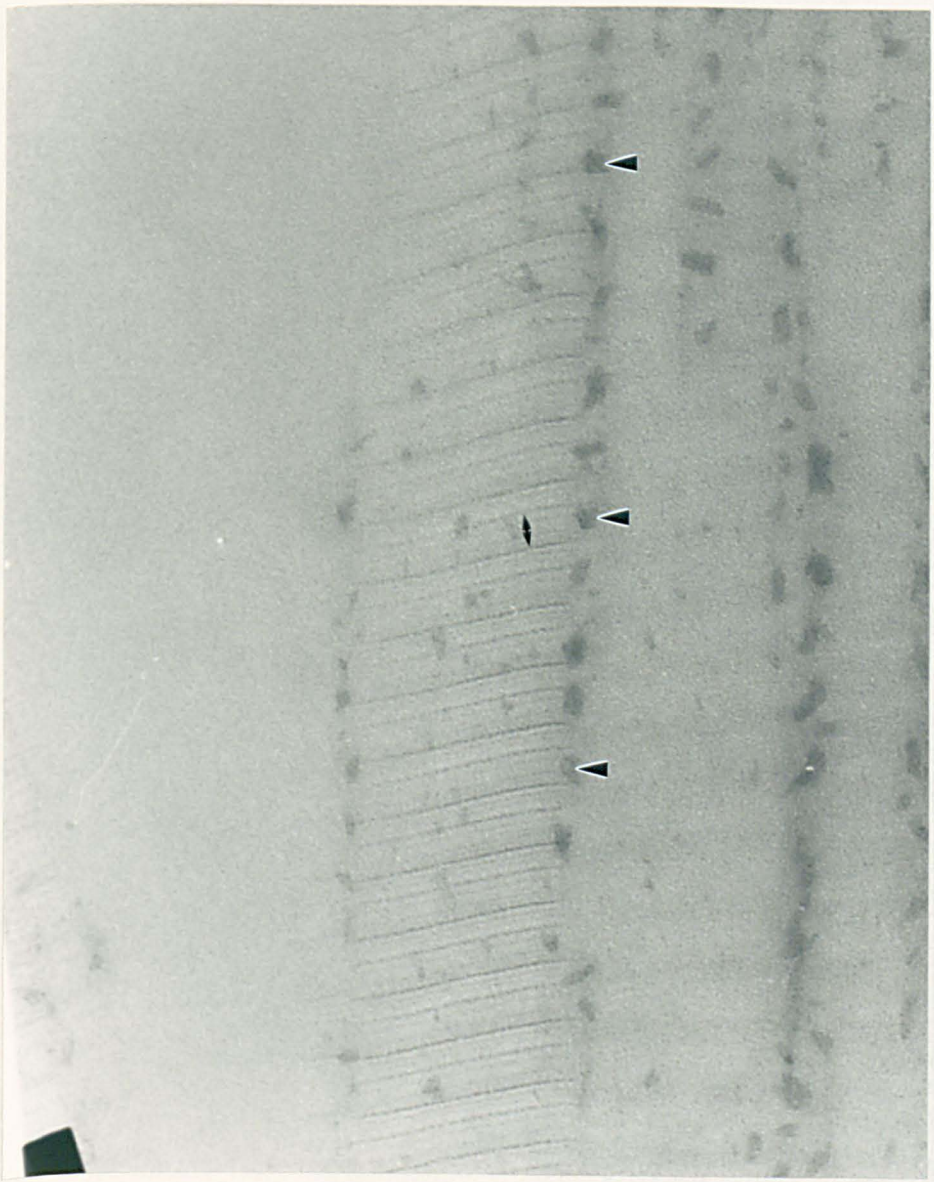

Figure 6.9 Shows the fibrous sclera of a myopic chick. It is evident that the small proteoglycans (arrows) are attached preferentially to the 'd' and '*e*'bands in the gap region (double arrow) of the collagen fibrils. ×142,000 magnification.

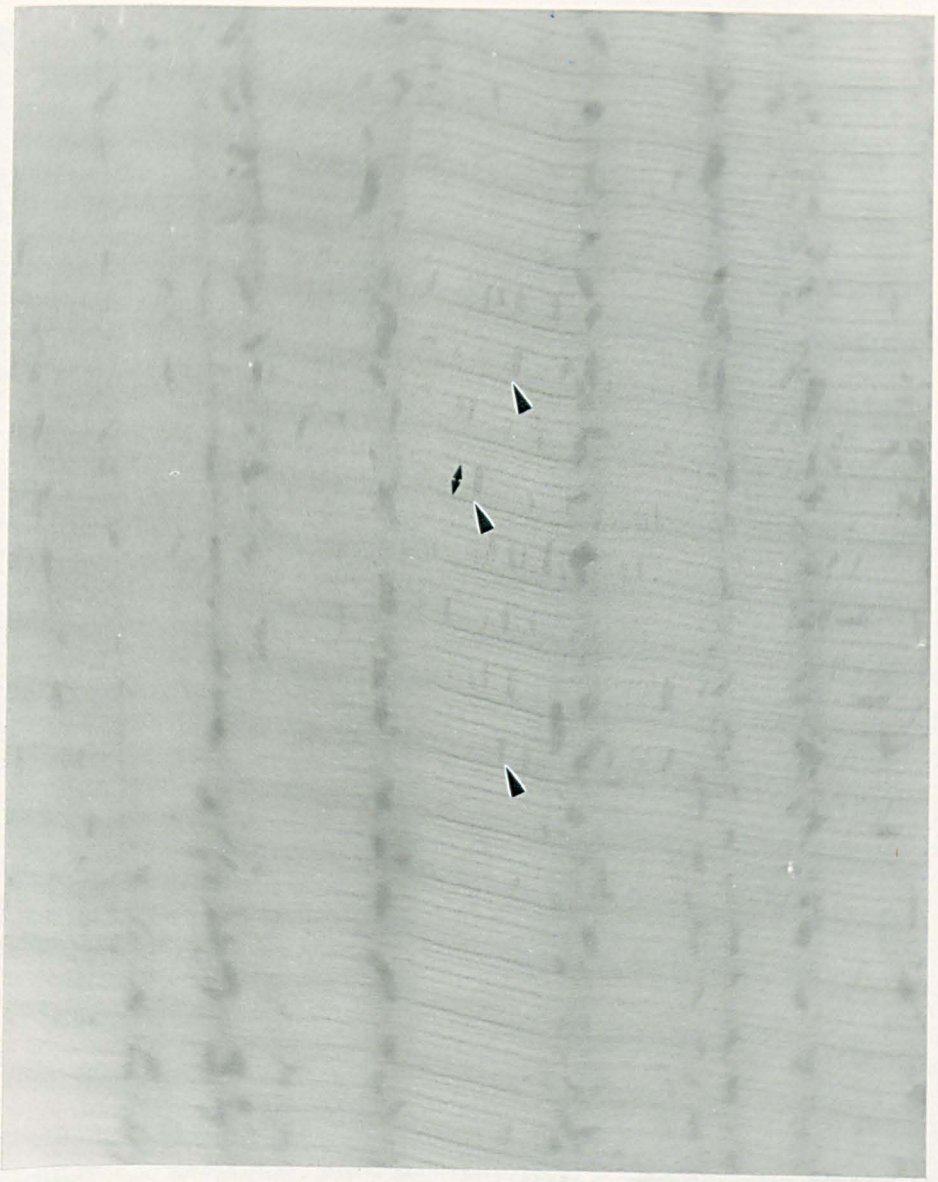

Figure 6.10 Shows the fibrous sclera from a control chick.The micrograph shows a longitudinal section through large diameter collagen fibrils, small intrafibrillar proteoglycans (arrows) are evident within the fibril located preferentially along the gap region (double arrow) of the fibril. ×142,000 magnification.

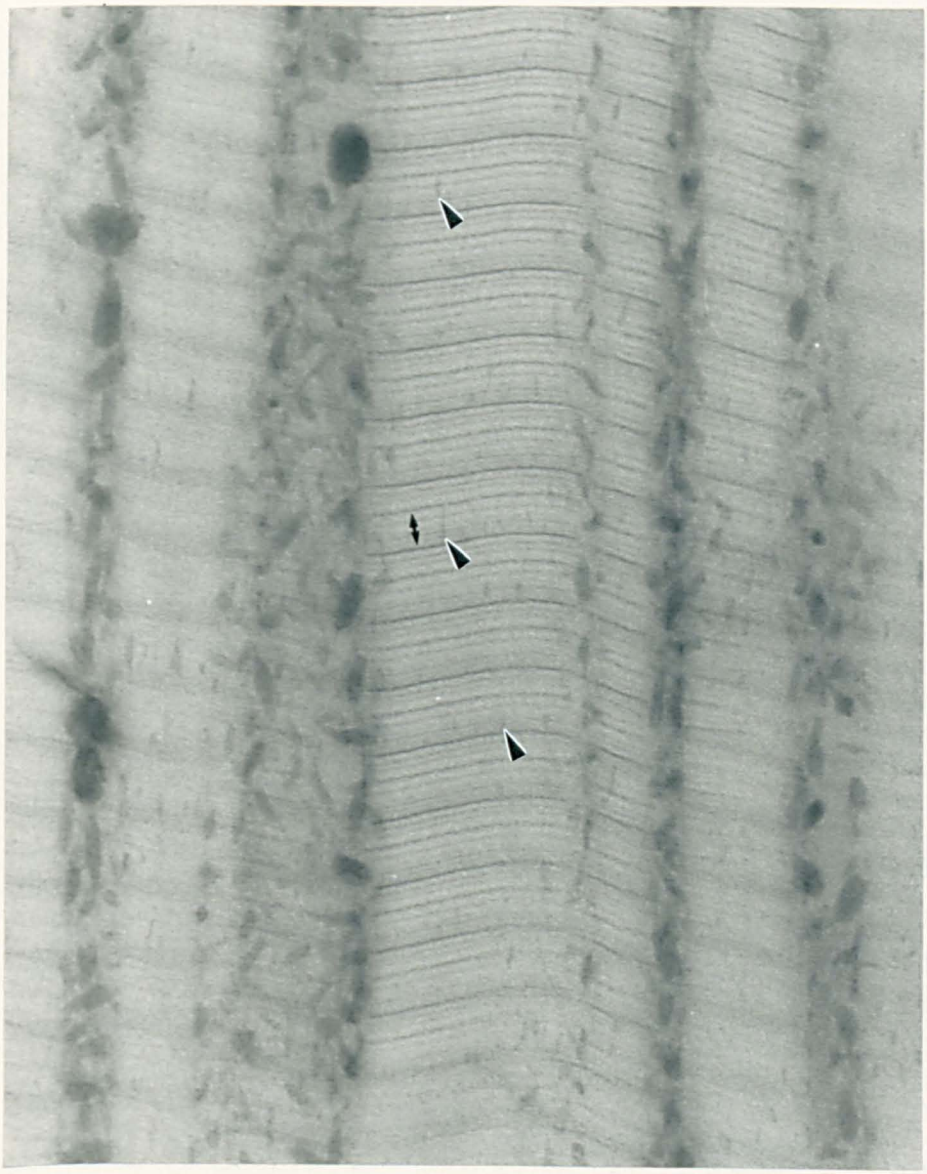

Figure 6.11 Shows the fibrous sclera from a myopic chick.The micrograph shows a longitudinal section through large diameter collagen fibrils, small intrafibrillar proteoglycans (arrows) are evident within the fibril located preferentially along the gap region of the fibril. $\times 142{,}000$ magnification.

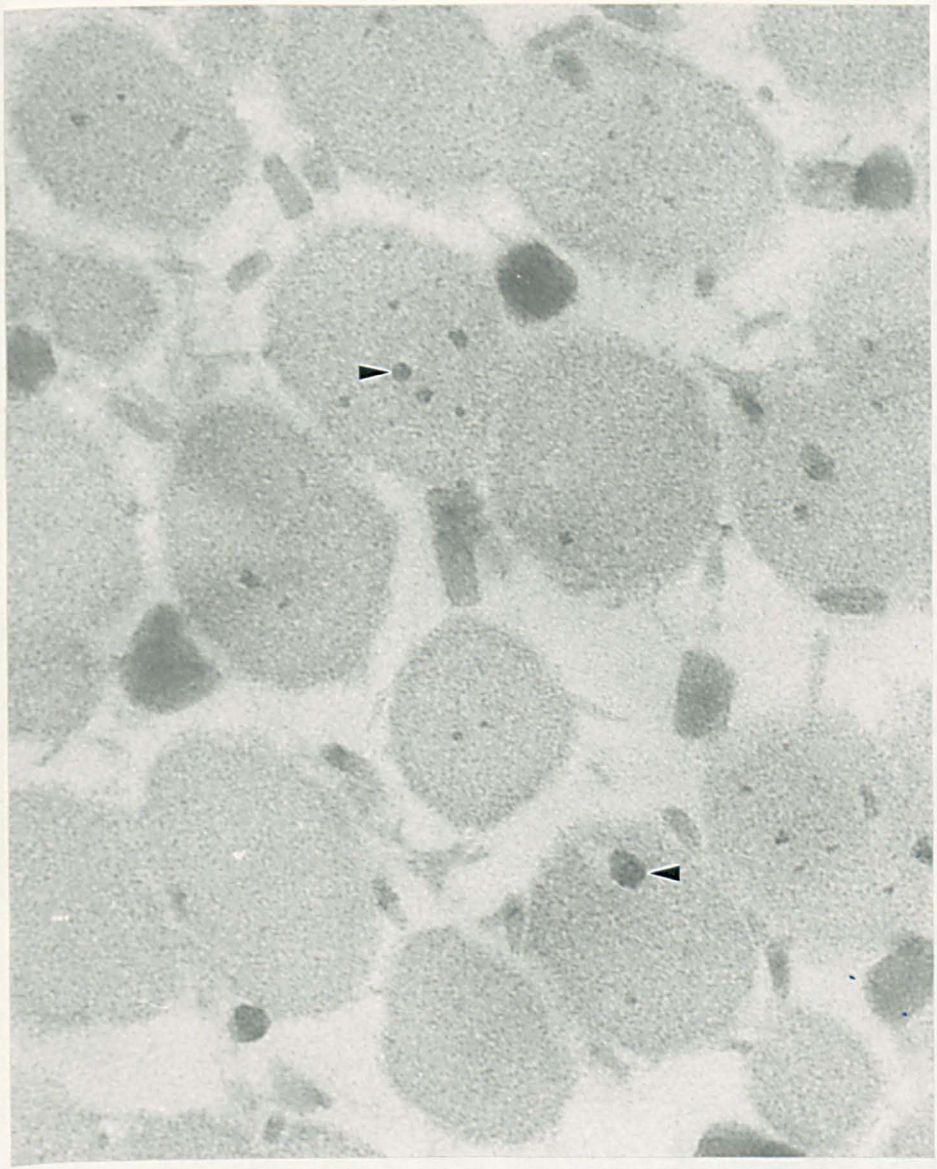

Figure 6.12 Shows transverse sections through the collagen fibrils of control chick sclera. Intrafibrillar proteoglycans (arrows) can be seen in the interior of the fibrils. ×151,000 magnification.

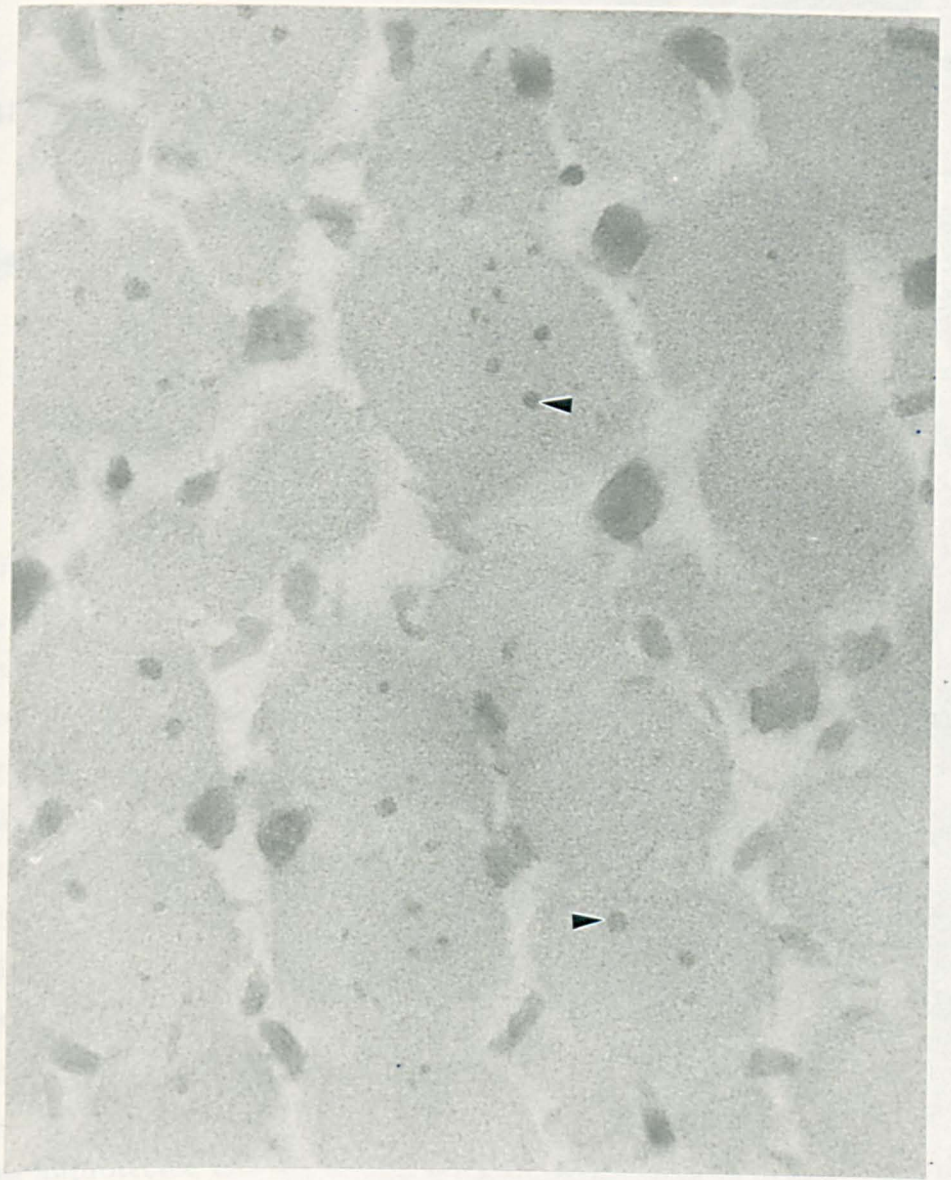

Figure 6.13 Shows transverse sections through the collagen fibrils of myopic chick sclera. Intrafibrillar proteoglycans (arrows) can be seen in the interior of the fibrils. $\times 151{,}000$ magnification.

Chapter 7

Discussion

7.1 Effect of Hydration on the Cornea

The investigation into the effect of the equilibration technique described in Chapter 2, has shown that the proteoglycans appear to be retained in the corneal stroma using this method. Proteoglycans are still visible attached to the collagen fibrils at hydrations below and above physiological, in contrast to what occurs when the cornea is placed unprotected into a swelling solution, when nearly all of the stromal proteoglycans are lost into the external solution. Examination of equilibrated samples by the TEM and SEM showed no detectable disruption of the tissue, suggesting that the equilibration technique used in this investigation is effective in changing the hydration of the stroma without otherwise affecting the tissue. This technique is therefore a much improved method of changing the hydration of the corneal stroma, compared to the previous technique of placing the cornea unprotected into distilled water (Goodfellow et al., 1978; Sayers et al., 1982).

The results from the swelling studies on bovine cornea clearly show that there is a linear relationship between interfibrillar spacing^2 and corneal hydration. Extrapolating the line down to zero hydration gives an interfibrillar spacing of ~34nm. We can calculate the fibril diameter at zero hydration by using the fibril diameter value of 37.4nm at physiological

hydration which was calculated in chapter 4, and adjusting this value by the percentage reduction in intermolecular spacings from physiological (1.60nm) to zero hydration (1.15nm). This leads to a value of ~27nm for fibril diameter at zero hydration. Thus, at zero hydration the fibrils in the corneal stroma are separated from each other by approximately 7nm presumably by the extra-fibrillar proteoglycans and other extra-fibrillar material in the stroma.

It is also possible to calculate the relative volumes of the non-aqueous component of the cornea and water at a specific hydration. Hydration (H) is defined as,

$$H = \frac{mass\ of\ water}{mass\ of\ cornea} = \frac{V_W}{V_C \times \rho_d} \tag{7.1}$$

where V_W and V_C are the volumes occupied by the water and the non-aqueous component of the cornea respectively, ρ_d is the density of the dry cornea. The density of water is taken as 1 g ml^{-1}, and Maurice (1969) has shown that ρ_d =1.28 g ml^{-1} for bovine cornea. Equation 7.1 can therefore be expressed as

$$V_W = V_C \times 1.28 \times H. \tag{7.2}$$

If V_H represents the volume of the hydrated cornea then

$$V_H = V_C + V_W = V_C(1 + 1.28H) \tag{7.3}$$

From Equation 7.3 it follows that at physiological hydration (H=3.2) water will occupy 4.1/5.1 of the volume of the cornea.

The volume fraction of collagen (f_c), water (f_w), and extra-fibrillar material (p) in the cornea can be calculated from data on the chemical composition of the bovine cornea (obtained from Maurice, 1969), and the densities of the various components of the cornea (obtained from Worthington 1984) . These are presented in Table 7.1, where all values are calculated at physiological hydration (H=3.2).

The volume fraction of the collagen in the cornea at physiological hydration (f_c) is calculated as 0.121. The fibril diameter at physiological hydration

Components	Weights	Densities	Areas	Vol. Fractions
Cornea	$w_s = 100$	$\rho_s = 1.05$	$A = 95.238$	1.000
Water	$w = 76.19$	$\rho_w = 1.00$	$wA = 76.190$	$f_w = 0.800$
Collagen	$w_c = 16.23$	$\rho_c = 1.41$	$f_cA = 11.511$	$f_c = 0.121$
Extra-material	$w_p = 7.57$	$\rho_p = 1.06$	$pA = 7.142$	$p = 0.075$

Table 7.1 Chemical composition, densities, and volume fractions of bovine cornea, calculated at physiological hydration. The values givern under the Weights and Areas headings are the relative weights and areas of the different components in the cornea.

has been determined in this investigation. If we assume liquid-like packing of fibrils as suggested by Worthington and Inouye (1985) and supported by this work, we can calculate the volume fraction of the fibril in the cornea (f) as,

$$f = \pi R_f^2/(d^2 \times 1.12) \tag{7.4}$$

where the fibril radius, $R_f = 18.7nm$; and the Bragg spacing, $d = 57.2nm$; giving us a fibril volume fraction in the cornea of $f = 0.300$ at physiological hydration. The volume fraction of the collagen in the fibril (c) can then be calculated from f_c/f, which gives a value of $c = 0.403$. Thus the volume of collagen in a fibril at any hydration, V_f is $\pi 18.7^2 \times 0.403 = 443nm^2$. The volume fraction of the extra-fibrillar material in the cornea (Table 7.1) is $p = 0.075$, so that the volume of extra-fibrillar material in each 'unit cell', V_p is $p \times d^2 \times 1.12 = 274nm^2$. Thus, the total volume of fibrillar and extra-fibrillar material in a 'unit cell' of the cornea, V_C is $443 + 274 = 717nm^2$. It is now possible, using Equation 7.3, to calculate the expected increase in volume with the increase in hydration if the water is evenly distributed around the fibrils.

This plot is shown in Figure 7.1. It is evident that that the slope of the theoretical line is greater that of the experimental; however the difference in slope is not very great, and at physiological hydration there is only a $\sim$5% difference in the theoretical and experimental volumes of the cornea. This $\sim$5% difference can be accounted for in several ways. Firstly it is possible that this 'missing volume' represents the volume of water which enters the

keratocytes in the corneal stroma - since the volume occupied by the keratocytes, though small, is an unknown quantity, this was left out of the volume calculations. Secondly, the 'missing volume' could be due to some of the extra-fibrillar material going into solution in the hydrated cornea. This would result in a lower value for V_C, and a lower gradient of the theoretical line. Lastly, it is possible that there is a change in the packing arrangement of the fibrils with hydration, into a less efficient form, or that some of the incoming water goes into regions of the corneal stroma where the fibrils are so disorganized that they do not contribute to the X-ray pattern. Up to around H=4 the small amount of 'missing volume' can easily be explained by either, or a combination of the first two possibilities. There is no evidence for a change in packing since the best-fit line is clearly a good fit to the experimental data (at least up to H=4). Electron microscopic observations during this investigation, using a range of preparation techniques, have produced no evidence of non-uniformity in the arrangement of the fibrils in corneas at physiological hydration. Thus, it appears that, at least up to physiological hydration the incoming water is evenly distributed around the fibrils.

The theoretical line and the experimental line have such similar slopes, at least up to ~H=4, that the small amount of 'missing volume' can easily be explained. However, above this hydration range the difference between the theoretical and experimental volume becomes quite large indicating that quite a lot of the incoming water is no longer being evenly distributed around the fibrils. One possibility is that a percentage of the incoming water is disappearing into 'lakes' in the corneal stroma. These 'lakes' (first proposed by Benedek, 1971) are regions in the corneal stroma almost devoid of fibrils, and filled with ground substance. Benedek postulated their existence in order to explain the opacity of the swollen cornea. Since Benedek (1971) subscribed to the destructive interference theory of transparency of the cornea, he proposed that loss of transparency at high hydrations is due to the 'lakes' reaching sizes of $\lambda/2$ or greater and thus scattering a large proportion of the incoming light. It seems possible that

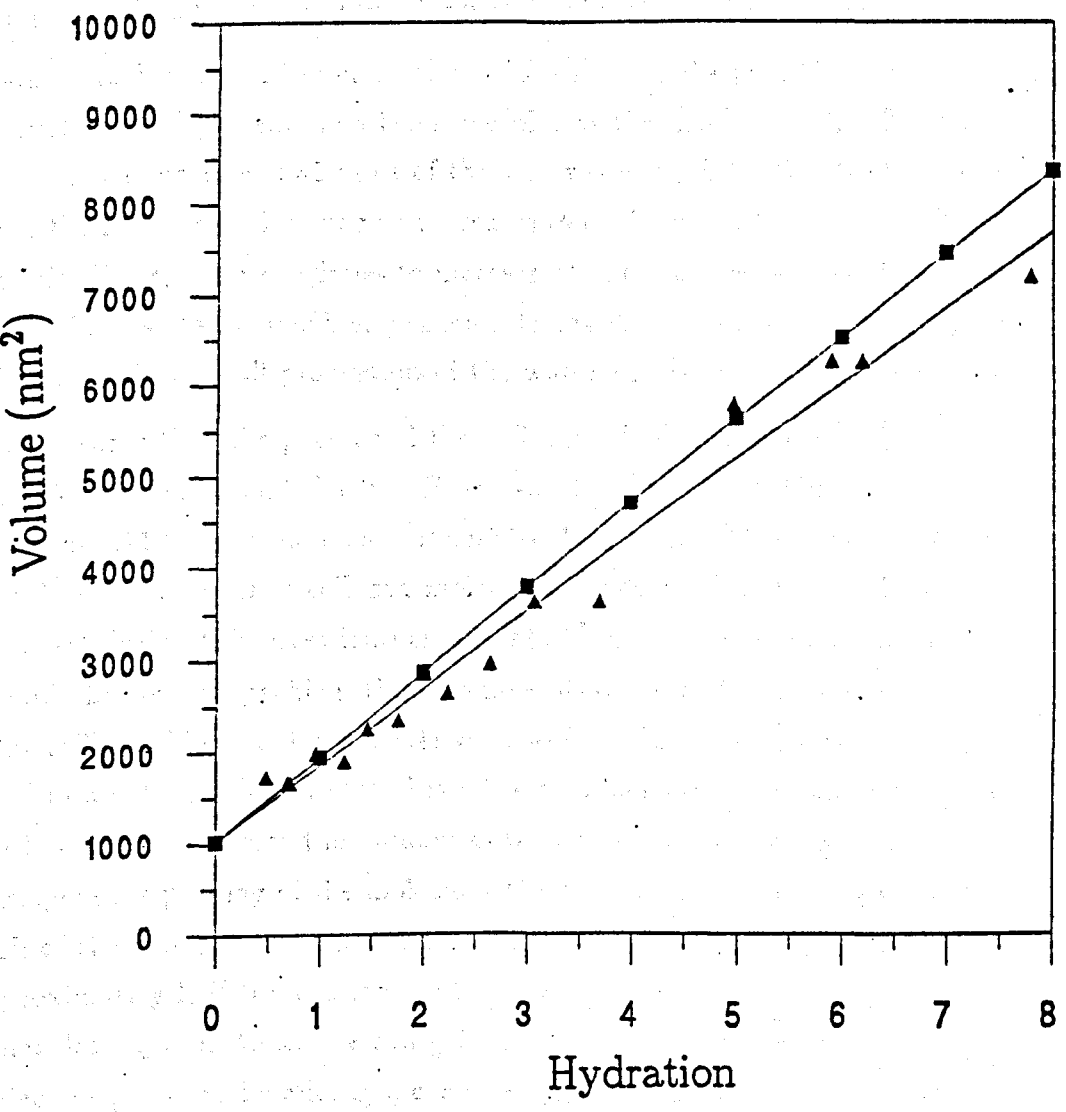

Figure 7.1 Experimental corneal interfibrillar volume from low-angle data is shown by the triangles with its corresponding least-squares, best-fit line. The theoretical increase in corneal volume, calculated by assuming the water to be absorbed uniformly throughout the tissue, is shown as squares with the corresponding lest-squares, best-fit line. In this calculation we have supposed the corneal tissue to swell in two-dimensions only, as is well supported by the low-angle data.

these 'lakes' may occur in some form in the highly swollen cornea.

Looking at Figure 3.12 in chapter 3, which showed the interfibrillar data normalized and presented on the same plot as the intermolecular data, it is obvious that up to ~H=1 most of the water is going into the fibrils. Above H=1 the intermolecular spacing increases only slightly, while the interfibrillar spacing continues to increase at the same rate, indicating that most of the water is now being taken into the spaces between the fibrils and that only a small proportion of the water enters the fibrils.

If we assume that the packing of the collagen molecules in the fibrils is 'pseudo-hexagonal' and that the Bragg spacing must be increased by a factor of 1.11 to give the mean intermolecular spacing, then it is possible to calculate the number of collagen molecules per fibril. The fibril volume obtained during this investigation was $\pi 18.7^2 = 1098.6nm^2$ and, assuming 'pseudo-hexagonal' packing, the volume associated with each molecule or 'unit cell' would equal $1.60^2 \times 1.11 = 2.84nm^2$. Thus the number of 'unit cells' in a cross-section of a fibril is ~386.8. The number of 'unit cells' in a fibril is not the same as the number of molecules. Even if we assume homogeneous packing of the molecules throughout the fibril cross-section, each of the molecules on the outer surface of the fibril requires a 'unit cell' approximately half the volume to maintain equal spacing with the molecules adjacent to it. We can get an estimate of the number of molecules per fibril by adding a correction factor for the 'edge effect' to the number of unit cells. This was calculated on the basis that the fraction of fibril volume associated with the collagen molecules on the edge of the fibrils is approximately half of that associated with the molecules inside the fibrils. Thus,

$$No.\ mols = \frac{\pi R_f^2}{d^2 \times 1.11} + \frac{2\pi R_f}{d \times 1.11} \div 2$$

where d in this equation is the Bragg spacing deriving from the intermolecular packing. The second term in the equation is an approximate correction for the 'edge effect' . This equation gives a value of 420 for the number of molecules in a fibril. With this value it is possible to calculate

the effective cross-sectional volume of a single collagen molecule as $V_f/420$ where $V_f = 443nm^2$ is the volume occupied by the collagen in a fibril. This gives a collagen molecular cross-sectional area of $1.05nm^2$, which is in very close agreement with the value of $1.04nm^2$, which was calculated directly from the diameter of a collagen molecule which is given as 1.15nm by Bigi and Roveri (1991).

Taking the diameter of a collagen molecule to be 1.15nm it is clear that at physiological hydration the molecules are separated by $1.78 - 1.15 = 0.63nm$. At zero hydration the collagen molecules are separated by $1.28 - 1.15 = 0.13nm$, this separation widens to $1.80 - 1.15 = 0.65nm$ at H=6, corresponding to an increase in spacing of 0.52nm. It seems probable that in order to encompass this range of intermolecular spacings, the covalent links between the molecules flex to some extent. Alternately the parts of the collagen molecules that are not crosslinked may bow away from adjacent molecules.

The results from the freezing section of this work demonstrate that there appears to be no effect on the intermolecular spacing as a result of freezing at $\sim -40°C$ and then thawing the corneas. However, during the freezing process there is some increase in intermolecular spacing and the pattern becomes sharper. The sharper ring could be a result of reduced thermal agitation, if the collagen molecules move about less during the exposure then the resultant pattern will be sharper. Freezing of the corneas at liquid nitrogen temperatures does appear to produce an irreversible reduction in intermolecular spacing. A possible explanation for this is that the extreme temperature leads to fractures within the now brittle cornea due to stresses caused by rapid uneven (outer to inner) cooling of the cornea, resulting in structural damage, which in turn causes a redistribution of water in the thawed cornea. Thus, it appears that freezing the cornea more slowly, in a conventional freezer to ~-40°C might produce less stress in a less brittle cornea, and so result in better preservation. Quantock et al., (1990) report that there appears to be no disruption of normal corneas at physiological hydration which have been stored frozen at -40°C.

The SEM studies clearly show that freezing has a considerable effect on the stroma of highly hydrated corneas. Large areas of disruption were observed in corneas hydrated above H=4, the higher the hydration the more disrupted is the tissue. The areas of disruption tend to occur in bands parallel to the lamellae in the corneas, which suggests that the areas are within or between the lamellae. The fact that the disruption is only obvious at higher than normal hydration may suggest that the abnormal swelling of the corneas has lead to structural weakening of certain regions of the stroma, which may in turn lead to concentration of the excess water in these regions during the relatively slow freezing process. One possibility is that these disrupted areas in frozen corneas correspond to the 'lakes' that Benedek (1971) proposed to occur in swollen corneas.

From this investigation it appears that the corneal stroma is a very robust structure and can be stored frozen without being detectably damaged so long as the cornea is at physiological hydration or lower. The corneal stroma is considerably disrupted while frozen, as shown by the reduction in the intermolecular spacing while frozen, and also by the various results of freeze fracture studies on the cornea (Itoh et al., 1981; Hirsch et al, 1982; and Williams, 1984) which indicate disruption caused by ice crystals. However, the corneal stroma appears to have the capacity to regain its normal arrangement on being thawed, suggesting some kind of self-ordering mechanism which can operate at physiological hydration but is lost in swollen corneas. This itself suggests that the critical factor may be the distance between fibrils, so that if this is too great, as is the case in swollen corneas, then the structures reordering the fibrils (possibly proteoglycans or type VI collagen attached to the fibrils) cannot interact.

7.2 Effects of Electron Microscopic Preparation on the Cornea

The results from this section indicate that glutaraldehyde fixation causes a significant increase in intermolecular spacing within the collagen fibril. It has been reported (Chapman et al., 1990) that polymeric crosslinks form, particularly between lysyl and hydroxylysyl residues (Bowes and Cater, 1968). The increase in intermolecular spacing might be due to swelling of the collagen fibrils in an hypertonic fixative solution before the glutaraldehyde intermolecular cross-links have formed. It might also be caused by the crosslinks pushing the collagen molecules further apart.

The reduction in D-periodicity is presumably the result of intramolecular crosslinks forming within the collagen molecule, possibly again between lysyl and hydroxylysyl residues, producing small conformational changes. Shrinkage has been reported to occur on a macroscopic scale (Chapman et al., 1990).

Dehydration appears to cause a reduction in interfibrillar spacing (TEM run 1). This could possibly be caused by the denaturing effect of ethanol; ethanol is also known to cause shrinkage and protein loss. Ethanol dehydration has been shown to cause ~10% shrinkage in muscle filaments (Page and Huxley, 1963). It has previously been established that fixation with osmium tetroxide results in significant loss of protein (Dallam, 1957). Since the proteoglycans in the cornea are implicated in maintaining fibril spacing, it is obvious that loss or denaturing of the protein cores will affect the fibril spacing. The reduction in interfibrillar spacing could also be due to the replacement of water by the much less polar ethanol, resulting in a loss of swelling pressure within the corneal stroma normally generated by the highly charged proteoglycans.

The stages between ethanol dehydration and resin polymerization is termed resin infiltration, however the specimens also pass through the intermediate solvent propylene oxide. The propylene oxide/resin infiltration stage only

produced a slight reduction in the D-period spacing of TEM run 1 processed specimens.

Resin polymerization clearly causes a decrease in interfibrillar spacing and of both the D-periodicity in samples fixed only in glutaraldehyde and in samples fixed in osmium tetroxide. Part of this shrinkage may be due to the ~3.5% volume reduction that epoxy resins are known to undergo as a result of thermal polymerization. The polymerization temperature of ~60°C is high enough to cause thermal shrinkage, reconstituted collagen fibrils are known to undergo shrinkage at 55-59°C (Danielsen, 1981), although the shrinkage temperature is increased following glutaraldehyde fixation.

Overall, TEM processing run 2 produced surprisingly little effect on the corneal stroma. The cross-linking produced by glutaraldehyde clearly stabilizes the structural components effectively enough to minimize extraction of proteins during the rest of the processing. Also, the extended fixation time in glutaraldehyde appears to have produced some fibril swelling which has compensated for the fibril shrinkage in later stages. The fact that the subsequent changes occurring in interfibrillar spacings in the corneal stroma are all reductions is significant. This suggests that there is some loss or weakening of the structural components which control the spacing of the fibrils. The proteoglycans have been implicated in controlling fibril spacing and loss of these molecules might well be expected to cause a decrease in interfibrillar spacing. The replacement of water by non-polar solvents and resins would also cause a reduction of swelling pressure in the cornea.

It is clear, comparing TEM runs 1 and 2, that post-fixation with osmium tetroxide has very drastic effects on the cornea. The osmium tetroxide must be affecting the packing of the collagen molecules in the fibrils to a large extent in order to lose the X-ray pattern from the intermolecular spacing. Osmium tetroxide also reduces the D-period spacing, although only slightly, but apparently has no effect on the interfibrillar spacing. This can be explained if we assume that osmium tetroxide has some ability to form

intermolecular crosslinks. Osmium tetroxide is known to oxidize α amino acids (Hake, 1965), and Deetz and Behrman (1981) report that osmium tetroxide reacts most rapidly with histidine, while Roth and Hinkley (1981) report stable products produced in reaction with glycine, alanine, valine, leucine, isoleucine, and phenylalanine. It is probable that osmium tetroxide can react with amino acids without being reduced to its lowest oxides, thus allowing it to react with other amino acids resulting in the formation of crosslinks. Osmium tetroxide is also known to cause massive loss of proteins, even if preceded by fixation in glutaraldehyde. This is presumably through the cleavage of proteins which has been shown to occur (Hopwood, 1969).

The results from the investigation of the different resins used in preparation of the cornea show, surprisingly that the more water soluble resins produce approximately the same amount of fibril shrinkage as does conventional epoxy resin. Assuming that the calculation of a fibril diameter of 37.4 ± 1.4nm is correct, then Nanoplast, which is 100% water soluble, undergoes $\sim$14% shrinkage, L.R. White resin, which is miscible in ethanol containing 12% water, undergoes $\sim$17% shrinkage, Lowicryl resin, which can tolerate 1% water, undergoes an $\sim$1% expansion, and Polarbed resin, which is totally immiscible with water undergoes, $\sim$10% shrinkage. As the preparation procedures differ, the changes in fibril diameter must be considered to be a result from the processing procedures (after glutaraldehyde fixation which was standard) and the resin used, rather than from the resin alone.

It is clear from the results that Nanoplast, a melamine resin which is totally water soluble, produces excellent ultrastructural preservation, and apparently preserves interfibrillar material which is lost using other embedding techniques. However, it is ineffective in preventing fibril shrinkage, and has the further disadvantages of difficult sectioning properties and a long embedding procedure.

L.R. White resin, an aromatic acrylic resin which has a limited miscibility

with water, showed the greatest amount of shrinkage. However, it has the advantages of good ultrastructural preservation, it readily takes up stain, has the shortest preparation procedure, and also, in contrast to all other resins used, is relatively safe to handle.

Lowicryl K4M is a methacrylate-acrylate resin and shows virtually (<1%) no change in fibril diameter and so probably gives the most accurate representation of the physiologically hydrated corneal stroma. It appears probable that the low-temperature preparation procedure for Lowicryl resin is responsible for preventing shrinkage of the collagen fibrils. At low temperatures the rearrangement of protein macromolecular systems in non-aqueous solutions is reduced due to the decrease in thermal vibration (Frauenfekder et al., 1979). Although the ultrastructural preservation using Lowicryl resins is not a good as that obtained with conventional epoxy resins, it is clear that the Lowicryl embedding technique produces effectively no volume changes. By following the Lowicryl low-temperature embedding procedure it is possible to obtain micrographs of cornea which are very close to the natural state of the cornea, making this method ideal for deriving the morphological data necessary to calculate the exact type of packing in the cornea.

The effect of critical point drying is a large reduction in all of the spacings monitored - interfibrillar, intermolecular and D-period. Clearly the process of removing all of the fluid from the tissue has a drastic effect. Although most of the fluid at this stage will be ethanol, the strength of the forces needed to keep the fibril spacing is still much less than if the fibrils are unsupported by any fluid. Also there is probably some strongly bound water still attached to the collagen molecule at the end of the ethanol dehydration. Critical point drying of the cornea would be expected to produce the kind of collapse of the corneal stroma that has actually occurred, the structures or forces holding the fibrils and collagen molecules apart are not strong enough to maintain their spacing when unsupported by fluid. In addition, critical point drying, through its combination of high pressure and elevated temperatures (up to 40°C) probably results in loss of

residual bound water in the collagen fibril, which would be expected to cause a contraction in the D-period.

It is clear that critical point drying is not an ideal preparation technique for SEM. Massive shrinkage occurs in interfibrillar spacing, intermolecular spacing and D-period spacing. Although post-fixation with osmium tetroxide is often used in SEM preparation to preserve lipids and reduce charging of the specimen in the electron beam, in the case of the cornea it would seem to be a particularly bad idea as it increases the already large shrinkage of the specimen.

7.2.1 Packing Analysis

The results from packing analysis of the changes occurring during electron microscopic preparation in effect show that there is minimal disruption to the packing arrangement. As a result of processing using TEM run 2 bovine corneas, there appears to be relatively little change in the packing arrangements within the stroma. The best fit theoretical scattering intensity curve after processing has values of N=5 and R_f=18nm. Thus the degree of order (and probably the packing arrangement) in the processed cornea appears to be the same as in the fresh bovine cornea. However, there may be changes in the fibril radius from ~20nm (Sayers et al., 1982) in the fresh cornea to 18nm in the embedded cornea, and of course, there is a considerable reduction in interfibrillar spacing.

The results of scattering intensity modelling of embedded cornea (TEM run 2) give a slightly higher value for fibril diameter (36nm) than from measurements made directly from micrographs of embedded corneas, which gave a fibril diameter of 33.6nm. The disparity may be due to the fact that only a small sample size (n=2) was used in the packing analysis compared to the morphological analysis. Another possibility is that one or more of the processes of sectioning, staining and exposure of the section to the electron beam in the TEM causes some shrinkage of the fibrils.

These results are encouraging in that they indicate that, if the correct processing schedule is used, (for bovine cornea the Lowicryl preparation procedure appears best), it should be possible to determine the exact type of packing in the cornea. As mentioned previously, several workers have already published analyses of electron micrographs of cornea, and the types of packing described range from a hexagonal lattice (Smith, 1969) to liquid-like packing (Worthington and Inouye, 1985), with most of the types of packing in between. The disagreement in the type of packing probably results from the different processing schedules used, these schedules are either not given at all, or would clearly result in corneal disruption, for example by the use of osmium as a fixative.

The effects of processing samples for the SEM clearly show much more shrinkage than occurs when processed for the TEM. The fibril radius decreases considerably from ~20nm to 15nm, a 25% decrease, while there is a similar decrease in interfibrillar spacing. However, again we essentially see no change in the packing arrangement of the stroma. Critical point drying although not perfect in that it does produce massive shrinkage, is far superior to air drying, which results in the interfibrillar pattern being lost totally.

The work on determining the fibril diameter has resulted in a value of 37.4nm±1.4nm. This value agrees well with the ~40nm fibril diameter reported by Sayers et al., (1982) obtained from the second of the models on X-ray data. During their modelling Sayers et al., (1982) used the value of R_f=20nm which was obtained from an extrapolation of a plot of interfibrillar spacing squared against hydration. Since this value produced a good fit to the data no attempt was made to refine the fit by using slightly higher or lower values for R_f, thus the value of R_f=20nm obtained from Sayers et al., (1982) could be ~ ±1nm in error. The value of 37.4nm also agrees well with the value of 39nm obtained by Worthington and Inouye (1985) for cow cornea. This value was obtained by assuming that the subsidary equatorial reflections from the interfibrillar spacing are solely due to the fibril transform, an assumption this investigation has shown not to

be totally correct, although it is a reasonable approximation. Another possible reason for the higher value obtained from the X-ray data could be that the fibril transform obtained from fresh hydrated fibrils in the corneal stroma includes not only the collagen fibrils but also material attached to the surface of the collagen fibrils, for example proteoglycans and non-fibrillar proteins, which effectively increase the diameter of the fibrils.

7.2.2 Transparency of the Cornea

By using the value of a fibril diameter of 37.4nm, and assuming liquid-like packing as proposed by Worthington and supported by this thesis, it is possible to calculate the different refractive indices of the fibrils (n_f) and the ground substance(n_g) of the cornea, and from these values work out the transmittance (T) of light through the cornea. The following calculations are based on the equations derived by Worthington (1984).

The refractive index of the corneal stroma (n_s) is the sum of the refractive indices of its components, as is shown in Equation 7.5, which is based on Gladstone and Dale's law of mixtures

$$n_s = n_w + fc(n_c - n_w) + p(n_p - n_w) \tag{7.5}$$

The following values are known from the work by Maurice (1969) on bovine cornea; the refractive index of the stroma, n_s=1.375; the refractive index of water, n_w=1.333; and the refractive index of dry collagen, n_c=1.547. Combining these values with the values of f_c and p from Table 7.1, the refractive index of the extra-fibrillar material (n_p) is calculated from Equation 7.5 as $n_p = 1.548$.

The next step is to calculate the refractive indices of the collagen fibrils in the stroma (n_f), and of the ground substance between the fibrils (n_g). The refractive index of the fibrils can be calculated from Equation 7.6

$$n_f = n_i + c(n_c - n_i) \tag{7.6}$$

where n_i is the refractive index of the fluid inside the fibril, and c, the collagen fraction in the fibril, has already been calculated as 0.403. It seems reasonable to assume that the fluid inside the fibril has the same refractive index as water, since virtually all of the extra-fibrillar material consists of macromolecules too large to invade the spaces between the collagen molecules. Thus if we assume $n_i = n_w$ in Equation 7.6, we obtain a value of n_f=1.419

The refractive index of the ground substance (n_g) can be calculated using Equation 7.7, where g is the volume fraction of the extra-fibrillar material in the extra-fibrillar volume of the cornea. The value of g can be calculated from $g = p/(1 - f)$ giving g=0.107, and hence n_g=1.356.

$$n_g = n_w + g(n_p - n_w) \tag{7.7}$$

The refractive index difference (Δv) between the refractive indices of the ground substance ($n_g = 1.356$), and the fibrils ($n_f = 1.419$) is $\Delta v = 0.063$.

With the values obtained above it is possible to calculate the transmittance (T) of the cornea. The attenuation of light through the cornea is described according to the well known exponential law Equation 7.8,

$$I = I_o exp(-\mu\sigma t). \tag{7.8}$$

where I_o is the incident intensity of light and I is the transmitted intensity, σ is the number density of the fibrils obtained from $\sigma = f/a$ ($a = \pi R_f^2$) and t is the thickness of the cornea. The value of μ is the cross-section for scattering over all possible scattering angles, Equation 7.9 defining μ was derived by Maurice (1957) and by Hart and Farrell (1969) and is written in the form used by Worthington (1984)

$$\mu = E(\pi/\lambda)^3 a^2 \Delta v^2. \tag{7.9}$$

Thus, the attenuation factor, $\mu\sigma t$, can be written as shown in Equation 7.10,

$$\mu\sigma t = Eaft\pi^3\Delta v^2/\lambda^3. \tag{7.10}$$

The factor E is a function of the refractive indices of the fibrils (n_f), and the ground substance (n_g). Equation 7.11, defining E was first derived by Maurice (1957), and is in the form used Worthington (1985):

$$E = (n_f + n_g)^2[(1/n_g) + 2n_g^3/(n_f^2 + n_g^2)^2] \qquad (7.11)$$

Using Equation 7.11 a value of $E = 8.267$ was obtained.

Taking a value of 500nm for the wavelength of light (λ), 8×10^5nm for the thickness of the cornea (t) from (Scott and Bosworth, 1990), and using Equation 7.10, $\mu\sigma t = 2.146$ for the attenuation factor is obtained. Using this value in Equation 7.8 we can obtain the transmittance of the cornea $T = I/I_o$. Thus we obtain a value of $T = 0.117$ for the transmittance of light through the bovine cornea at $\lambda = 500nm$.

It should be emphasized that this value is the maximum realistic value; since the chemical composition of the bovine cornea was published by Maurice (1969), work done by Winterhalter (1988) has shown that possibly as much as 50% of the 'extra-material' in the human cornea is other types of collagen (mostly type VI), and might be associated with the fibrils under normal physiological conditions. If this is also the case in the bovine cornea, then it would mean that the refractive index of the fibrils would increase and the refractive index of the ground substance decrease, increasing the value of Δv and considerably reducing the transmittance of light through the cornea.

Since the experimental value for the transmittance of light through the cornea is ~0.99, it is obvious that the cornea is not transparent as the result of a uniform refractive index as first considered by Maurice (1957), and Smith (1969). Consequently, it would appear that the destructive interference theory (Maurice, 1957) is the correct theory. The results from the work on the packing arrangement of the corneas by Sayers et al., (1982) indicate short range order, ($N = 5$). Various workers, notably Hart and Farrell (1969), and Bendeck (1971) have shown theoretically that short range order in the corneal stroma should be sufficient to ensure transparency.

7.3 Keratoconus

7.3.1 Human Keratoconus

The SEM micrographs show the characteristic Z-shaped lamellae in the central region of the keratoconus cornea (Figure 5.6), unlike the parallel arrangement seen in normal cornea (Figure 5.7). The 'Z' shaped folds are possibly an artifact caused by the release of tension when the keratoconus cornea is removed from the eye, since the central region is thinner and weaker than normal. Under the SEM the thinning in the central area appears to be due to fewer lamellae and a reduction in the mean thickness of individual lamellae (Figure 5.1). Since results from the low-angle X-ray patterns have shown that there is no reduction in the interfibrillar packing of the collagen fibrils, the reduction in the thickness of the lamellae is possibly due to a loss of collagen fibrils from the lamellae. The elongated appearance of the epithelial cells in the central region (Figure 5.3) is possibly a secondary effect of the formation of the ectasia, the epithelial cells over the rest of the keratoconus cornea appear normal in shape but with a larger variation in size in comparison to normal corneas.

TEM results from the cuprolinic blue-staining clearly demonstrate an abnormal arrangement of proteoglycans in keratoconus corneas (Figure 5.9), compared to normal (Figure 5.8). It is possible that this arrangement is due to secondary scarring of the cornea, however the orientation of the proteoglycans is unusual and unlike the expected orientation of proteoglycans in scarred tissue (Rawe et al., 1991). The arrangement may be due to stresses within the stroma causing slipping between adjacent collagen fibrils and thus displacing the proteoglycans into a parallel arrangement with respect to collagen fibrils; this is supported by the elongated arrangement of the epithelial cells which suggests that they may also have been stretched in one direction. This explanation obviously supports the theory that keratoconus results from ocular trauma.

An alternative possibility is that the abnormal arrangement is due to a

difference in the nature of the proteoglycans; a recent report (Funderburgh et al., 1989) states that in keratoconus corneas the keratan sulphate proteoglycan core has fewer keratan sulphate chains attached. This difference in proteoglycan structure could explain the lower levels of staining and abnormal proteoglycan arrangement which we have observed.

The results from Figure 5.10 suggest that the interfibrillar spacing is the same at any given hydration in both keratoconus and control corneas. This implies that the uptake of water around the diffracting fibrils in the corneal stroma is the same in both tissues. However, measurements of the peak profiles indicate that keratoconus corneas have a wider range of spacings than control corneas, indicating a more disordered arrangement of fibrils in keratoconus.

By equilibrating corneas to a specific hydration ($H=2.4\pm0.2$) it was possible to compare the interfibrillar spacings of large numbers of corneas, and from this experiment it became clear that there is no significant ($p>0.2$) difference between control and keratoconus corneas. This result was confirmed using "fresh" control and keratoconus corneas at physiological hydration (Table 5.3), where once again no difference in interfibrillar spacing was observed. The X-ray results on interfibrillar spacing have clearly demonstrated that the thinning which occurs in the central region of the keratoconus cornea (up to 60%) is not due to compression of the fibrils, but is due to loss of fibrils from this region.

Figure 5.12 shows that the intermolecular spacing in keratoconus fibrils does not increase above $H=2$, in agreement with results obtained from bovine corneas during work on this thesis and from human normal corneas (N.S. Malik, personal communication). Results from control and keratoconus corneas equilibrated at $H=2.4$ show a significantly ($p<0.01$) lower (3.3%) intermolecular spacing in keratoconus. Results from control and keratoconus corneas at normal physiological hydration show a highly significant ($p<0.001$) reduction (7.5%) in intermolecular spacing in keratoconus corneas. It has been shown (Malik et al., 1992) that there is a

4% increase in the intermolecular spacing in normal human corneas with age, resulting in a 4% increase in intermolecular spacing between birth and 90 years. However, most of this increase occurs up to the age of 40 years, beyond which the spacing remains constant. Between the ages of 31 years (the mean age of keratoconus corneas), and 58 years (the mean age of the control corneas), there is less than a 1% increase in intermolecular spacing. The age effect is, therefore, not likely to be the cause of the significant difference in intermolecular spacing found between keratoconus and control corneas. The reduction in intermolecular spacing in keratoconus corneas would result in a reduction in fibril diameter of up to 7.5% assuming the same number of collagen molecules per fibril as normal.

A possible reason for the small but significant change in intermolecular spacing in keratoconus corneas could be a change in the crosslinking of the collagen. Abnormal crosslinking in keratoconus has been reported (Cannon and Foster 1978) where the collagen has increased levels of lysinonorleucine crosslinks, however later workers were unable to confirm this finding (Oxlund and Simonsen, 1985).

An alternative explanation is that the change in intermolecular spacing is due to a change in the relative osmotic strengths of the interfibrillar and intrafibrillar environments. An increase in the osmotic strength of the interfibrillar environment relative to the intrafibrillar environment would cause water to move out from between the collagen molecules into the interfibrillar space and result in closer intermolecular spacing, and a reduction in fibril diameter. This effect has been demonstrated in cartilage collagen by Katz et al., (1986). Increased levels of polyanions including glycosaminoglycans have been shown to occur in the stroma of keratoconus corneas (Yue et al., 1988), and more recent work (Yue et al., 1990) suggests that there is an increase in the 4-sulphated disaccharides of chondroitin and dermatan sulphates, but a reduction in the sulphated epitopes of keratan sulphate, giving an overall increase in polyanion levels in keratoconus corneal stroma. Higher levels of glycosaminoglycans within the interfibrillar space might attract permeant ions from the intrafibrillar space, reducing

the osmotic potential of the intrafibrillar space and decreasing intermolecular spacing.

The results obtained from analysis of the meridional patterns show that there is very little difference in electron density along the collagen fibrils between normal and keratoconus corneas (R=0.17). However, analysis of cupromeronic-blue stained material shows large differences (R=0.39) between normal and keratoconus corneas which probably reflect some alteration of the ordered proteoglycans along the collagen fibrils. Further analyses of the integrated intensities by the use of Patterson functions again show very little difference in the electron density vectors along the unstained collagen fibril between normal and keratoconus corneas. In cupromeronic blue-stained material, the Patterson functions for normal and for keratoconus corneas are very different. This difference is probably due to certain keratoconus proteoglycans taking up less stain than their normal counterparts or may be because they are less ordered than normal. There does not appear to be a uniform reduction of proteoglycan staining in keratoconus, but rather a bias towards certain proteoglycans or towards certain proteoglycan binding sites along the collagen fibril. The abnormal form of keratan sulphate proteoglycan, with fewer keratan sulphate chains (Yue et al., 1990) or with a modified structure (Funderburgh et al., 1989) as reported in keratoconus corneas, would result in lower staining by cupromeronic blue for the ordered keratan sulphate proteoglycans along the collagen fibril. This might be expected to lead to the kind of Patterson function seen in Figure 5.14.

In conclusion, it has been shown that there is no overall change in interfibrillar spacing, a reduction of up to 7.5% in intermolecular spacing, and an uneven reduction in staining of the ordered proteoglycans along the collagen fibril axis in keratoconus corneas compared to control corneas.

7.3.2 Chicken Keratoconus

The low-angle results clearly show chicken keratoconus corneas to have a significantly ($p>0.0001$) higher interfibrillar spacing than normal corneas. The difference in means between 63.8nm for keratoconus corneas and 58.4nm for normal corneas would represent a 9% increase of corneal thickness in keratoconus corneas, assuming the same number of fibrils in normal and keratoconus corneas. Unfortunately, the thickness of chicken keratoconus and normal corneas was not accurately determined, it should be possible to detect the 9% increase in thickness in chicken keratoconus corneas suggested by these results. The wide-angle data suggest that there are higher intermolecular spacings in chicken keratoconus corneas than in normal corneas, although the difference is not clearly significant ($0.1>p>0.05$). Both of these results are in contrast to the human keratoconus data, where it was shown that there is no difference in interfibrillar spacing between normal and keratoconus human corneas, and a significantly *lower* intermolecular spacing in keratoconus human corneas. The abnormal arrangement of proteoglycans (Figure 5.9) observed in certain regions of human keratoconus corneas was not seen in chicken keratoconus corneas (Figure 5.16), although the lower levels of proteoglycan staining in chicken keratoconus corneas was sometimes observed in human keratoconus corneas. Although the chicken model of keratoconus may follow the development of human keratoconus in many respects (Whitley et al., 1986), it appears that, with regard to interfibrillar spacings, intermolecular spacings, and the arrangement of the proteoglycans in the stroma, the chicken model of keratoconus differs to some degree with what was observed in human keratoconus.

7.4 Myopia

The X-ray results on cornea show no significant difference in interfibrillar spacing or in intermolecular spacing, although in both instances, myopic

corneas have the higher spacing. The X-ray results on sclera show that myopic sclera has a higher intermolecular spacing than normal. The intermolecular spacing of bovine sclera increases with hydration (Chapter 3). Thus, a possible explanation for the increased intermolecular spacing in myopic sclera is that the tissue is more hydrated. Recent work by Christensen and Wallman (1991) has shown that the sclera of myopic chicks is more hydrated than normal sclera.

Two morphologically distinct types of proteoglycan were observed in both normal and myopic sclera. This finding agrees well with work by Rada et al., (1991), who report finding the proteoglycans decorin ($M_r \sim 43,000$), and aggrecan ($M_r > 1 \times 10^6$)

The preferential binding of the proteoglycans in both normal and myopic sclera to the 'd' and 'e' bands of the collagen fibrils agrees with the observation of Quantock and Meek (1988) working on human sclera, and Young (1985) who reported binding of proteoglycans to the 'd' region in rabbit sclera.

Sclera has previously been reported as containing 'almost no' intrafibrillar proteoglycans (Scott 1991) with no indication of any preferential binding sites in sclera. Scott (1990) reports that the intrafibrillar proteoglycans present in rat-tail tendon are located along the gap region of the fibrils, this is in agreement with our findings in chick sclera. Scott suggests that in rat-tail tendon the intrafibrillar proteoglycans are attached to the surface of collagen protofibrils, and that a possible function of the proteoglycans is to prevent the assembly of the protofibrils into larger fibrils.

Most of the swelling pressure in sclera is caused by the proteoglycans. The proteoglycans have charged groups on their glycosaminoglycans which attract a cloud of permeant ions, producing a high osmotic potential. Thus an increase in the intrafibrillar proteoglycans, would result in an increased intermolecular spacing. The wider range of intermolecular spacings observed in myopic sclera might have a number of explanations. It is possible that the collagen in the myopic chicks is undergoing a more rapid

turnover than in the control chicks. This might lead to a wider range of intermolecular spacings derived from the higher proportion of collagen undergoing change in the myopic sclera. Alternatively, the larger range could be due a difference in the number or distribution of intrafibrillar proteoglycans in myopic sclera, leading to more irregular packing of the collagen molecules within the fibrils. No obvious difference in the number or distribution of the intrafibrillar proteoglycans was observed.

The higher proportion of spaces between collagen bundles, usually associated with aggregations of large proteoglycans (possibly the proteoglycan aggrecan) present in myopic sclera, may account for the higher levels of hydration observed in this tissue (Christensen and Wallman 1991). The clumping may be due to the presence of hyaluronic acid, or may be related to the findings of Rada et al., (1991) who report unexpectedly high levels of aggrecan core protein in myopic sclera. These clumps of proteoglycans associated with gaps between the collagen bundles bear a resemblance to micrographs of the corneal stroma during wound healing, when very large proteoglycans are present in spaces within the damaged lamellae (Cintron et al., 1990; Rawe et al., 1991). In wound healing the large proteoglycans are precursors of the synthesis of collagen fibrils by the keratocytes in the damaged area of the corneal stroma. It seems possible that the aggregations of proteoglycans in chick sclera may facilitate the growth of the fibrous sclera in chicks, and that this higher proportion of space in myopic sclera reflects that this process is occurring a faster rate in myopic chicks.

The results from this investigation show the binding sites of the proteoglycans to be along the 'd' and 'e' bands of the collagen fibrils in both control and myopic chicks. Also, both types of sclera had intrafibrillar proteoglycans located preferentially along the gap region of the fibrils. Differences in the appearance of the proteoglycans were found, but these were of a quantitative rather than a qualitative nature; the myopic sclera appears to have more spaces associated with aggregates of large proteoglycans than control sclera. Also, the higher intermolecular spacing

in myopic sclera, together with the wider range of spacings observed, suggests the possibility of more rapid turnover of the collagen or differences in the intrafibrillar proteoglycans in myopic sclera. If these differences observed between myopic and normal sclera are related to the abnormal expansion of the sclera in myopic chicks, then it appears that this process is only a more exaggerated form of what is already occurring during the normal growth of the sclera. These findings do not support evidence for a distinct mechanism of scleral expansion in chick myopia.

7.5 Main Conclusions

The main findings of this project are listed as follows:

1. The findings of Goodfellow et al., (1978) and Sayers et al., (1982), that the plot of interfibrillar spacing^2 against hydration is a linear relationship, has been confirmed using fresh equilibrated bovine corneas.

2. The effect of hydration on intermolecular spacing in cornea, sclera and rat-tail tendon has been documented. Similar behaviour is observed in all three cases, a rapid increase in intermolecular spacing in the range H=0 to H$\approx$1, after which there is virtually no change with hydration.

3. Intermolecular and interfibrillar spacings in bovine cornea have been shown to rise in unison over the hydration range H=0 to H$\approx$1, after which nearly all of the water enters the interfibrillar spaces.

4. Freezing corneas to -40°C and then thawing has been shown to have little effect on corneas at physiological hydration and below, but to cause disruption in the stroma of swollen corneas. In contrast, freezing to -180°C and thawing results in permanent damage to corneas at physiological hydration.

5. The structural changes occuring during each stage of several different processing runs for the TEM and the SEM have been described. The parameters monitored were interfibrillar spacing, intermolecular spacing, D-period spacing, fibril diameter, and fibril packing. The optimum preparation technique for TEM involves extended fixation in glutaraldehyde followed by low temperature embedding in Lowicryl K4M resin.

6. The fibril diameter in bovine cornea at physiological hydration has been established to be 37.4nm±1.4.

7. Analysis of embedded corneas by fitting X-ray data with models of fibril packing, and examination under the TEM, indicates that the packing of fibrils in the cornea is probably liquid-like, as proposed by Worthington and Inoyue (1985).

8. By plotting the experimental increase in volume with hydration of the cornea against the theoretical increase (calculated from data obtained in this investigation), it is evident that the water entering the stroma is evenly distributed around the fibrils over the hydration range H=0 to H=4. Above H=4 its distribution around the fibrils appears to become less even, suggesting the possibility that the extra water is entering the 'lakes', proposed by Benedek (1971).

9. Using results from Chapters 3 and 4, it has been possible to calculate the theoretical transmittance of light through the bovine cornea (excluding interference effects); a value of $T \approx 12\%$ was obtained. Thus, most of the transparency of the cornea must be due to constructive interference as first proposed by Maurice (1957).

10. SEM and TEM micrographs of keratoconus corneas have shown abnormally elongated epithelial cells, disrupted lamellae, and abnormally arranged proteoglycans. X-ray data have shown that the thinning of the stroma is not due to closer packing of the fibrils. Increased intermolecular spacing in keratoconus is probably due to

higher levels of polyanions (proteoglycans) increasing the osmotic potential of the interfibrillar space. Analysis of meridional patterns has shown an abnormality in the distribution of proteoglycans along the collagen fibrils in keratoconus.

11. No differences were found between the corneas of normal and myopic chicks, or between the attachment sites of the inter- and intra-fibrillar proteoglycans in normal and myopic chick sclera. Myopic chicks were found to have more of a large proteoglycan (probably aggrecan) which was associated with larger empty spaces than normal sclera. Analysis of X-ray data showed that myopic sclera had a significantly higher intermolecular spacing than normal.

7.6 Future Work

Much of this thesis has been spent developing a TEM preparation procedure which results in minimal disruption to the corneal stroma. This allows the possibility of obtaining from micrographs, information such as mean interfibrillar spacing, radial distribution functions, and fibril number density, any of which which cannot be obtained directly from X-ray data. With this information it should be possible to determine the exact type of packing in the cornea. The next step would be to use these experimental values to calculate exactly how much constructive interference of light occurs, using the equations already derived by Maurice (1957), and Hart and Farrell (1969) for the cornea. This would hopefully lead to a clear understanding of the basis of transparency in the normal cornea, and also as to why transparency is lost in a number of corneal disfunctions.

7.7 Publications

To date three papers, and two refereed abstracts have been published from the work in this thesis. Three abstracts are currently under consideration at the present time.

Papers

Fullwood, N.J., Meek, K.M., Malik, N.S., and Tuft, S.J. A comparison of proteoglycan arrangement in normal and keratoconus human corneas. Biochem. Soc. Trans. **18:** 961-962. 1990.

Meek, K.M., Fullwood, N.J., Cooke, P.H., Elliott, G.F., Maurice, D.M., Quantock, A.J., Wall, R.S., and Worthington, C.R. Synchrotron X-ray studies of the cornea, with implications for stromal hydration. Biophysical Journal **60:** 467-474. 1991.

Fullwood, N.J., Tuft, S.J., Malik, K.M., Meek, K.M., Ridgway, A.E.A., and Harrison, R.J. Synchrotron X-ray diffraction studies of keratoconus corneal stroma. Invest. Ophthal. Vis. Sci. **33:** 1166-1173. 1992.

Refereed Abstracts

Fullwood, N.J., Cooke, P.M., Elliott, G.M., Meek, K.M., and Maurice, D.M. High angle X-ray diffraction studies of the corneal stroma: The effect of hydration on the intermolecular spacing. Invest. Ophthal. Vis. Sci. (Suppl) **31:** 32. 1990.

Fullwood, N.J. and Meek, K.M. A comparison of proteoglycan arrangement in normal and keratoconus human corneas. Structure, Biology and Pathology of Proteoglycans Colloquia. 634th Meeting of Biochemical Society. Abstract No 147. April 1990.

Under consideration

Fullwood, N.J. and Meek, K.M. X-ray diffraction and ultrastructural studies on freezing in the cornea. Submitted to 33rd meeting of the Association for Eye Research. June 1992.

Fullwood, N.J. and Meek, K.M. Changes in the cornea during preparation

for electron microscopy. Submitted to 10th meeting of the International Congress of Eye Research. September 1992.

Meek, K.M. and Fullwood, N.J. Structure of corneal collagen using synchrotron X-ray diffraction and transmission electron microscopy. Submitted to 10th meeting of the International Congress of Eye Research. September 1992.

Chapter 8

References

Adler, H.J., Gross, S.T. and Lambert,J.M. Physical studies on corneal tissues. Science (Wash. DC). **109:** 383. 1949.

Agarwal, L.P., Chand, D., Mishra, R.K. and Khosla, P.K. X-ray diffraction patterns of the rabbit cornea. Orient. Arch. Ophthal. **10:** 236. 1972.

Anseth, A. Studies on corneal polysaccharides. Exp. Eye. Res. **8:** 438. 1969.

Axelsson, I. and Heinegård, D. Fractionation of proteoglycans from bovine corneal stroma. Biochem. J., **145:** 491. 1975.

Azaroff, C.V. Elements of X-ray crystallography. McGraw-Hill Book Company, N.Y. 1968.

Bear, R.S. and Bolduan, O.E.A. Diffraction by cylindrical bodies with periodic axial structure. Acta Crystallogr. **3:** 236. 1950.

Benedek, G.B. Theory of transparency of the eye. Applied Optics. **10:** 459. 1971.

Bigi, A. and Roveri, N. Fibre diffraction: collagen. *In:* Handbook on synchrotron radiation. Vol. 4. (Eds. Ebashi, S., Koch, M. and Rubenstein, E.). Elsevier Science Publishers B.V., 1991.

Buckley, R.J. The Cornea *In:* Clinical Ophthalmology (Ed. Miller, S.)

I.O.P. Publishing Ltd., Bristol. 1987.

Buddecke, E. and Wollensak, J. Saure mucopolysaccharide und glykoproteine der menschlichen cornea in abhangigkeit vom lebensalter und bei keratoconus. Graefes. Arch. Klin. Exp. Ophthalmol. **171:** 105. 1966.

Bowes, J.H. and Cater, C.W. The interaction of aldehydes with collagen. Biochem. Biophys. Acta. **168:** 341. 1968.

Cannon, J. and Foster, C.S. Collagen crosslinking in keratoconus. Invest. Ophthalmol. Visual. Sci. **17:** 63. 1978.

Chapman, J.A. and Hulmes, D.J.S. Electron microscopy of the collagen fibril. *In:* Ultrastructure of the connective tissue matrix. (Eds. Ruggeri, A. and Motta, P.M.). Martinus Nijhoff. Boston. 1984.

Chapman, J.A., Tzaphildou, M., Meek, K.M. and Kadler, K.E. The collagen fibril - A model system for studying the staining and fixation of a protein. Electron. Microsc. Rev. **3:** 143. 1990.

Christensen, A.M. and Wallman, J. Evidence that increased scleral growth underlies visual deprivation myopia in chicks. Invest. Ophthamol. Vis. Sci. **32:** 2143. 1991.

Cintron, C., Covington, H.I. and Kublin, C.L. Morphologic analysis of proteoglycans in rabbit corneal scars. Invest. Ophthalmol. Vis. Sci. **31,** 1789. 1990.

Craig, A.S. and Parry, D.A.D. Collagen fibrils of the vertebrate corneal stroma. J. Ultrastruct. Mol. Struct. Res. **74:** 232. 1981.

Craig, A.S., Robertson, J.G. and Parry, D.A.D. Preservation of corneal collagen fibril structure using low temperature procedures for electron microscopy. J. Ultrastruct. Mol. Struct. Res., **96:** 172. 1987.

Cooke, P.H., Maurice, D.M., Elliott, G.F. and Meek, K.M. Moderate to high-angle X-ray diffraction studies of the corneal stroma, with implications for fibril hydration. Unpublished manuscript. 1987.

Cöster, L. and Fransson, L-A. Isolation and characterization of dermatan sulphate proteoglycans from bovine sclera. Biochem. J. **193:** 143. 1981.

Cox, J.L., Farrell, R.A., Hart, R.W. and Langham, M.E. the transparency of the cornea. J. Physiol. **21:** 601. 1970.

Curtin, B.J., Iwamoto, T. and Renaldo, D.P. Normal and staphylomatous sclera of high myopia. Arch. Ophthalmol. **97,** 912. 1979.

Curtin, B.J. and Teng, C.C. Scleral changes in pathological myopia. Trans. Amer. Acad. Ophthalmol. Otolaryngol. **62:** 777. 1957.

Dallam, R.D. Determination of protein and lipid lost during osmic fixation of tissues and cellular particulates. J. Histochem. Cytochem. **5:** 178. 1957.

Danielsen, C.C. Thermal stability of reconstituted collagen fibrils. Shrinkage characteristics upon *in vitro* maturation. Mech. Ageing. Devel. **15:** 269. 1981.

Deetz, J.S. and Behrman, E.J. Reaction of osmium reagents with amino acids and proteins. Int. J. Peptide Protein Res. **17:** 495. 1981.

Fischbarg, J., Hernandez, J., Leibovitch, L.S. and Koniarek, J.P. The mechanism of fluid and electrolyte transport across corneal endothelium: Critical revision and update of a model. Curr. Eye. Res. **4:** 351. 1985.

Frauenfelder, H., Petsko, G.A. and Tsernoglou, D. Temperature-dependant X-ray diffraction as a probe of protein structure dynamics. Nature Lond. **280:** 558. 1979.

Friend, J. Physiology of the cornea: Metabolism and biochemistry, *In:* The Corneas. Scientific Foundations and Clinical Practice, 2nd ed (Eds. Smolin,G. and Thoft,R.A.), Little, Brown, Boston. 1987.

Fullwood, N.J., Meek, K.M., Malik, N.S. and Tuft, S.J. A comparison of proteoglycan arrangement in normal and keratoconus corneas. Biochem. Soc. Trans. **18:** 961. 1990a.

Fullwood, N.J., Cooke, P.M., Elliott, G.M., Meek, K.M. and Maurice, D.M. High angle X-ray diffraction studies of the corneal stroma: The effect of hydration on the intermolecular spacing. Invest. Ophthal. Vis. Sci. (Suppl.) **31:** 32. 1990b.

Funderburgh, J.L., Panjwani, N., Conrad, G.W. and Baum, J. Altered keratan sulphate epitopes in keratoconus. Invest. Ophthalmol. Vis. Sci. **30:** 2278. 1989.

Gernet, H. Oculometric findings in myopia. *In:* 3rd International Conference on Myopia. Doc. Ophthal. Proc. Series 28. (Eds Fledelius,H.C., Alsbirk,P.H. and Goldschmidt,E.) The Hague. 1981.

Girauld, J.P., Pouliquen, Y., Offret, G. and Payrau, P. Statistical morphometric studies in normal human and rabbit corneal stroma. Exp. Eye Res. **21:** 221. 1975.

Gipson, I.K., Spurr-Michaud, S.J. & Tisdale, A.S. Anchoring fibrils form a complex network in human and rabbit cornea. Invest. Ophthalmol. Vis. Sci., **28:** 212. 1987.

Goodfellow, J.M., Elliott, G.F., and Woolgar, A.E. X-ray diffraction studies of the corneal stroma. J. Mol. Biol. **119:** 237. 1978.

Gottlieb, M.D., Joshi, H.B. and Nickla, D.L. Scleral changes in chicks with form deprivation myopia. Curr. Eye Res. **9:** 1157. 1991.

Gyi, T.J. A comparison of the structure of the corneal stroma in a variety of animal species. PhD Thesis, The Open University, U.K. 1988.

Hake, T. Studies on the reaction of OsO_4 and $KMnO_4$ with amino acids, peptides and proteins. Lab. Invest. **14:** 470. 1965.

Hamilton, W.C. Statistics in physical science. The Ronald Press Company, N.Y. 1964.

Hardingham, T.E., Beardmore-Gray, M., Dunham, G and Ratcliffe, A. Cartilage proteoglycans. *In:* Functions of the proteoglycans. CIBA

Foundation Symposium 24 (Eds. Evered,D. and Whelan,J.) **30:** John Wiley and Sons, U.K. 1986.

Hart, R.W. and Farrell, R.A. Light scattering in the cornea. J. Opt. Soc. Am. **59:** 766. 1969.

Hayat, M.A. Principles and techniques of electron microscopy. Biological applications. Macmillan Press, London. 1989.

Hertel, V.E. The application and significance of structural research by means of X-rays in ophthalmology. Archiv. fr. Augenheilknde. **106:** 260. 1933.

Hirsch, M., Nicolas, G. and Pouliquen, Y. Interfibrillar structures in fast-frozen, deep-etched and rotary-shadowed extracellular matrix in the rabbit corneal stroma. Exp. Eye Res. **49:** 311. 1989.

Hodge, A.J. and Schmitt, F.O. The charge profile of the tropocollagen macromolecule and the packing arrangement in native-type collagen fibrils. Proc. Natl. Acad. Sci. USA, **46:** 186. 1960.

Hopwood, D. Fixation of proteins by osmium tetroxide, potassium dichromate and potassium permanganate. Histochemie. **24:** 50. 1969.

Hosaka, A. The growth of the eye and its components. Japanese Studies. Acta. Ophthalmol. (Suppl). **185:** 65. 1988.

Ihalainen, A., Salo, T., Forsius, H. and Peltonen, L. Increase in type I and type IV collagenylic activity in primary cultures of keratoconus cornea. Eur. J. Clin. Invest. **16:** 78. 1986.

Itoh, T., Klein, L. and Geil, P.H. Age dependance of collagen fibril and subfibril diameters revealed by transverse freeze-fracture and -etching technique. J. Micros. **125:** 343. 1982.

Jakus, M.A. Studies on the cornea, I. The fine structure of the rat cornea. Am. J. Ophthalmol., **38:** 40. 1954.

Kanski, J.J. Disorders of the cornea and sclera. *In*: Clinical Ophthalomology, 2nd edition (Ed. Kanski, J.) 87, Butterworth & Co. Ltd., London. 1984.

Katz, E.P., Wachtel, E.J. and Maroudas, A. Extrafibrillar proteoglycans osmotically regulate the molecular packing of collagen in cartilage. Biochim. Biophys. Acta. **882:** 136. 1986.

Kimura, J.H., Thonar, E.J-M., Hascall, V.C., Reiner, A. and Poole, A.R. Identification of core protein, an intermediate in proteoglycan biosynthesis in cultured rat chondrocytes from the swarm rat chondrosarcoma. J. Biol. Chem. **256:** 7890. 1981.

Kjellen, L. and Lindahl, U. Proteoglycans: structures and interactions. Ann. Rev. Biochem. **60:** 443. 1991.

Komai, Y. and Ushiki, T. The three-dimentional organization of collagen fibrils in the human cornea and sclera. Invest. Ophthalmol. Vis. Sci. **32:** 224. 1991.

Krachmer, J.H.,Feder, R.S. and Belin, M.W. Keratoconus and related noninflammatory corneal thinning disorders. Surv. Ophthalmol. **28:** 293. 1984.

Labermeier, U. and Kenney, M.C. The prescence of EC collagen and type IV collagen in bovine Descemet's membranes. Biochem. Biophys. Res. Commun. **116:** 619. 1983.

Malik, S.M., Moss, S.J., Ahmed, N., Furth, A.J., Wall, R.S. and Meek, K.M. Aging in the human corneal stroma: structural and biochemical changes. Biochim. Biophys. Acta. *In press.* 1992.

Marchini, M., Moracutti, M., Ruggeri, A., Koch, M.H.J., Bigi, N. and Roveri, N. Differences in the fibril structure of cornea and tendon collagen. An electron microscopy and X-ray diffraction investigation. Conn. Tiss. Res. **15:** 269. 1986.

Maroudas, A., Wachtel, E., Grushko, G., Katz, E.P. and Weinberg, P. The effect of osmotic and mechanical pressures on water partitioning in articular cartilage. Biochim. Biophys. Acta. **1073:** 285. 1991.

Maurice, D.M. The structure and transparency of the cornea. J. Physiol. (London), **136:** 263. 1957.

Maurice, D.M. The cornea and the sclera. *In*: The Eye, Vol. 1, (Ed. Davson, H.), Academic Press, New York. 1969.

Maurice, D.M. Mechanics of the cornea *In*: The Cornea: Transactions of the World Congress on the Cornea III. (Ed. Cavanagh, H.D.) Raven Press Ltd., New York. 1988.

Meek, K.M., Blamires, T., Elliott, G.F., Gyi, T.J. and Nave, C. The organisation of collagen fibrils in the corneal stroma; a synchrotron x-ray diffraction study. Curr. Eye Res., **6:** 841. 1987a.

Meek, K.M., Elliott, G.F., Gyi, T.J. & Wall, R.S. The structure of normal and keratoconus human corneas. Ophthalmic Res., **19:** 6. 1987b.

Meek, K.M., Elliott, G.F., Hughes, R.A., and Nave, C. The axial density in collagen fibrils from human corneal stroma. Curr. Eye Res. **2:** 471. 1983.

Meek, K.M., Elliott, G.F., and Nave, C. A synchrotron X-ray diffraction study of bovine corneal stroma stained with Cupromeronic blue. Coll. Res. Rel. **6:** 203. 1986.

Meek, K.M., Elliott, G.F., Sayers, Z., Whitburn, S.B. and Koch, M.H. Interpretation of the meridional X-ray diffraction pattern from collagen fibrils in corneal stroma. J. Mol. Biol. **149:** 477. 1981.

Meek, K.M., Scott, J.E., and Nave, C. An X-ray diffraction analysis of rat tail tendons treated with Cupromeronic blue. J. Micros. **139:** 205. 1985.

Muir, H. Proteoglycans as organizers of the intercellular matrix. Biochem. Soc. Trans. 17^{th} CIBA Med. Lect. **11:** 613. 1982.

Murphy, C., Alvarado, J. and Juster, R. Prenatal and postnatal growth of the human Descemet's membrane. Invest. Ophthalmol. Vis. Sci. **25:** 1402. 1984.

Nakayasu, K., Chuman, Y., Tanaka, M., Kanai, A. and Itoi, M. A statistical study on keratoconus. Jpn. J. Clin. Ophthalmol. **18:** 807. 1981.

Nakayasu, K., Tanaka, M., Konomi, H., and Hayashi, T. Distribution of types I, II, III, IV, and V collagen in normal and keratoconus corneas. Ophthalmic Res. **18:** 1. 1986.

Newsome, D.A., Foidart, J.M., Hassel, J.R., Krachmer, J.H., Rodrigues, M.M. and Karz, S.I. Detection of specific collagen types in normal and keratoconus corneas. Invest. Ophthalmol. Vis. Sci. **20:** 738. 1981.

Nimni, M.E. and Harkness, R.D. Molecular structure and functions of collagen. *In*: Collagen, Volume 1; Biochemistry. (Ed. Nimni, M.E.), C.R.C. Press Inc., Boca Raton, Florida. 1988.

Oster, G. and Riley, D.P. Scattering from cylindrically symmetric systems. Acta Crystallogr. **5:** 272. 1952.

Oxlund, H. and Simonsen, A.H. Biochemical studies of normal and keratoconus corneas. Acta. Ophthalmol. (Copenh). **63:** 666. 1985.

Parry, D.A.D. The molecular and fibrillar structure of collagen and its relationship to the mechanical properties of connective tissue. Biophys. Chem. **29:** 195. 1987.

Page, S.G. and Huxley, H.E. Filament lengths in striated muscle. J. Cell Biol. **19:** 369. 1963.

Perkins, E.S. Myopia and scleral stress. *In:* 3rd International Conference on Myopia. Doc. Ophthal. Proc. Series 28. The Hague. 1981.

Polack, F.M. Contributions of electron microscopy to the study of corneal pathology. Surv. Ophthalmol. **20:** 497. 1976.

Pouliquen, Y., Graf, B., DeKozak, Y., Bisson, J., Faure, J-P., Bourles, F., and Frouin, M.A. Etude morphologique et biochimique du keratocone: I etude morphologique. Arch. Ophthalmol.(Paris). **30:** 497. 1970.

Quantock, A.J. and Meek, K.M. Axial electron density of human scleral collagen. Biophys. J. **54:** 159. 1988.

Quantock, A.J, Meek. K.M., Ridgway, A.E.A., Bron, A.J. and Thonar, E.J-M.A. Macular corneal dystrophy: reduction in both corneal thickness and collagen interfibrillar spacing. Curr. Eye Res. **9:** 393. 1990.

Rada, J.R., Thoft, R.A. and Hassel, J.R. Increased aggrecan (cartilage proteoglycan) production in the sclera of myopic chicks. Develop. Biol. **147:** 303. 1991.

Ramachandran, G.N. Structure of collagen at the molecular level. *In:* Treatise on collagen. (Ed. Ramachandran, G.N.) Academic Press, New York. 1967.

Raviola, E. and Wiesel, T.N. Animal model of myopia. New Eng. J. Med. **312:** 1609. 1985.

Rawe, I.M., Tuft, S.J. and Meek, K.M. Proteoglycan and collagen morphology in superficially scarred rabbit cornea. Histochem. J. *In press.* 1992.

Roth, W.J. and Hinckley, C.C. Synthesis and characterization of Osmyl-amino acid complexes. Inorg. Chem. **20:** 2023. 1981.

Sawaguchi, S., Yue, B.Y.J.T., Chang, I., Sugar, J. and Robin, J. Proteoglycan molecules in keratoconus corneas. Invest. Ophthalmol. Vis. Sci. **32:** 1846. 1991.

Sayers, Z., Koch, M.H.J., Whitburn, S.B., Meek, K.M., Elliott, G.F. and Harmsen, A. Synchrotron X-ray diffraction study of corneal stroma. J. Mol. Biol. **160:** 593. 1982.

Schwartz, W. Elektronenmicroskopische untersuchungen uber die

differenzierung der cornea und sklera fibrillen des menschen. Z. Zellforsch, **38:** 78. 1953.

Scott, J.E. Collagen-proteoglycan interactions. Localization of proteoglycans in tendon by electron microscopy. Biochem. J. **187:** 887. 1980.

Scott, J.E. Proteoglycans: collagen interactions and subfibrillar structure in collagen fibrils. Implications in the development and aging of connective tissues. J. Anat. **169:** 23. 1990.

Scott, J.E. Proteoglycan: collagen interactions in connective tissues. Ultrastructural, biochemical, functional and evolutionary aspects. Int. J. Biol. Macromol. **13:** 157. 1991.

Scott, J.E. and Bosworth, T.R. A comparative biochemical and ultrastructural study of proteoglycan-collagen interactions in corneal stroma. Biochem. J. **270:** 491. 1990.

Scott, J.E. and Orford, C.R. Dermatan sulphate-rich proteoglycan associates with rat tail-tendon collagen at the d band in the gap region. Biochem. J. **197:** 213. 1981.

Scott, J.E., Orford, C.R. and Hughes, E.W. Proteoglycan-collagen arrangements in developing rat tail tendon. An electron microscopical and biochemical investigation. Biochem. J. **195:** 573. 1981.

Smith, J.W. The transparency of the corneal stroma. Vision Res. **9:** 393. 1969.

Stryer, L. Biochemistry. 3rd edition. W.H. Freeman and Company, New York. 1988.

Tomlin, S.G. and Worthington, C.R. Low-angle X-ray diffraction patterns of collagen. Proc. Roy. Soc. Ser. A. **235:** 189. 1956.

Vainshtein, B.K. Diffraction of X-rays by chain molecules. Elsevier Publishing Company Ltd: Amsterdam. 1966.

Wallman, J., Gottlieb, M.D., Rajaram, V., and Fugate-Wentzek, L.A. Local retinal regions control local eye growth and myopia. Science. **237:** 73. 1987.

Wallman, J., Turkel, J. and Trachtman, J. Extreme myopia produced by modest changes in early visual experience. Science. **201:** 1249. 1978.

Whitley, R.D., Garcia, G.A., Samuelson, D.A., Hager, D.A., Houde, W.L. and Bitgood, J.J. Inherited keratoconus in the chicken. Preliminary findings. Trans, Am. Coll. Vet. Ophthalmol. and Intl. Soc. Vet. Ophthalmol. **17:** 376. 1986.

Williams, L.R. Ultracryotometry and the cornea. Open University Thesis. 1984.

Winterhalter, K.H. 8^{th} Int. Congress On Eye Research, San Francisco; Workshop proceedings (unpublished). 1988.

Worthington, C.R. The structure of cornea. Quart. Rev. Biophys. **17:** 423. 1984.

Worthington, C.R. and Inouye, H. X-ray diffraction study of the cornea. Int. J. Biol. Macromol. **7:** 2. 1985.

Young, R.D. The ultrastructural organization of proteoglycans and collagens in human and rabbit scleral matrix. J. Cell. Sci. **74:** 95. 1985.

Yue, B.Y.J.T., Sugar, J. and Schrode, K. Histochemical studies of keratoconus. Curr. Eye Res. **7:** 81. 1988.

Yue, B., Sawaguchi, S., Twining, S., and Sugar, J. Biochemical studies of keratoconus corneas. Proceedings of the International Society for Eye Research. **6:** 198. 1990.